



National Library
of Canada

Bibliothèque nationale
du Canada

Canadian Theses Service Service des thèses canadiennes

Ottawa, Canada
K1A 0N4

NOTICE

The quality of this microform is heavily dependent upon the quality of the original thesis submitted for microfilming. Every effort has been made to ensure the highest quality of reproduction possible.

If pages are missing, contact the university which granted the degree.

Some pages may have indistinct print especially if the original pages were typed with a poor typewriter ribbon or if the university sent us an inferior photocopy.

Previously copyrighted materials (journal articles, published tests, etc.) are not filmed.

Reproduction in full or in part of this microform is governed by the Canadian Copyright Act, R.S.C. 1970, c. C 30.

AVIS

La qualité de cette microforme dépend grandement de la qualité de la thèse soumise au microfilmage. Nous avons tout fait pour assurer une qualité supérieure de reproduction.

Si manque des pages, veuillez communiquer avec l'université qui a conféré le grade.

La qualité d'impression de certaines pages peut laisser à désirer, surtout si les pages originales ont été dactylographiées à l'aide d'un ruban usé ou si l'université nous a fait parvenir une photocopie de qualité inférieure.

Les documents qui font déjà l'objet d'un droit d'auteur (articles de revue, tests publiés, etc.) ne sont pas microfilmés.

La reproduction, même partielle, de cette microforme est soumise à la Loi canadienne sur le droit d'auteur, S.R.C. 1970, c. C 30.

THE UNIVERSITY OF ALBERTA

NMR STUDIES OF CHEMICAL EXCHANGE

by

DAYA RANJITH MUHANDIRAM

A THESIS SUBMITTED

TO THE FACULTY OF GRADUATE STUDIES AND RESEARCH

IN PARTIAL FULFILMENT OF THE REQUIREMENTS

FOR THE DEGREE OF DOCTOR OF PHILOSOPHY

DEPARTMENT OF CHEMISTRY

EDMONTON, ALBERTA

FALL, 1987

Permission has been granted to the National Library of Canada to microfilm this thesis and to lend or sell copies of the film.

The author (copyright owner) has reserved other publication rights, and neither the thesis nor extensive extracts from it may be printed or otherwise reproduced without his/her written permission.

L'autorisation a été accordée à la Bibliothèque nationale du Canada de microfilmer cette thèse et de prêter ou de vendre des exemplaires du film.

L'auteur (titulaire du droit d'auteur) se réserve les autres droits de publication; ni la thèse ni de longs extraits de celle-ci ne doivent être imprimés ou autrement reproduits sans son autorisation écrite.

ISBN 0-315-41030-2

THE UNIVERSITY OF ALBERTA

RELEASE FORM

NAME OF AUTHOR Daya Ranjith Muhandiram
TITLE OF THESIS NMR Studies of Chemical Exchange
DEGREE FOR WHICH THESIS WAS PRESENTED Ph. D.
YEAR THIS DEGREE GRANTED 1987

Permission is hereby granted to the UNIVERSITY OF ALBERTA LIBRARY to reproduce single copies of this thesis and to lend or sell such copies for private, scholarly or scientific research purposes only.

The author reserves other publication rights, and neither the thesis nor extensive extracts from it may be printed or otherwise reproduced without the author's written permission.

Muhandiram

(Signed)

Permanent Address:

133/89 D. C. R. Wijesinghe Mawatha

Off Ratnapura Road

Avissawella

Sri Lanka

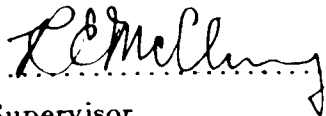
Date *September 29th* 1987

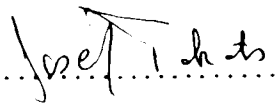
THE UNIVERSITY OF ALBERTA
FACULTY OF GRADUATE STUDIES AND RESEARCH

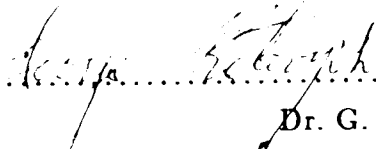
The undersigned certify that they have read, and recommend to the Faculty of
Graduate Studies and Research for acceptance, a thesis entitled


NMR STUDIES OF CHEMICAL EXCHANGE


submitted by D. R. Muhandiram in partial fulfilment of the requirements for the
degree of Doctor of Philosophy.

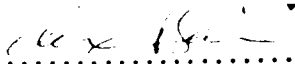

.....
Supervisor Dr. R. E. D. McClung


.....
Dr. J. Takats


.....
Dr. G. Kotovych


.....
Dr. J. S. Martin


.....
Dr. A. N. Kamal


.....
External Examiner Dr. A. D. Bain

Date .. September 29th .. 1987 ..

To My Parents

ABSTRACT

In this thesis, a theoretical description of the effects of chemical exchange in NMR experiments has been developed using product operators, and a magnetization transfer method has been developed to delineate exchange mechanisms in complex multisite exchange situations. The description of the ^1H - ^{13}C DEPT, heteronuclear magnetization transfer experiment on exchanging $\text{CH}_2 \dots \text{CH}$ and $\text{CH}_3 \dots \text{CH}_3$ has been developed in detail to demonstrate the general applicability of the product operator description to experiments employing sophisticated pulse sequences which generate multiple quantum coherences. In the region of intermediate exchange, the comparison of observed and calculated ^{13}C DEPT intensities for N-acetylpyrrole and N,N-dimethylacetamide, afforded the determination of the exchange rate to within 5-15%.

The multisite magnetization transfer method in which the magnetization at one site is selectively inverted, was employed in the study of chemical exchange in several organometallic complexes, which are multisite networks involving several exchange mechanisms. A method of least squares analysis which allows precise determination of the contributing exchange mechanisms and their rates is presented. It has been used to quantitatively establish the fluxional behaviour of a mixture of asymmetric/meridional and symmetric/facial isomers of $(\eta^3\text{-C}_7\text{H}_7)\text{-Os}(\text{CO})_3\text{-SnPh}_3$ as due to "1-2" metal migrations, which occur with different activation energies in the two isomers. Fluxionality of transition metal complexes $(\eta^5\text{-C}_7\text{H}_7)\text{-M}(\text{CO})_2\text{-SnPh}_3$, $\text{M}=\text{Fe}, \text{Ru}, \text{Os}$ has also been investigated in detail using this method, which enabled the delineation and precise quantitative determination of the rates of competing "1-2" and "1-3" metal shifts in the Fe complex

which is of C_1 symmetry, and the rates of dominant "1 2" and slower "1 3" shifts in the Os complex which is of C_s symmetry. The enantiomer interconversion of the asymmetric isomer of the Ru complex, which exists as a mixture of symmetric (C_s) and asymmetric (C_1) isomers was found to occur via the symmetric species. The metal migration in this complex, was also established as only due to "1 3" shifts.

ACKNOWLEDGEMENTS

I wish to express my deep sincere gratitude to Professor R. E. D. McClung for his encouragement, guidance and help throughout the course of this work. His efforts in trying to instill the fundamentals of magnetic resonance in me, are greatly appreciated.

I owe special gratitude to Professor J. Takats and Dr. G. Y. Kiel for the samples of organometallic complexes and for their collaboration in some of the experiments. Special thanks are due to Dr. Takats for numerous discussions and for his help in the preparation of chapters 5 and 6 of this thesis.

I thank Dr. Boban John for initial guidance with the instrumentation and Dr. T. T. Nakashima for his help on various instrumental and data processing aspects.

Special thanks are due to my wife Jennifer for her help in the preparation of this manuscript and Dr. Albin Otter for continuous moral support.

Financial assistance from the Department of Chemistry and Natural Sciences and Engineering Research Council of Canada is gratefully acknowledged.

TABLE OF CONTENTS

Chapter	Page
1. Introduction	1
2. Product Operator Description of Chemical Exchange in NMR Experiments with Application to ^1H - ^{13}C DEPT Magnetization Transfer	7
2.1 Introduction	7
2.2 Theory: Product Operator Description of Chemical Exchange	8
2.3 Effects of Chemical Exchange in DEPT Magnetization Transfer Experiments	10
2.3.1 CH...CH Exchange	13
2.3.2 CH ₃ ...CH ₃ Exchange	19
2.4 Experimental	25
2.5 Results	25
2.5.1 CH...CH Exchange	26
2.5.2 CH ₃ ...CH ₃ Exchange	30
2.6 Summary	33
3. Development of Multisite Magnetization Transfer Experiments and Method of Data Analysis	35
3.1 Introduction	35
3.2 Basic Concepts of Magnetization Transfer Experiments	36
3.3 Modified Bloch Equations for z -Magnetization	37
3.4 Saturation Transfer Experiments	39
3.4.1 Decay of Signal <i>A</i> upon Saturation of Signal <i>B</i>	39
3.4.2 Cases (b) to (d) - Temporal Magnetization (Saturation) Transfer	41
3.5 Selective Pulse Experiments	41

3.5.1 Simplest Two Site Exchange	44
3.6 General <i>N</i> -Site Exchange - Selective Inversion Method	47
3.6.1 Least Squares Analysis of Selective Inversion-Magnetization Transfer Data	48
3.6.2 Analytic First Derivatives of $M_1(t)$	51
3.6.3 New Parameters for Iteration and Convergence	53
3.6.4 Estimation of Errors in Rate Constants	55
3.7 Summary	56
4. Details of Selective Inversion Experiment and Evaluation of the Method ..	58
4.1 Introduction	58
4.2 Experimental Details	58
4.3 Application of the Selective Inversion Method to a Study of the Fluxional Behaviour of $(\eta^3\text{-C}_7\text{H}_7)\text{-Os}(\text{CO})_3\text{-SnPh}_3$	61
4.3.1 Qualitative Determination of Exchange Mechanism	64
4.3.2 Quantitative Determination of Rate Constants	66
4.3.3 Importance of the "1-3" Exchange Process	67
4.3.4 Clockwise vs Anticlockwise Metal Migration	67
4.3.5 Reliability of Rate Constants	68
4.3.6 Effects of Imperfect Selectivity of Inversion	68
4.3.7 Effect of absence of Data from One Site on the Rate Constant ..	69
4.4 Application of the Method to the Study of the Fluxional Behaviour of the Symmetric Isomer, in the Presence of rapidly Exchanging Asymmetric Isomer	71
4.5 Limitations of the Multisite Magnetization Transfer Method	75
4.5.1 Inefficient Selective Inversion	75
4.5.2 Effect of Inaccurate T_1 Values	76

4.5.3 Effects of Cross Relaxation	78
4.6 Summary	79
5. Fluxionality of $(\eta^3\text{-C}_7\text{H}_7)\text{-Os}(\text{CO})_3\text{-SnPh}_3$	80
5.1 Introduction	80
5.2 Experimental	82
5.3 Results of Selective Inversion Experiments on $(\eta^3\text{-C}_7\text{H}_7)\text{-Os}(\text{CO})_3\text{-SnPh}_3$	82
5.3.1 Rate Constants and Activation Parameters for the Asymmetric Isomer	82
5.3.2 Rate Constants and Activation Parameters for the Symmetric Isomer	84
5.3.3 Comparison of Fluxional Behaviour of $(\eta^3\text{-C}_7\text{H}_7)\text{-M}(\text{CO})_3\text{-SnPh}_3$ systems	87
5.4 Comparison of Fluxional Behaviour of $(\eta^3\text{-C}_7\text{H}_7)\text{-Os}(\text{CO})_3\text{-SnPh}_3$ with other Fluxional $\eta^3\text{-C}_7\text{H}_7$ Systems with Symmetric and Asymmetric Isomers	89
5.5 Summary	90
6. Fluxionality of $(\eta^5\text{-C}_7\text{H}_7)\text{-M}(\text{CO})_2\text{-SnPh}_3$, M=Fe, Ru, Os	92
6.1 Introduction	92
6.2 Experimental	93
6.3 Fluxional Behaviour of $(\eta^5\text{-C}_7\text{H}_7)\text{-Fe}(\text{CO})_2\text{-SnPh}_3$	100
6.3.1 Delineation of the Exchange Mechanism of $(\eta^5\text{-C}_7\text{H}_7)\text{-Fe}(\text{CO})_2\text{-SnPh}_3$	101
6.3.2 Rate Constants and Activation Parameters for $(\eta^5\text{-C}_7\text{H}_7)\text{-Fe}(\text{CO})_2\text{-SnPh}_3$	108
6.4 Fluxional Behaviour of $(\eta^5\text{-C}_7\text{H}_7)\text{-Os}(\text{CO})_2\text{-SnPh}_3$	112

6.4.1 Delineation of the Exchange Mechanism of $(\eta^5\text{-C}_7\text{H}_7)\text{-Os}(\text{CO})_2\text{-SnPh}_3$	112
6.4.2 Rate Constants and Activation Parameters for $(\eta^5\text{-C}_7\text{H}_7)\text{-Os}(\text{CO})_2\text{-SnPh}_3$	116
6.5 Fluxional Behaviour of $(\eta^5\text{-C}_7\text{H}_7)\text{-Ru}(\text{CO})_2\text{-SnPh}_3$	120
6.5.1 Isomer interconversion in $(\eta^5\text{-C}_7\text{H}_7)\text{-Ru}(\text{CO})_2\text{-SnPh}_3$	120
6.5.2 Delineation of the Metal Migration Mechanism in $(\eta^5\text{-C}_7\text{H}_7)\text{-Ru}(\text{CO})_2\text{-SnPh}_3$	131
6.5.3 Estimation of Activation Parameters for $(\eta^5\text{-C}_7\text{H}_7)\text{-Ru}(\text{CO})_2\text{-SnPh}_3$	136
6.6 Comparison of the Fluxional Behaviour of $(\eta^5\text{-C}_7\text{H}_7)\text{-M}(\text{CO})_2\text{-SnPh}_3$ systems (M=Fe, Ru, os)	137
6.7 Comparison of the Fluxionality of General $\eta^5\text{-C}_7\text{H}_7$ transition metal complexes	139
6.8 Summary	141
7. Conclusions and Suggestions for Future Consideration	143
REFERENCES	149
APPENDIX A	155

LIST OF TABLES

Table		Page
2. 1	Basis Operators, Traces and Commutators for CH exchange	14
2. 2	Basis Operators, Traces and Commutators for CH ₃ exchange	20
4. 1	Effect of absence of data from one site on the rate constant	70
4. 2	Dependence of k on $1/T_1$	78
5. 1	Rate constants for exchange in asymmetric (η^3 -C ₇ H ₇)-Os(CO) ₃ -SnPh ₃	83
5. 2	Rate constants for exchange in symmetric (η^3 -C ₇ H ₇)-Os(CO) ₃ -SnPh ₃	84
5. 3	Activation parameters for (η^3 -C ₇ H ₇)-Os(CO) ₃ -SnPh ₃	85
5. 4	Activation parameters for symmetric (η^3 -C ₇ H ₇)-M(CO) ₃ -SnPh ₃	88
6. 1	Rate constants for exchange in (η^5 -C ₇ H ₇)-Fe(CO) ₂ -SnPh ₃	109
6. 2	Activation parameters for (η^5 -C ₇ H ₇)-Fe(CO) ₂ -SnPh ₃	111
6. 3	Comparison of variance for "1 2" and "1 3" vs only "1 2" shifts in (η^5 -C ₇ H ₇)-Os(CO) ₂ -SnPh ₃	116
6. 4	Rate constants for exchange in (η^5 -C ₇ H ₇)-Os(CO) ₂ -SnPh ₃	117
6. 5	Activation parameters for (η^5 -C ₇ H ₇)-Os(CO) ₂ -SnPh ₃	119
6. 6	Effect of $k_{(AA')}$ on variance for isomer interconversion in (η^5 -C ₇ H ₇)- Ru(CO) ₂ -SnPh ₃	126
6. 7	Rate constants for isomer interconversion in (η^5 -C ₇ H ₇)-Ru(CO) ₂ - SnPh ₃	130
6. 8	Activation parameters for isomer interconversion in (η^5 -C ₇ H ₇)-Ru(CO) ₂ - SnPh ₃	130
6. 9	Variance for only "1-3" vs "1-3" and "1-4" shifts in (η^5 -C ₇ H ₇)-Ru(CO) ₂ - SnPh ₃	133

6. 10	Variance for only "1-3" vs "1-3" and "1-4" shifts in $(\eta^5\text{-C}_7\text{H}_7)\text{-Ru}(\text{CO})_2$ SnPh ₃	135
6. 11	Exchange processes and activation parameters for $(\eta^5\text{-C}_7\text{H}_7)\text{-M}(\text{CO})_2$ SnPh ₃	137
6. 12	Fluxional $(\eta^5\text{-C}_7\text{H}_7)\text{-ML}_2$ complexes	140

LIST OF FIGURES

Figure	Page
2-1 Pulse sequence and coherence transfer pathways for DEPT	11
2-2 Comparison of Observed and calculated DEPT intensities for N-acetylpyrrole	27
2-3 Comparison of Observed and calculated DEPT intensities for N,N-dimethylacetamide	31
3-1 Behaviour of the z -magnetizations in the simplest two site exchange ...	45
3-2 Dependence of the temporal response of z -magnetization at site B on the exchange rate and relaxation rate	46
4-1 DANTE selective inversion recovery pulse sequence	59
4-2 ^1H NMR spectrum of the C_7H_7 region for $(\eta^3\text{-C}_7\text{H}_7)\text{-Os}(\text{CO})_3\text{-SnPh}_3$ at 188 K	62
4-3 Comparison of the observed and calculated magnetizations for the asymmetric isomer at 188 K	65
4-4 ^1H NMR spectra of the C_7H_7 region for $(\eta^3\text{-C}_7\text{H}_7)\text{-Os}(\text{CO})_3\text{-SnPh}_3$ at 214, 223 and 233 K	72
4-5 Comparison of the observed and calculated magnetizations for the symmetric isomer at 214 K	74
6-1 ^1H NMR spectra of the C_7H_7 region for $(\eta^5\text{-C}_7\text{H}_7)\text{-Fe}(\text{CO})_2\text{-SnPh}_3$ at 258, 268 and 278 K	94
6-2 ^1H NMR spectra of the C_7H_7 region for $(\eta^5\text{-C}_7\text{H}_7)\text{-Os}(\text{CO})_2\text{-SnPh}_3$ at 273, 282 and 291 K	95
6-3 ^1H NMR spectrum of the C_7H_7 region for $(\eta^5\text{-C}_7\text{H}_7)\text{-Ru}(\text{CO})_2\text{-SnPh}_3$ at 183 K	96

6-4	^1H NMR spectra of the C_7H_7 region for $(\eta^5\text{-C}_7\text{H}_7)\text{-Ru}(\text{CO})_2\text{-SnPh}_3$ in toluene- d_8 at 221, 231 and 234 K	97
6-5	^1H NMR spectrum of the C_7H_7 region for $(\eta^5\text{-C}_7\text{H}_7)\text{-Ru}(\text{CO})_2\text{-SnPh}_3$ in CD_2Cl_2 at 232 K	98
6-6	Comparison of the observed and calculated magnetizations for "1-2" and "1-3" shifts in $(\eta^5\text{-C}_7\text{H}_7)\text{-Fe}(\text{CO})_2\text{-SnPh}_3$	103
6-7	Comparison of the observed and calculated magnetizations for "1-2" shifts in $(\eta^5\text{-C}_7\text{H}_7)\text{-Fe}(\text{CO})_2\text{-SnPh}_3$	104
6-8	Comparison of the observed and calculated magnetizations for "1-3" shifts in $(\eta^5\text{-C}_7\text{H}_7)\text{-Fe}(\text{CO})_2\text{-SnPh}_3$	105
6-9	Comparison of the observed and calculated magnetizations for "1-2" and "1-3" shifts in $(\eta^5\text{-C}_7\text{H}_7)\text{-Fe}(\text{CO})_2\text{-SnPh}_3$	106
6-10	Arrhenius plot for $(\eta^5\text{-C}_7\text{H}_7)\text{-Fe}(\text{CO})_2\text{-SnPh}_3$	110
6-11	Comparison of the observed and calculated magnetizations for "1-2" and "1-3" shifts in $(\eta^5\text{-C}_7\text{H}_7)\text{-Os}(\text{CO})_2\text{-SnPh}_3$	113
6-12	Comparison of the observed and calculated magnetizations for "1-2" shifts in $(\eta^5\text{-C}_7\text{H}_7)\text{-Os}(\text{CO})_2\text{-SnPh}_3$	114
6-13	Arrhenius plot for $(\eta^5\text{-C}_7\text{H}_7)\text{-Os}(\text{CO})_2\text{-SnPh}_3$	118
6-14	Comparison of the observed and calculated magnetizations for $(\eta^5\text{-C}_7\text{H}_7)\text{-Ru}(\text{CO})_2\text{-SnPh}_3$ isomer interconversion	128
6-15	Comparison of the observed and calculated magnetizations for $(\eta^5\text{-C}_7\text{H}_7)\text{-Ru}(\text{CO})_2\text{-SnPh}_3$ isomer interconversion	129
6-16	Comparison of the observed and calculated magnetizations for "1-3" shifts in $(\eta^5\text{-C}_7\text{H}_7)\text{-Ru}(\text{CO})_2\text{-SnPh}_3$	134

ABBREVIATIONS

Me₃ (CH₃)₃

Ph₃ (C₆H₅)₃

EPTB 4-ethyl-1-phospha-2,6,7-trioxabicyclo[2.2.2]octane

CHAPTER 1

INTRODUCTION

Effects of chemical exchange on NMR spectra were recognized early in the development of NMR spectroscopy and NMR is now an elegant technique for investigating a variety of exchange processes (1,2). Analysis of the exchange modified lineshape of conventional NMR spectra has been the major NMR technique used in the elucidation of exchange mechanisms and in the determination of exchange rate constants in a large number of chemical exchange processes (1,3-11). The phenomena of exchange broadening, coalescence and exchange narrowing of resonances in conventional NMR spectra have been described theoretically by many workers (12-16,17,18,19-24). The first theoretical treatments (12-16) were based on the classical Bloch equation description of NMR (25), and were limited to exchange between uncoupled spins. Exchange involving scalar coupled nuclear spins required a more general quantum mechanical description (19-24) based on the density matrix approach (26). The formal theory of exchange-modified lineshapes was subsequently reviewed, refined and especially developed in a more computational sense by many workers (3,27-34) in order to improve the reliability of rate constants determined from lineshape analysis, and for efficient handling of larger spin systems. The most reliable rate constants are obtained from lineshape analysis by fitting the observed NMR lineshape to the calculated lineshape. This method can be used to study exchange processes with exchange rate constants in the range of $\sim 1 - 10^6 \text{ s}^{-1}$. The NMR lineshape is found to be insensitive to very slow and very fast exchange processes with exchange rate constants outside these limits. In the intermediate exchange region, sometimes, significantly

broadened or coalesced resonances may be of poor signal-to-noise, making precise visual comparison of calculated and observed spectra difficult, especially in the case of less sensitive nuclei such as ^{13}C . Although the theoretical treatments have been generalized to handle exchange involving a large number of sites, classical lineshape analysis does not always produce unambiguous or precise results when there are several different, but simultaneous exchange processes occurring in complex systems. This work is concerned with the delineation of the effects of chemical exchange on sophisticated pulse sequences to probe the potential utility of modern NMR experiments to study chemical exchange processes, and with the development of a multisite magnetization transfer method to delineate exchange mechanisms in complex exchange situations.

With the increased utilization of sophisticated NMR experiments involving complicated pulse sequences (35,36), it is useful to investigate the effects of chemical exchange on these pulse sequences in order to find out the effects of chemical exchange on the outcome of these experiments, and to assess the potential utility of modern experiments to investigate exchange processes. Although the Carr-Purcell spin echo (37) experiment has been recognized as a useful pulse sequence for the elucidation of exchange processes (38-41) at early stages of the development of pulsed NMR, its application has not been widespread (42,43). In the Carr-Purcell spin echo, 2D exchange (44), and many heteronuclear correlation experiments, exchange effects are easily described by classical Bloch equations since only transverse and longitudinal magnetizations are involved. In many modern experiments multiple quantum coherences are generated and used to obtain information about the spin system under investigation. The effects of chemical exchange on the behaviour of multiple quantum coherences cannot be treated using simple Bloch equations and hence a more general description is required. In

principle the density matrix formalism can be used to study the effects of chemical exchange on more complicated pulse sequences, but in practice explicit density matrix calculations become very complicated as the size of the spin system increases. The product operator representation of the density operator (45-47) provides a convenient method of following the density operator during a pulse experiment. In this thesis the effects of chemical exchange on complicated pulse sequences are investigated using the product operator formalism.

In chapter 2, a product operator description of chemical exchange is presented and it is used to investigate the effects of intramolecular CH...CH and CH₃...CH₃ exchange on the ¹H-¹³C DEPT heteronuclear magnetization transfer experiment (48). The DEPT experiment can be considered as a representative example of many sophisticated pulse sequences. In the ¹H-¹³C DEPT experiment, ¹H magnetization is transferred to ¹³C magnetization via ¹H-¹³C multiple quantum coherences, and it allows one to observe edited ¹³C NMR spectra for CH, CH₂ and CH₃ groups, with enhanced sensitivity. The effects of chemical exchange on the ¹H-¹³C multiple quantum coherences are delineated using the product operator description. Theoretical predictions are tested and the potential applicability of the DEPT sequences to investigate exchange processes is probed using N-acetylpyrrole (CH...CH exchange) and NN-dimethylacetamide (CH₃...CH₃ exchange) as test molecules. Kinetic information about these molecules is readily available from previous studies (11,49,50,51-53).

Chapters 4 to 6 deal with multisite chemical exchange processes in which more than one exchange mechanism may be operative. It is not always possible to use classical lineshape analysis to delineate exchange mechanisms and to determine quantitative rate constants when several simultaneous exchange processes are occurring in a complex system, even though this is possible in principle. For example,

lineshape analysis had failed to yield unambiguous mechanisms for the fluxional behaviour in some fluxional organometallic complexes (54). With the introduction of double resonance techniques, Forsen and Hoffmann (55-57) developed a homonuclear magnetization transfer experiment which is especially suitable for the study of exchange processes with rates slower than $\sim 1 \text{ s}^{-1}$ which are inaccessible by classical lineshape methods. A non-equilibrium magnetization is produced at one of the exchanging sites by application of a saturating rf field (55-57), or a selective 180° pulse (58-62), and the mechanisms and rate constants are deduced by observing the transfer of this non-equilibrium magnetization to other exchanging sites. This technique is suitable for the delineation of exchange mechanisms in multisite exchange processes but most studies which employed this method have been limited to simple two site exchange cases (63,64). The extension of this method to delineate exchange mechanisms and to determine rate constants for these mechanisms in a multisite exchange network is presented in detail in Chapter 3. The Forsen-Hoffmann saturation transfer experiment is discussed briefly, and the application of selective inversion method in delineating exchange mechanisms is illustrated using the simple two site exchange case. The modified Bloch equation description of the selective inversion experiment for the general N -site exchange problem is developed and the least squares method of data analysis is described.

In Chapter 4, the power of the selective inversion, multisite magnetization transfer method developed in Chapter 3 in delineating exchange mechanisms and determining exchange rate constants is demonstrated using the fluxional organometallic complex $(\eta^3\text{-C}_7\text{H}_7)\text{-Os}(\text{CO})_3\text{-SnPh}_3$ as a test case. This complex exists as a mixture of two fluxional but noninterconverting isomers (65). Fluxionality arises due to the migration of the Os atom around the C_7H_7 ring and in

one of the isomers, all seven sites on the C_7H_7 ring are nonequivalent, providing a challenging seven site exchange problem. Although it is possible to study this isomer in the low temperature range where only this isomer is fluxional, the other isomer which corresponds to a four site exchange case can only be studied in the high temperature region where both isomers are fluxional. The successful handling of both cases is described in detail in Chapter 4.

Chapters 5 and 6 deal with the application of the selective inversion multisite magnetization transfer method to study the fluxional behaviour of some $(\eta^3-C_7H_7)$ and $(\eta^5-C_7H_7)$ transition metal organometallic complexes. Exchange reactions in organometallic compounds have been studied extensively using NMR (5,7,9,66-70), and there is significant interest in the delineation of exchange mechanisms responsible for fluxional behaviour in stereochemically nonrigid complexes (66-70). The majority of investigations of the fluxional behaviour of transition metal organometallic complexes have been carried out using lineshape analysis (66-70), but only qualitative or semi-quantitative information is available from many of the studies. Fluxional behaviour of complexes of the type $(\eta^m-C_nH_n)-ML_x$ where $m \leq n$, M is a transition metal and L_x represents other ligands, has been explained (69-71) using the Woodward-Hoffmann orbital symmetry rules (72). However many transition metal complexes, especially $(\eta^5-C_7H_7)$ complexes were found to be fluxional in violation of the predictions based on the Woodward-Hoffmann rules. The lack of precise quantitative information on rate constants and activation parameters for the exchange processes which are responsible for the fluxional behaviour has made it difficult to assess the validity of these rules in explaining the fluxionality of transition metal organometallic complexes. In Chapter 5, results of the selective inversion magnetization transfer experiments on the $(\eta^3-C_7H_7)-Os(CO)_3-SnPh_3$ complex are presented. The results of the in-

investigation of the group 8B transition metal organometallic complexes ($\eta^5\text{-C}_7\text{H}_7$)- $\text{M}(\text{CO})_2\text{-SnPh}_3$, $\text{M}=\text{Fe,Ru,Os}$ are presented in Chapter 6.

The final chapter, chapter 7, summarizes briefly the conclusions from the investigations of effects of chemical exchange on the DEPT heteronuclear magnetization transfer experiment, and the selective inversion, multisite magnetization transfer experiments. A few suggestions for future consideration are included.

CHAPTER 2

Product Operator Description of Chemical Exchange in NMR Experiments with Application to ^1H - ^{13}C DEPT Magnetization Transfer

2.1 Introduction

The effects of chemical exchange on NMR spectra were recognized early in the development of NMR spectroscopy, and NMR is now an elegant and useful tool for the delineation of exchange processes and the determination of exchange rates (1,2). With the increasing utilization of more sophisticated experiments employing more complicated pulse sequences (35,36) it is useful to investigate the effects of chemical exchange in such experiments. In the 2D exchange experiment (4) and some heteronuclear correlation experiments, the chemical exchange effects are easily handled in terms of modified Bloch equations since only transverse and longitudinal magnetizations (coherences of levels $0, \pm 1$) are involved. However, many modern experiments involve multiple quantum coherences which cannot be described in simple terms. The potential application of such experiments in the study of chemical exchange can only be assessed and exploited with a more general description of the effect of chemical exchange on the state of a spin system.

The product operator representation of the density operator (45,46) has revolutionized the description of the evolution of the spin system in modern NMR experiments. In this chapter, we present a product operator description of chemical exchange, and use it to investigate the effects of $\text{CH}\dots\text{CH}$ and $\text{CH}_3\dots\text{CH}_3$ exchange in the DEPT ^1H - ^{13}C magnetization transfer experiment (48). Experimental results from DEPT experiments on N-acetylpyrrole and N,N-

dimethylacetamide are reported and the utility of the DEPT experiment in the study of chemical exchange in these systems is evaluated.

2.2 Theory: Product Operator Description of Chemical Exchange

Conventionally, the effects of chemical exchange in NMR spectroscopy have been described by the use of exchange-modified Bloch equations, or density matrix lineshape calculations (3). In more complicated pulse sequences like DEPT (48), the effects of chemical exchange are most easily described by following the density operator. We have adopted the product operator formalism (45,46) as a convenient representation of the density operator. The state of a spin system is described by the density operator, ρ , which is governed by the equation of motion (3)

$$\frac{d\rho}{dt} = i[\rho, \mathcal{H}] - k(\rho - P\rho P), \quad [2-1]$$

in the presence of chemical exchange. In Eq. [2-1], \mathcal{H} is the spin Hamiltonian (in s^{-1}) for the spin system of interest in the absence of rf fields, P is a permutation operator which describes the nuclear interchanges which occur in the exchange process, and k is the rate constant for exchange. ρ can be represented as a linear combination of basis operators $\{B_s\}$ (26):

$$\rho(t) = \sum_s b_s(t) B_s. \quad [2-2]$$

Following the product operator formalism (45,46), we select the basis operators to be a complete set of spherical tensor basis product operators (47) which satisfy the orthogonality relation

$$\text{Tr}\{B_r^\dagger B_s\} = C_N \delta_{r,s}, \quad [2-3]$$

where $C_N = 2^{N-2}$, and N is the number of spin 1/2 nuclei in the spin system. The value of the coefficient $b_s(t)$ in Eq. [2-2] represents the magnitude of the coherence (or magnetization) associated with product operator B_s at time t .

The effects of free precession and of rf pulses on the density operator are well-known (45-47). In the presence of chemical exchange, however, the behaviour of the coefficients $b_s(t)$ in Eq. [2-2] requires further analysis. From Eq. [2-1] and [2-2], one obtains the equation of motion

$$\sum_s \frac{db_s(t)}{dt} B_s = i \sum_s b_s(t) [B_s, \mathcal{H}] - k \sum_s b_s(t) (B_s - P B_s P) \quad [2-4]$$

for the coefficients $b_s(t)$. Multiplying Eq. [2-4] on the left by B_r^\dagger , taking the trace, and making use of the orthogonality relation [2-3], one obtains

$$\frac{db_r(t)}{dt} = \sum_s \left\{ -k\delta_{r,s} - \frac{i}{C_N} \text{Tr}([B_r^\dagger, \mathcal{H} | B_s]) + \frac{k}{C_N} \text{Tr}(B_r^\dagger P B_s P) \right\} b_s(t), \quad [2-5]$$

which can be written in matrix form as

$$\frac{d\mathbf{b}}{dt} = \mathbf{K}\mathbf{b}, \quad [2-6]$$

where $\text{Tr}(\)$ represents the trace operation, \mathbf{b} is a column matrix of the coefficients b_r , and \mathbf{K} is a square matrix, which describes the effects of free precession and chemical exchange, with elements

$$K_{rs} = -k\delta_{r,s} - \frac{i}{C_N} \text{Tr}([B_r^\dagger, \mathcal{H} | B_s]) + \frac{k}{C_N} \text{Tr}(B_r^\dagger P B_s P). \quad [2-7]$$

Solution of Eq. [2-6] gives the coefficients $\mathbf{b}(t)$ at time t during a period of evolution:

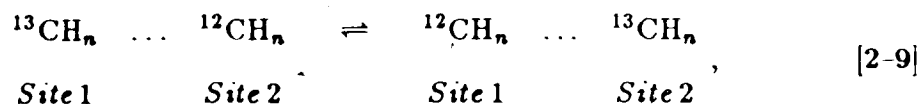
$$\mathbf{b}(t) = \mathbf{U} \exp(\mathbf{K}t) \mathbf{U}^{-1} \mathbf{b}(0), \quad [2-8]$$

where Λ and U are the eigenvalues and eigenvectors of the matrix K . It should be pointed out that the only coefficients b_r which need be included in the description of a period of free evolution are those which are non-zero at the beginning of the period, and those associated with operators B_r which are connected via spin-spin interactions or by chemical exchange to operators B_r with non-zero coefficients. This means that only a small subset of the 4^N coefficients b_r need be included, as demonstrated in the following section.

There is a close parallel between the product operator description of chemical exchange and the density matrix description (3,28), but the product operator description is more convenient for the present purposes.

2.3 Effects of Chemical Exchange in DEPT Magnetization Transfer Experiments

In studying the effects of exchange on magnetization transfer, we shall restrict ourselves to intramolecular 2 site exchange reactions of the form



where Sites 1 and 2 are chemically nonequivalent. The DEPT pulse sequence is shown in Fig. 2-1. It is a sequence in which ${}^1\text{H}$ magnetization is transferred to ${}^{13}\text{C}$ magnetization via ${}^1\text{H}$ - ${}^{13}\text{C}$ zero and double quantum coherences as shown in the coherence transfer pathways given in Fig. 2-1. The behaviour of the magnetizations and multiple quantum coherences will be affected by chemical exchange, and it is these effects of chemical exchange on DEPT magnetization transfer which we wish to delineate. To this end, we investigate the behaviour of spin systems under the action of the DEPT sequence for various values of τ , not only the $1/2J_{CH}$ value normally employed (48).

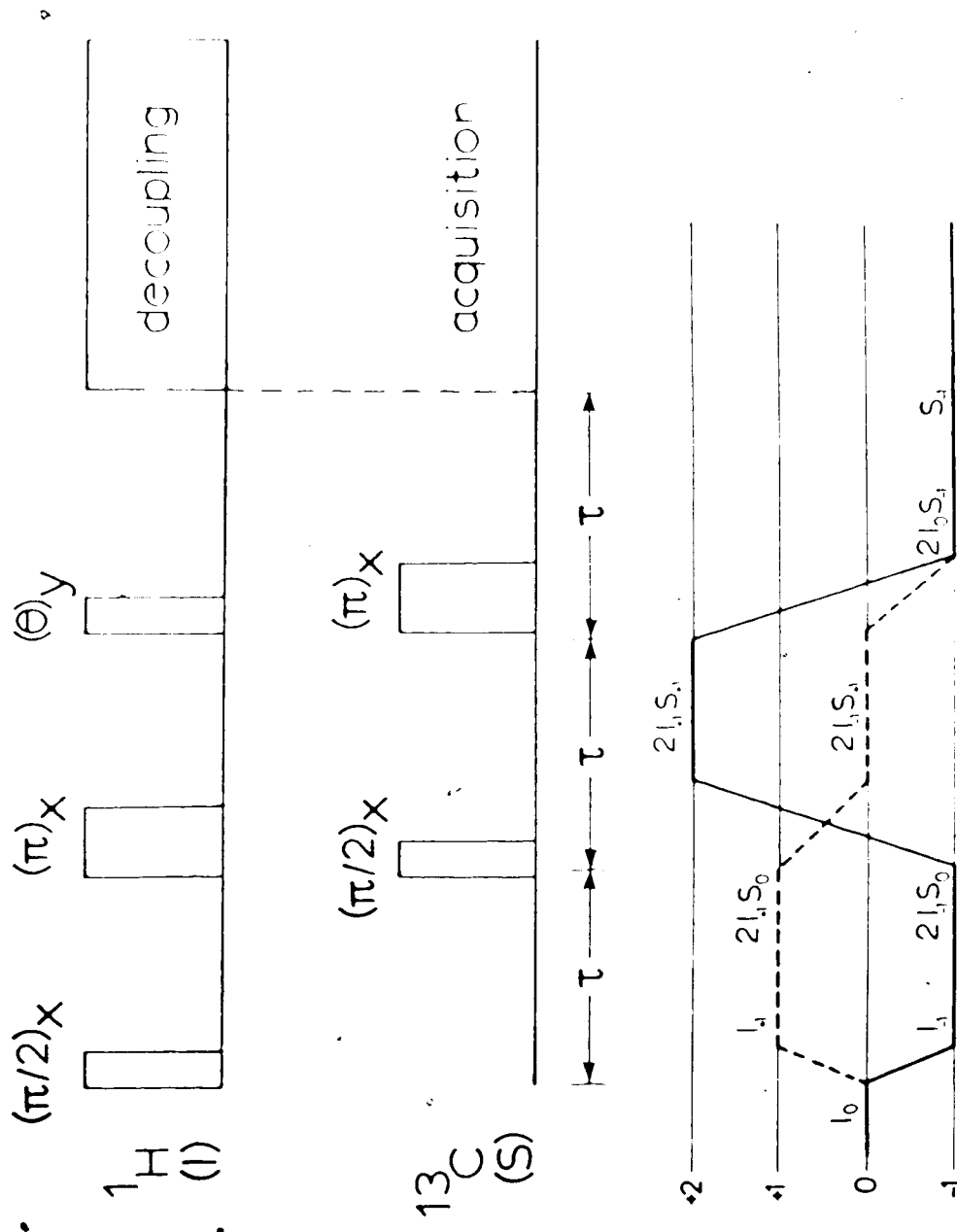


Fig. 2-1 Pulse sequence and coherence transfer pathways for DEPT.

The coherence transfer pathways shown in Fig. 2-1 show clearly how the DEPT magnetization transfer process is related to the evolution of the various terms (product operators) in the density operator. Schematically, we can represent the DEPT sequence with chemical exchange by the operator sequence

$$\begin{array}{cccccccc}
 I_{+1} & \xrightarrow{K_1\tau} & 2I_{+1}S_0 & \xrightarrow{\pi I_x} & (\pi/2)S_x & \xrightarrow{2I_{-1}S_{+1}} & 2I_{-1}S_{+1} & \xrightarrow{K_2\tau} & 2I_{-1}S_{+1} \\
 I_0 & \xrightarrow{(\pi/2)I_x} & \uparrow & & & & & & \downarrow \xrightarrow{\pi S_x} \\
 I_{-1} & \xrightarrow{K_1\tau} & 2I_{-1}S_0 & \xrightarrow{\pi I_x} & (\pi/2)S_x & \xrightarrow{2I_{+1}S_{+1}} & 2I_{+1}S_{+1} & \xrightarrow{K_2\tau} & 2I_{+1}S_{+1} \\
 & & & & & & \xrightarrow{\theta I_y} & 2I_0S_{-1} & \xrightarrow{K_3\tau} & S_{-1} & [2-10]
 \end{array}$$

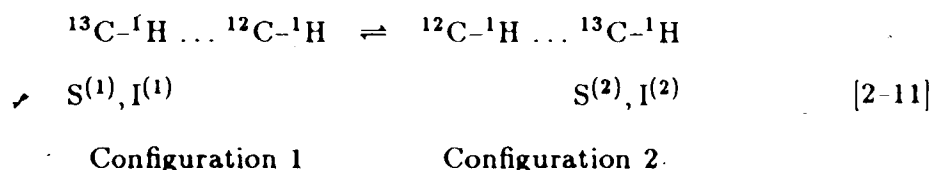
where I_m is the m -th spherical tensor component of the total proton spin angular momentum operator, and $S_{m'}$ is the m' -th spherical tensor component of the carbon spin angular momentum operator. The evolution operators $K_1\tau$, $K_2\tau$ and $K_3\tau$ represent the evolution of the spin system under chemical shift, spin-spin coupling and chemical exchange for each of the periods of free evolution (see Eq. [2-6]) in the DEPT sequence which have duration τ . The labels 1, 2 and 3 on K are used to identify the particular evolutionary period. In the schematic operator sequence [2-10], only the essential product operators involved are shown. It is shown below that other product operators (which are connected to the essential operators by spin-spin coupling) are involved, but in a subsidiary way. The upper operator sequence in [2-10] corresponds to the coherence transfer pathway shown as dashed lines in Fig. 2-1, and the lower operator sequence in [2-10] corresponds to the solid pathway in Fig. 2-1.

The evolution of the terms in the density operator in the presence of chemical exchange is described by Eqs. [2-6]-[2-8] above. In order to determine the ^{13}C signal intensity to be expected in a DEPT experiment, it is necessary to establish the identity of the product operators involved in each τ period, and

to determine the elements of the corresponding \mathbf{K} matrices. Since the product operators involved and the structure of the \mathbf{K} matrices depends on the particular chemical system, we shall consider the $\text{CH}\dots\text{CH}$ and $\text{CH}_3\dots\text{CH}_3$ exchange cases in detail.

2.3.1. $\text{CH}\dots\text{CH}$ Exchange

Consider the intramolecular exchange



The complete set of 16 basis operators required to describe each of the configurations consists of the unit operator, 6 single spin operators and 9 product operators involving two spins. Fortunately, only a subset is required to describe the behaviour of this exchanging spin system during the DEPT magnetization transfer experiment. The basis operators required here are given in Table 2.1 together with their traces, and their commutators with the Hamiltonian

$$\mathcal{H}^{(\ell)} = \omega_I^{(\ell)} I_x^{(\ell)} + \omega_S^{(\ell)} S_x^{(\ell)} + J^{(\ell)} I_x^{(\ell)} S_x^{(\ell)}, \quad (\ell = 1, 2), \quad [2-12]$$

for the appropriate configuration. In Eq. [2-12], the Hamiltonian has units of s^{-1} , $\omega_I^{(\ell)}$ is the proton resonance frequency, $\omega_S^{(\ell)}$ is the ${}^{13}\text{C}$ frequency and $J^{(\ell)}$ is the ${}^1\text{H}$ - ${}^{13}\text{C}$ spin-spin coupling (in s^{-1}) in configuration ℓ .

The magnetization transfer experiment begins with the system having initial density operator

$$\rho(0) = [H_0 / (4k_B T)] \left\{ \gamma_H (I_0^{(1)} + I_0^{(2)}) + \gamma_C (S_0^{(1)} + S_0^{(2)}) \right\}, \quad [2-13]$$

Table 2.1 Basis Operators, Traces and Commutators for CH Exchange¹

B_r	$\text{Tr}\{B_r^\dagger B_r\}$	$[B_r, \mathcal{H}^{(\ell)}]$
$I_{+1}^{(\ell)}$	C_2	$+\{\omega_I^{(\ell)} I_{+1}^{(\ell)} + (J^{(\ell)}/2) 2I_{+1}^{(\ell)} S_z^{(\ell)}\}^\dagger$
$S_1^{(\ell)}$	C_2	$\{\omega_S^{(\ell)} S_1^{(\ell)} + (J^{(\ell)}/2) 2I_z^{(\ell)} S_1^{(\ell)}\}^\dagger$
$2I_{+1}^{(\ell)} S_z^{(\ell)}$	C_2	$+\{\omega_I^{(\ell)} (2I_{+1}^{(\ell)} S_z^{(\ell)}) + (J^{(\ell)}/2) I_{+1}^{(\ell)}\}^\dagger$
$2I_{+1}^{(\ell)} S_{+1}^{(\ell)}$	C_2	$+\{\omega_I^{(\ell)} + \omega_S^{(\ell)}\} (2I_{+1}^{(\ell)} S_{+1}^{(\ell)})^\dagger$
$2I_z^{(\ell)} S_1^{(\ell)}$	C_2	$-\{\omega_I^{(\ell)} (2I_z^{(\ell)} S_{-1}^{(\ell)}) + (J^{(\ell)}/2) S_1^{(\ell)}\}^\dagger$

¹ $\ell = 1, 2$ for configurations 1 and 2 respectively.

where γ_H and γ_C are the 1H and ^{13}C magnetogyric ratios, H_o is the applied magnetic field, k_B is the Boltzmann constant, and T is the absolute temperature. Since the ^{13}C magnetization is not of interest in the DEPT magnetization transfer experiment, we shall henceforth ignore the second term in Eq. [2-13], and shall drop the factor $\gamma_H H_o / (4k_B T)$ in the first term for clarity. When the $(\pi/2)_z$ 1H pulse is applied, the density operator is transformed to

$$\rho(0^+) = -(i/\sqrt{2})(I_{+1}^{(1)} + I_{+1}^{(2)} + I_{-1}^{(1)} + I_{-1}^{(2)}) . \quad [2-14]$$

The spin system undergoes free precession and chemical exchange for time τ . The evolution of the +1 coherence and the -1 coherence during this interval can be treated independently because no transfers between these coherence levels occur in the absence of rf pulses. Chemical exchange events convert coherences associated with configuration 1 into coherences associated with configuration 2 and vice-versa. Hence the +1 coherence level operators $I_{+1}^{(1)}, I_{+1}^{(2)}$ are connected by chemical exchange, and these operators are connected via spin-spin coupling (see commutators in Table 2.1) to $2I_{+1}^{(1)}S_o^{(1)}$ and $2I_{+1}^{(2)}S_o^{(2)}$. Therefore one need consider only the operators ${}^+1B_1 = I_{+1}^{(1)}$, ${}^+1B_2 = 2I_{+1}^{(1)}S_o^{(1)}$, ${}^+1B_3 = I_{+1}^{(2)}$, and ${}^+1B_4 = 2I_{+1}^{(2)}S_o^{(2)}$ in describing the evolution of the +1 coherence during the first precession period. The coefficients ${}^+1b_1, {}^+1b_2, {}^+1b_3, {}^+1b_4$, associated with these operators in the expansion [2-2], have initial values $b_1(0^+) = b_3(0^+) = -i/\sqrt{2}$, $b_2(0^+) = b_4(0^+) = 0$, and follow Eq. [2-6] with K matrix:

$${}^+1K_1 = \begin{pmatrix} -i\omega_I^{(1)} - k & -iJ^{(1)}/2 & k & 0 \\ -iJ^{(1)}/2 & -i\omega_I^{(1)} - k & 0 & k \\ k & 0 & -i\omega_I^{(2)} - k & -iJ^{(2)}/2 \\ 0 & k & -iJ^{(2)}/2 & -i\omega_I^{(2)} - k \end{pmatrix} . \quad [2-15]$$

The evolution of the -1 coherence can be treated in an exactly analogous fashion and the coefficients corresponding to the product operators $I_{-1}^{(1)}$, $2I_{-1}^{(1)}S_0^{(1)}$, $I_{-1}^{(2)}$, $2I_{-1}^{(2)}S_0^{(2)}$ follow Eq. [2-6] with a \mathbf{K} -matrix which is the complex conjugate of ${}^{+1}\mathbf{K}_1$ in Eq. [2-15]. Solution of the equations of motion (see Eq. [2-8]) yields the values of the coefficients ${}^{\pm 1}b_1(\tau)$, ${}^{\pm 1}b_2(\tau)$, ${}^{\pm 1}b_3(\tau)$, and ${}^{\pm 1}b_4(\tau)$ associated with the $+1$ and -1 coherences at the end of the first τ delay.

At the end of the first precession-exchange period, the system contains I_{+1} and $2I_{+1}S_0$ coherences. The I_{+1} coherences are of no further interest because they are not converted into ${}^{13}\text{C}$ magnetization later in the sequence, and therefore do not lead to any detectable signals. Application of the $(\pi/2)_x$ carbon and $(\pi)_x$ proton pulses converts the $+1$ and -1 coherences into coherences in levels 0, $+2$ and -2 . Since only those coherences associated with product operators containing an $S_{+1}^{(\ell)}$ operator will ultimately reach the detector (see Eq. [2-10] and Fig. 2-1), we shall focus our attention on the zero quantum coherences $2I_{-1}^{(1)}S_{+1}^{(1)}$, $2I_{-1}^{(2)}S_{+1}^{(2)}$, and on the two quantum coherences (coherence level $+2$) $2I_{+1}^{(1)}S_{+1}^{(1)}$, $2I_{+1}^{(2)}S_{+1}^{(2)}$ which are produced from the $2I_{+1}S_0$ and $2I_{-1}S_0$ coherences respectively by the rf pulses.

During the second precession-exchange period, the coefficients 0b_1 and 0b_2 associated with the coherence level 0 product operators ${}^0B_1 = 2I_{-1}^{(1)}S_{+1}^{(1)}$ and ${}^0B_2 = 2I_{-1}^{(2)}S_{+1}^{(2)}$ follow Eq. [2-6] with \mathbf{K} -matrix

$${}^0\mathbf{K}_2 = \begin{pmatrix} -i(\omega_I^{(1)} - \omega_S^{(1)}) - k & k \\ k & -i(\omega_I^{(2)} - \omega_S^{(2)}) - k \end{pmatrix}, \quad [2-16]$$

and have initial values ${}^0b_1(\tau^+) = (i/\sqrt{2}) {}^{+1}b_2(\tau)$, ${}^0b_2(\tau^+) = (i/\sqrt{2}) {}^{+1}b_4(\tau)$. The coefficients ${}^{+2}b_1$ and ${}^{+2}b_2$ associated with the coherence level $+2$ operators ${}^{+2}B_1 = 2I_{+1}^{(1)}S_{+1}^{(1)}$ and ${}^{+2}B_2 = 2I_{+1}^{(2)}S_{+1}^{(2)}$ follow Eq. [2-6] with \mathbf{K} -matrix

$${}^{+2}\mathbf{K}_2 = \begin{pmatrix} -i(\omega_I^{(1)} + \omega_S^{(1)}) - k & k \\ k & -i(\omega_I^{(2)} + \omega_S^{(2)}) - k \end{pmatrix}, \quad [2-17]$$

and have initial values ${}^{+2}b_1(\tau^+) = (i/\sqrt{2})^{-1}b_2(\tau)$, ${}^{+2}b_2(\tau^+) = (i/\sqrt{2})^{-1}b_4(\tau)$. The values of ${}^0b_1(2\tau)$, ${}^0b_2(2\tau)$, ${}^{+2}b_1(2\tau)$, and ${}^{+2}b_2(2\tau)$ are obtained by solution of Eq. [2-6] with **K**-matrices given by Eqs. [2-16] and [2-17].

The $(\theta)_y$ proton and $(\pi)_x$ carbon pulses at time 2τ convert the +2 and 0 coherences into -2, -1, 0, +1 and +2 coherences, but only the -1 coherence is of further interest. The evolution of the -1 coherence during the third precession-exchange period is described by the behaviour of the coefficients ${}^{-1}b_{1'}$, ${}^{-1}b_{2'}$, ${}^{-1}b_{3'}$ and ${}^{-1}b_{4'}$ associated with the operators ${}^{-1}B_{1'} = 2I_0^{(1)}S_{-1}^{(1)}$, ${}^{-1}B_{2'} = S_{-1}^{(1)}$, ${}^{-1}B_{3'} = 2I_0^{(2)}S_{-1}^{(2)}$, and ${}^{-1}B_{4'} = S_{-1}^{(2)}$. These coefficients are governed by Eq. [2-6] with **K**-matrix

$${}^{-1}\mathbf{K}_3 = \begin{pmatrix} i\omega_S^{(1)} - k & iJ^{(1)}/2 & k & 0 \\ iJ^{(1)}/2 & i\omega_S^{(1)} - k & 0 & k \\ k & 0 & i\omega_S^{(2)} - k & iJ^{(2)}/2 \\ 0 & k & iJ^{(2)}/2 & i\omega_S^{(2)} - k \end{pmatrix}, \quad [2-18]$$

with initial conditions ${}^{-1}b_{1'}(2\tau^+) = {}^{-1}b_{3'}(2\tau^+) = 0$, ${}^{-1}b_{2'}(2\tau^+) = \sin\theta[{}^0b_1(2\tau) - {}^{+2}b_1(2\tau)]/\sqrt{2}$, ${}^{-1}b_{4'}(2\tau^+) = \sin\theta[{}^0b_2(2\tau) - {}^{+2}b_2(2\tau)]/\sqrt{2}$. Solution of the equations of motion [2-6] for these coefficients yields ${}^{-1}b_{1'}(3\tau)$, ${}^{-1}b_{2'}(3\tau)$, ${}^{-1}b_{3'}(3\tau)$ and ${}^{-1}b_{4'}(3\tau)$. The intensity, $S_{CH}(3\tau)$, of the ${}^{13}\text{C}$ signal detected (the sum of the intensities of the peaks near $\omega_S^{(1)}$ and $\omega_S^{(2)}$ in the slow exchange limit, or the intensity of the peak at $(\omega_S^{(1)} + \omega_S^{(2)})/2$ in the fast exchange region) is given by

$$S_{CH}(3\tau) = {}^{-1}b_{2'}(3\tau) + {}^{-1}b_{4'}(3\tau). \quad [2-19]$$

Relaxation effects have been omitted in the description of the DEPT CH...CH exchange given above. The inclusion of relaxation in an exact fashion would be rather complicated since relaxation in the first precession period will be

governed by ^1H T_2 's, relaxation in the second τ period by decay of zero and double quantum ^{13}C - ^1H coherences, and relaxation in the third τ period by ^{13}C T_2 's. We therefore propose to include relaxation effects in a phenomenological fashion with the decay rate characterized by an effective relaxation time, $T_{2\text{eff}}$, so that the ^{13}C signal intensities are given by

$$S_{\text{CH}}(3\tau) = [^{-1}b_{2'}(3\tau) + ^{-1}b_{4'}(3\tau)] \exp(-3\tau/T_{2\text{eff}}). \quad [2-20]$$

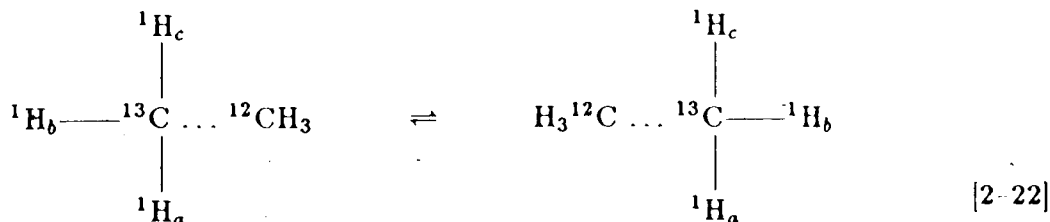
In the slow exchange limit, $k \ll |\Delta\omega_I|, |\Delta\omega_S|, |\Delta\omega_I \pm \Delta\omega_S|$, where $\Delta\omega_I = \omega_I^{(1)} - \omega_I^{(2)}$ and $\Delta\omega_S = \omega_S^{(1)} - \omega_S^{(2)}$. The presence of the term $-k$ in all diagonal elements of the matrices $^{\pm 1}\mathbf{K}_1$, $^{0,2}\mathbf{K}_2$, and $^{-1}\mathbf{K}_3$ implies that $^{-1}b_{2'}(3\tau) + ^{-1}b_{4'}(3\tau)$ is approximately equal to $[^{-1}b_{2'}(3\tau) + ^{-1}b_{4'}(3\tau)]_{\text{no exchange}}$ multiplied by the damping factor $\exp[-3k\tau]$ in the slow exchange limit. Investigation of the DEPT experiment without exchange (47) shows that, *in the slow exchange limit*, the ^{13}C signal intensity is given by

$$S_{\text{CH}}(3\tau) \cong \sin\theta [1 - \cos(2\pi J_{\text{CH}}\tau)] \exp[-3k\tau] \exp[-3\tau/T_{2\text{eff}}]. \quad [2-21]$$

where J_{CH} is the average of $J^{(1)}$ and $J^{(2)}$.

2.3.2 CH₃...CH₃ Exchange

For the intramolecular exchange



$S^{(1)}, I_a^{(1)}, I_b^{(1)}, I_c^{(1)}$

Configuration 1

$S^{(2)}, I_a^{(2)}, I_b^{(2)}, I_c^{(2)}$

Configuration 2

a complete description of the density operator could require up to 511 basis functions. The subset of basis product operators required to describe the behaviour of the exchanging system during the DEPT sequence is given in Table 2.2 together with the traces of these operators and their commutators with the Hamiltonian

$$\mathcal{H}^{(\ell)} = \omega_I^{(\ell)} (I)_0^{(\ell)} + \omega_S^{(\ell)} S_z^{(\ell)} + J^{(\ell)} (I)_0^{(\ell)} S_z^{(\ell)} \quad [2-23]$$

for the appropriate configuration. In Eq. [2-23], and in Table 2.2, the linear combinations of product operators defined by

$$\begin{aligned}
 \text{(I)}_m^{(\ell)} &= I_{ma}^{(\ell)} + I_{mb}^{(\ell)} + I_{mc}^{(\ell)}, \quad m = +1, 0, -1 \\
 \text{(II)}_0^{(\ell)} &= I_{0a}^{(\ell)} I_{0b}^{(\ell)} + I_{0b}^{(\ell)} I_{0c}^{(\ell)} + I_{0c}^{(\ell)} I_{0a}^{(\ell)}, \\
 \text{(II)}_{\pm 1}^{(\ell)} &= I_{\pm 1a}^{(\ell)} (I_{0b}^{(\ell)} + I_{0c}^{(\ell)}) + I_{\pm 1b}^{(\ell)} (I_{0a}^{(\ell)} + I_{0c}^{(\ell)}) + I_{\pm 1c}^{(\ell)} (I_{0a}^{(\ell)} + I_{0b}^{(\ell)}), \quad [2-24] \\
 \text{(III)}_0^{(\ell)} &= I_{0a}^{(\ell)} I_{0b}^{(\ell)} I_{0c}^{(\ell)}, \\
 \text{(III)}_{\pm 1}^{(\ell)} &= I_{\pm 1a}^{(\ell)} I_{0b}^{(\ell)} I_{0c}^{(\ell)} + I_{0a}^{(\ell)} I_{\pm 1b}^{(\ell)} I_{0c}^{(\ell)} + I_{0a}^{(\ell)} I_{0b}^{(\ell)} I_{\pm 1c}^{(\ell)},
 \end{aligned}$$

are employed to facilitate a compact formulation of the exchange and magnetization transfer processes.

Table 2.2 Basis Operators, Traces and Commutators for CH₃ Exchange¹

B_r	$\text{Tr}\{B_r^\dagger B_r\}$	$[B_r, \mathcal{H}^{(t)}]$
${}^{+1}B_1 = (I)_{\pm 1}^{(1)}$	$3C_4$	$\pm \{\omega_1^{(1)} {}^{+1}B_1 + (J^{(1)}/2) {}^{+1}B_2\}^\dagger$
${}^{+1}B_2 = 2(I)_{\pm 1}^{(1)} S_0^{(1)}$	$3C_4$	$\pm \{\omega_1^{(1)} {}^{+1}B_2 + (J^{(1)}/2) {}^{+1}B_1\}^\dagger$
${}^{1+1}B_1 = 2(I)_{\pm 1}^{(1)} S_{\pm 1}^{(1)}$	$3C_4$	$\pm \{(\omega_1^{(1)} \pm \omega_S^{(1)}) {}^{1+1}B_1 + (J^{(1)}/2) {}^{1+1}B_2\}^\dagger$
${}^{1+1}B_2 = 4(II)_{\pm 1}^{(1)} S_{\pm 1}^{(1)}$	$6C_4$	$\pm \{(\omega_1^{(1)} \pm \omega_S^{(1)}) {}^{1+1}B_2 \pm (J^{(1)}/2) ({}^{1+1}B_1 + {}^{1+1}B_3)\}^\dagger$
${}^{1+1}B_3 = 8(III)_{\pm 1}^{(1)} S_{\pm 1}^{(1)}$	$3C_4$	$\pm \{(\omega_1^{(1)} \pm \omega_S^{(1)}) {}^{1+1}B_3 \pm (J^{(1)}/2) {}^{1+1}B_2\}^\dagger$
${}^{-1}B_{1'} = S_{-1}^{(1)}$	C_4	$\pm \{ -\omega_S^{(1)} {}^{-1}B_{1'} - (J^{(1)}/2) {}^{-1}B_{2'}\}^\dagger$
${}^{-1}B_{2'} = 2(I)_0^{(1)} S_1^{(1)}$	$3C_4$	$\{ -\omega_S^{(1)} {}^{-1}B_{2'} - (3J^{(1)}/2) {}^{-1}B_{1'} - J^{(1)} {}^{-1}B_{3'}\}^\dagger$
${}^{-1}B_{3'} = 4(II)_0^{(1)} S_{-1}^{(1)}$	$3C_4$	$\{ -\omega_S^{(1)} {}^{-1}B_{3'} - J^{(1)} {}^{-1}B_{2'} - (3J^{(1)}/2) {}^{-1}B_{3'}\}^\dagger$
${}^{-1}B_{4'} = 8(III)_0^{(1)} S_{-1}^{(1)}$	C_4	$\{ -\omega_S^{(1)} {}^{-1}B_{4'} - (J^{(1)}/2) {}^{-1}B_{3'}\}^\dagger$

¹ Operators for configuration 1 only are given. The operators ${}^{\pm 1}B_{3,4}$, ${}^{1\pm 1}B_{4,5,6}$ and ${}^{-1}B_{5',6',7',8'}$ are obtained from the respective operators ${}^{\pm 1}B_{1,2}$, ${}^{1\pm 1}B_{1,2,3}$ and ${}^{-1}B_{1',2',3',4'}$ by using spin operators for configuration 2 in place of the configuration 1 spin operators.

The analysis of the CH₃ exchange problem follows exactly the analysis of the CH exchange case given in section 2.3.1 above. The behaviour of the CH₃ system is formally identical to that of the CH case up to time τ^+ , where the terms of interest in the density operator are

$$\rho(\tau^+) = (i/\sqrt{2}) \left\{ \begin{aligned} &+^1 b_2(\tau) [2(I)_{+1}^{(1)} S_{+1}^{(1)}] + +^1 b_4(\tau) [2(I)_{+1}^{(2)} S_{+1}^{(2)}] \\ &+ -^1 b_2(\tau) [2(I)_{-1}^{(1)} S_{-1}^{(1)}] + -^1 b_4(\tau) [2(I)_{-1}^{(2)} S_{+1}^{(2)}] \end{aligned} \right\} \quad [2-25]$$

During the second precession-exchange interval, the coefficients ${}^0 b_1, {}^0 b_2, \dots, {}^0 b_6$ associated with the zero quantum coherences ${}^0 B_1, {}^0 B_2, \dots, {}^0 B_6$ are governed by Eq. [2-6] with K-matrix given by

$${}^0 \mathbf{K}_2 = \begin{pmatrix} A_0^{(1)} & -iJ^{(1)} & 0 & k & 0 & 0 \\ -iJ^{(1)}/2 & A_0^{(1)} & -iJ^{(1)}/2 & 0 & k & 0 \\ 0 & -iJ^{(1)} & A_0^{(1)} & 0 & 0 & k \\ k & 0 & 0 & A_0^{(2)} & -iJ^{(2)} & 0 \\ 0 & k & 0 & -iJ^{(2)}/2 & A_0^{(2)} & -iJ^{(2)}/2 \\ 0 & 0 & k & 0 & -iJ^{(2)} & A_0^{(2)} \end{pmatrix} \quad (A_0^{(\ell)} = i(\omega_I^{(\ell)} - \omega_S^{(\ell)}) - k) \quad [2-26]$$

with initial conditions

$$\begin{aligned} {}^0 b_1(\tau^+) &= -^1 b_2(\tau) , \\ {}^0 b_4(\tau^+) &= -^1 b_4(\tau) , \\ {}^0 b_2(\tau^+) &= {}^0 b_3(\tau^+) = {}^0 b_5(\tau^+) = {}^0 b_6(\tau^+) = 0 . \end{aligned} \quad [2-27]$$

The coefficients ${}^2 b_1, {}^2 b_2, \dots, {}^2 b_6$ associated with +2 coherence level operators ${}^2 B_1,$

${}^2B_2, \dots, {}^2B_6$ (See Table 2.2) follow the equation of motion [2-6] with \mathbf{K} -matrix:

$${}^{+2}\mathbf{K}_2 = \begin{pmatrix} A_2^{(1)} & -iJ^{(1)} & 0 & k & 0 & 0 \\ -iJ^{(1)}/2 & A_2^{(1)} & -iJ^{(1)}/2 & 0 & k & 0 \\ 0 & -iJ^{(1)} & A_2^{(1)} & 0 & 0 & k \\ k & 0 & 0 & A_2^{(2)} & -iJ^{(2)} & 0 \\ 0 & k & 0 & -iJ^{(2)}/2 & A_2^{(2)} & -iJ^{(2)}/2 \\ 0 & 0 & k & 0 & -iJ^{(2)} & A_2^{(2)} \end{pmatrix},$$

$$(A_2^{(\ell)} = -i(\omega_1^{(\ell)} + \omega_S^{(\ell)}) - k) \quad [2-28]$$

and have initial values

$$\begin{aligned} {}^2b_1(\tau^+) &= {}^{+1}b_2(\tau), \\ {}^2b_4(\tau^+) &= {}^{+1}b_4(\tau), \\ {}^2b_2(\tau^+) &= {}^2b_3(\tau^+) = {}^2b_5(\tau^+) = {}^2b_6(\tau^+) = 0. \end{aligned} \quad [2-29]$$

The values of ${}^0b_\alpha(2\tau)$ and ${}^2b_\alpha(2\tau)$ ($\alpha = 1, 2, \dots, 6$) are obtained by solution of Eq. [2-6] with \mathbf{K} matrices given by Eqs. [2-26] and [2-28].

Following the $(\theta)_y$ proton and $(\pi)_z$ carbon pulses, the coherences of interest are associated with operators ${}^{-1}B_\alpha$ ($\alpha = 1', 2', \dots, 8'$) and the corresponding coefficients have values

$$\begin{aligned} {}^{-1}b_{1'}(2\tau^+) &= {}^{-1}b_{5'}(2\tau^+) = 0, \\ {}^{-1}b_{2'}(2\tau^+) &= (1/\sqrt{2})\{{}^0b_1(2\tau) - {}^2b_1(2\tau)\} \sin \theta, \\ {}^{-1}b_{3'}(2\tau^+) &= \sqrt{2}\{{}^0b_2(2\tau) - {}^2b_2(2\tau)\} \sin \theta \cos \theta, \\ {}^{-1}b_{4'}(2\tau^+) &= (3/\sqrt{2})\{{}^0b_3(2\tau) - {}^2b_3(2\tau)\} \sin \theta \cos^2 \theta, \\ {}^{-1}b_{6'}(2\tau^+) &= (1/\sqrt{2})\{{}^0b_4(2\tau) - {}^2b_4(2\tau)\} \sin \theta, \\ {}^{-1}b_{7'}(2\tau^+) &= \sqrt{2}\{{}^0b_5(2\tau) - {}^2b_5(2\tau)\} \sin \theta \cos \theta, \\ {}^{-1}b_{8'}(2\tau^+) &= (3/\sqrt{2})\{{}^0b_6(2\tau) - {}^2b_6(2\tau)\} \sin \theta \cos^2 \theta. \end{aligned} \quad [2-30]$$

During the third τ interval, these coefficients follow Eq. [2-6] with \mathbf{K} -matrix:

$${}^0\mathbf{K}_2 = \begin{pmatrix} A^{(1)} & 3iJ^{(1)}/2 & 0 & 0 & k & 0 & 0 & 0 \\ iJ^{(1)}/2 & A^{(1)} & iJ^{(1)} & 0 & 0 & k & 0 & 0 \\ 0 & iJ^{(1)} & A^{(1)} & iJ^{(1)}/2 & 0 & 0 & k & 0 \\ 0 & 0 & 3iJ^{(1)}/2 & A^{(1)} & 0 & 0 & 0 & k \\ k & 0 & 0 & 0 & A^{(2)} & 3iJ^{(2)}/2 & 0 & 0 \\ 0 & k & 0 & 0 & iJ^{(2)}/2 & A^{(2)} & iJ^{(2)} & 0 \\ 0 & 0 & k & 0 & 0 & iJ^{(2)} & A^{(2)} & iJ^{(2)}/2 \\ 0 & 0 & 0 & k & 0 & 0 & 3iJ^{(2)}/2 & A^{(2)} \end{pmatrix} \quad (A^{(\ell)} = i\omega_S^{(\ell)} - k) \quad [2-31]$$

Solution of the equation of motion [2-6] yields the values of ${}^{-1}b_\alpha(3\tau)$ ($\alpha = 1', \dots, 8'$), and the intensity $S_{\text{CH}_3}(3\tau)$, of the ^{13}C signal detected (the sum of the intensities of the peaks near $\omega_S^{(1)}$ and $\omega_S^{(2)}$ in the slow exchange limit, or the intensity of the peak at $(\omega_S^{(1)} + \omega_S^{(2)})/2$ in the fast exchange region) is

$$S_{\text{CH}_3}(3\tau) = {}^{-1}b_1(3\tau) + {}^{-1}b_5(3\tau) \quad [2-32]$$

Relaxation effects have not been included in the analysis of the $\text{CH}_3 \dots \text{CH}_3$ exchange given above. As in the $\text{CH} \dots \text{CH}$ exchange case, we introduce an effective relaxation time, $T_{2\text{eff}}$, so that

$$S_{\text{CH}_3}(3\tau) = [{}^{-1}b_1(3\tau) + {}^{-1}b_5(3\tau)] \exp(-3\tau/T_{2\text{eff}}) \quad [2-33]$$

In the slow exchange limit, the presence of $-k$ in each of the diagonal elements in the matrices ${}^{\pm 1}\mathbf{K}_1$, ${}^{0,2}\mathbf{K}_2$, and ${}^{-1}\mathbf{K}_3$, implies that ${}^{-1}b_1(3\tau) + {}^{-1}b_5(3\tau)$ is approximately equal to $[{}^{-1}b_1(3\tau) + {}^{-1}b_5(3\tau)]_{\text{noexchange}}$ multiplied by the damping factor $\exp[-3k\tau]$. Investigation of the no exchange case (47) shows that, in the

slow exchange limit, the ^{13}C signal intensity is given by

$$\begin{aligned}
 S_{\text{CH}_3}(3\tau) \cong & \{ [18 \sin \theta + 6 \sin(2\theta) + 10 \sin(3\theta)] \\
 & - [11 \sin \theta + 4 \sin(2\theta) + 15 \sin(3\theta)] \cos(2\pi J_{\text{CH}}\tau) \\
 & - [2 \sin \theta + 8 \sin(2\theta) - 6 \sin(3\theta)] \cos(4\pi J_{\text{CH}}\tau) \\
 & - [5 \sin \theta - 4 \sin(2\theta) + \sin(3\theta)] \cos(6\pi J_{\text{CH}}\tau) \} \\
 & \times \exp[-3k\tau] \exp[-3\tau/T_{2\text{eff}}] ,
 \end{aligned} \tag{2-34}$$

where $2J_{\text{CH}}$ is the average of $J^{(1)}$ and $J^{(2)}$.

2.4 Experimental

^{13}C (50.3 MHz) and ^1H (200.0 MHz) NMR spectra were recorded on a Bruker WH-200 spectrometer. Samples of 50% (v/v) N-acetylpyrrole in CD_2Cl_2 ($\text{CH}\dots\text{CH}$ exchange case) and 80% (v/v) N,N-dimethylacetamide in $\text{DMSO}-d_6$ ($\text{CH}_3\dots\text{CH}_3$ exchange case) were prepared in 5 mm tubes, degassed and sealed under vacuum. N acetylpyrrole was prepared according to the procedure given by Reddy (73) and purified by distillation under reduced pressure. Dimethylacetamide (Eastman-Kodak) was purified by distillation prior to use.

DEPT magnetization transfer experiments using the pulse sequence shown in Fig. 2-1 were performed on N-acetylpyrrole from 213 to 307 K, and on dimethylacetamide between 300 and 353 K. Temperatures were measured using a copper-constantan thermocouple inserted into a 5 mm tube containing CH_2Cl_2 or DMSO. At each temperature, the ^{13}C fid's from DEPT transfer experiments with τ values in the range 0.4 to 12.4 ms were collected. The proton $(\theta)_y$ pulses (see Fig. 2-1) had flip angles of 90° for N-acetylpyrrole and 36° for dimethylacetamide. All fid's were transformed using a Lorentzian linebroadening of 3 Hz, and spectra were normalized with respect to the lowest temperature spectrum with $\tau = 1.9$ ms. ^{13}C - ^1H coupling constants were determined from DEPT experiments without proton decoupling during acquisition at the lowest temperatures studied.

Proton spectra for N-acetylpyrrole were measured at the temperatures at which the DEPT experiments were performed, and the rate constants for the exchange process were determined from lineshape analysis of these spectra (3).

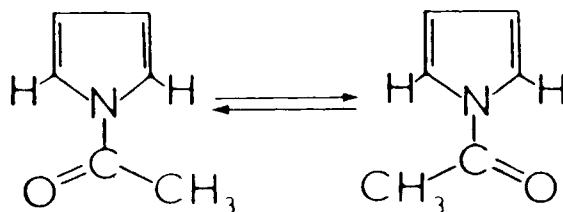
2.5 Results

The behavior of the various terms in the density operator during a DEPT magnetization transfer experiment on a system undergoing chemical exchange has

been described in detail in the previous sections of this chapter. The experimental verification of the theoretical predictions for CH...CH exchange and CH₃...CH₃ exchange cases is presented below, followed by a discussion of the general applicability of the DEPT method in the measurement of rate constants for exchange processes.

2.5.1 CH...CH Exchange

The hindered internal rotation about the C-N bond in N-acetylpyrrole:



provides a suitable example of CH...CH exchange since the 2 and 5 positions on the pyrrole ring are interchanged by the exchange process. Although the protons at positions 2 and 5 on the pyrrole ring are coupled to the protons at positions 3 and 4, the couplings are small enough that their effects are not significant over the time intervals involved in the DEPT magnetization transfer experiments. The variation of the C-2 and C-5 ¹³C signal intensities with the duration of the τ -delays in DEPT experiments on N-acetylpyrrole is shown in Fig. 2-2 along with the ¹³C spectra obtained from the DEPT experiments with $\tau = 2.9$ ms. The variation of the ¹³C intensities with τ has a damped periodic time dependence, with the degree of damping being strongly dependent on the exchange rate. At the lowest temperature, where exchange is very slow, the periodic signal is not significantly damped. As the exchange rate increases, the ¹³C signal intensity decreases and the periodic τ -dependence is increasingly damped, so that near coalescence of the ¹³C

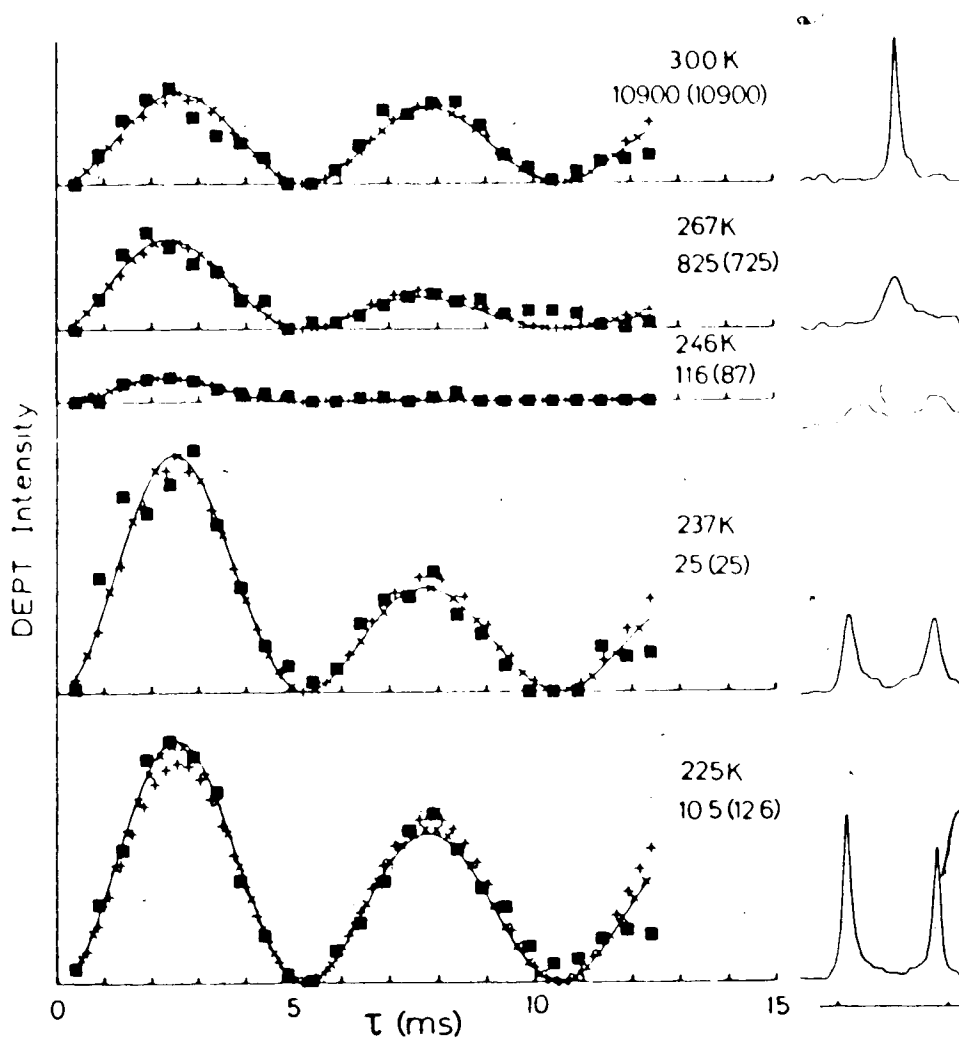


Fig. 2-2 Comparison of observed and calculated DEPT intensities, of 2 and 5 C-H fragments of N-acetylpyrrole, and the corresponding ^{13}C spectra for $\tau = 2.9$ ms. Values of k (in s^{-1}) from ^1H lineshape measurements and best fit values (in parenthesis) are given at each temperature. ■ - observed intensities, + - intensities calculated from Eq. [2-19] with k from lineshape measurement, \times - intensities calculated from Eq. [2-20] with k from lineshape measurement and $T_{2\text{eff}} = 0.10$ s, — - intensities calculated from Eq. [2-20] with best fit k and $T_{2\text{eff}} = 0.10$ s. Marks on horizontal axis under spectra are 100 Hz apart.

spectrum (between 246 K and 267 K) the signal is very weak. After coalescence, the intensity of the signal increases and the damping of the periodic τ -dependence decreases so that significant intensities at large τ are again observed in the case of fast exchange (300 K).

In order to compare the observed τ -dependence of the ^{13}C signal intensities in N-acetylpyrrole with that predicted by the theory presented in the previous section, the rate constant, k , was determined at each temperature by fitting the lineshape of the ^1H NMR spectrum in the conventional manner (3). The rate constants obtained compare favorably to literature values (51-53). The carbon-proton coupling constant, $^1J_{\text{CH}}$, and the chemical shift differences, $\Delta\omega_{\text{H}}$ and $\Delta\omega_{\text{C}}$, were obtained from ^1H and ^{13}C spectra at 213 K, and have values $^1J_{\text{CH}} = 190$. Hz (average for 2 and 5 positions), $\Delta\omega_{\text{H}}/2\pi = 78$. Hz and $\Delta\omega_{\text{C}}/2\pi = 90$. Hz. The observed intensities are compared in Fig. 2-2 with the intensities calculated using Eq. [2-20]. The calculated intensities were multiplied by the factor $\sum_i (S_i^{\text{obs}} S_i^{\text{calc}}) / \sum_i (S_i^{\text{calc}})^2$ in order to facilitate comparison of observed and calculated results. (S^{obs} and S^{calc} are the observed and calculated intensities for the i th value of τ , and the sum over i includes all τ values at which measurements were made). The intensities calculated from Eq. [2-20] with $T_{2\text{eff}} = \infty$ (no relaxation) and the values of k determined from the lineshape analysis of the proton spectra are shown for each temperature. The intensities calculated assuming no relaxation agree very well with the observed intensities except at the lowest and highest temperatures studied. In order to investigate the importance of relaxation effects on the results, we estimated $T_{2\text{eff}}$ to be 0.10 s from the τ -dependence of the exchange-narrowed resonance for C-3, C-4 in the DEPT experiments on N-acetylpyrrole at 300 K. The intensities calculated from Eq. [2-20] with $T_{2\text{eff}} = 0.10$ s are shown, in Fig. 2-2, to agree more closely with the observed data than those calculated assuming

$T_{2\text{eff}} = \infty$, particularly at the extremes of the temperature range where exchange effects and relaxation effects are of comparable magnitude.

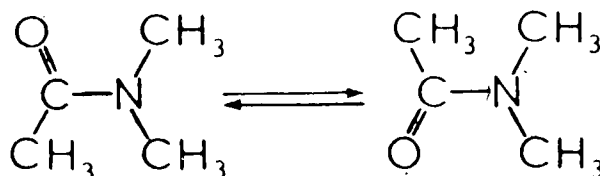
It is useful to study the sensitivity of the calculated intensities to the value of the rate constant k for the exchange process in order to assess the utility of DEPT experiments in the measurement of exchange rates. We have therefore varied k at each temperature (keeping $T_{2\text{eff}}$ fixed at 0.10s) and found the values of k which give best fits of the experimental data. The best fit lines and the corresponding values of k are given in Fig. 2-2. It is clear that the intensities calculated using the values of k obtained from the proton NMR lineshapes closely resemble the best fit intensities. The differences between the values of k from the lineshape analysis, and the values from fitting the τ -dependent DEPT intensities to Eq. [2-20] reflect the sensitivity of the DEPT intensities to changes in k . In the very slow and very fast exchange limits, where relaxation effects are as important as exchange effects, the fitting of the DEPT intensities yields values of k with estimated errors of 20-30%. When the exchange rate lies between these extremes, the τ -dependent DEPT intensities are more sensitive to the exchange rate, and the values of k obtained by fitting the DEPT intensities are expected to have uncertainties of 5-15%.

It has been shown above that the τ -dependence of the ^{13}C intensities in the DEPT experiment is expected to follow the simple form of Eq. [2-21] when exchange is very slow. We have attempted, unsuccessfully, to fit the data for N-acetylpyrrole at 225 and 237 K to this form using standard least squares procedures (74) in the expectation that this procedure might provide an easy practical way to determine k in the slow exchange region. In the fits, the predicted oscillatory behaviour was not identical with the observed data. The reason that the observed data do not follow the simple functional form of Eq. [2-21] is that $|\Delta\omega_{\text{H}} - \Delta\omega_{\text{C}}| \sim$

75 s^{-1} so that, even at 225 K where $k \sim 10.5 \text{ s}^{-1}$, the N-acetylpyrrole exchange is not in the very slow exchange region. When $|\Delta\omega_{\text{H}} - \Delta\omega_{\text{C}}| \gg k$, the calculated DEPT intensities are found to follow Eq. [2-21] exactly, so the simple fitting procedure may be useful in other cases.

2.5.2 $\text{CH}_3 \dots \text{CH}_3$ Exchange

The hindered rotation about the C-N bond in N,N-dimethylacetamide (DMA):



provides a good example of $\text{CH}_3 \dots \text{CH}_3$ exchange. DMA has been studied extensively by several workers (11,49,50) who used mainly conventional ^1H NMR lineshape analysis to determine the rate constant for the exchange process. The variation of the intensities of the N-methyl ^{13}C signals with the duration of the τ -delays in DEPT experiments on DMA is shown in Fig. 2-3. The accessible temperature range (300–353 K) permitted the study of the slow exchange region only. The observed intensities show the damped periodic dependence on τ as expected, with the degree of damping increasing with increasing temperature. The ^{13}C signal intensities of DMA calculated with Eq. [2-33] are compared with the observed data in Fig. 2-3. The carbon-proton coupling constant, $^1J_{\text{CH}} = 136. \text{ Hz}$ (average for N- CH_3 groups), and the chemical shift differences, $\Delta\omega_{\text{H}}/2\pi = 35.0 \text{ Hz}$, and $\Delta\omega_{\text{C}}/2\pi = 156. \text{ Hz}$, were obtained from the proton and carbon NMR spectra at 300 K. Since the investigation of the $\text{CH} \dots \text{CH}$ exchange showed that relaxation

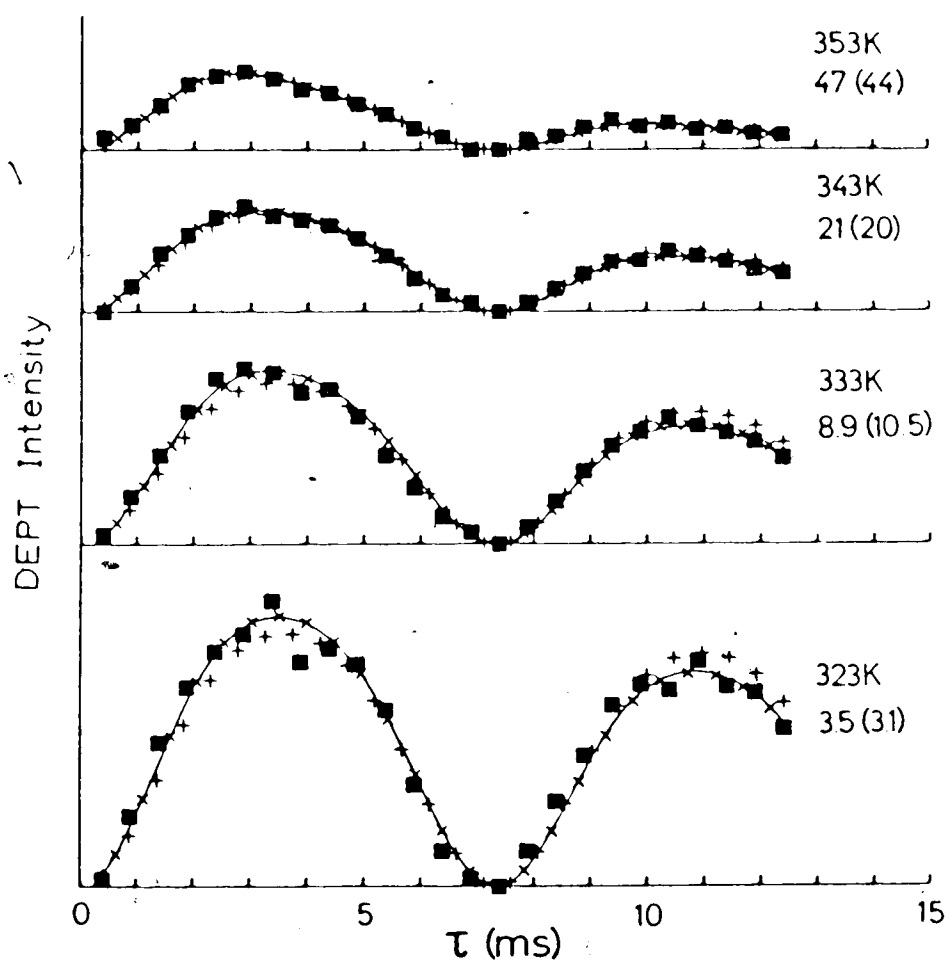


Fig. 2-3 Comparison of observed and calculated DEPT intensities of $\overset{\circ}{\text{C}}\text{-CH}_3$ fragments of N,N-dimethylacetamide. Literature values of k (in s^{-1}) from ref. (50) and best fit values (in parenthesis) are given at each temperature. ■ - observed intensities, + - intensities calculated from Eq. [2-32] with k from literature, × - intensities calculated from Eq. [2-33] with k from literature and $T_{2\text{eff}} = 0.14 \text{ s}$, — - intensities calculated from Eq. [2-33] with best fit k and $T_{2\text{eff}} = 0.14 \text{ s}$.

effects are important when exchange is very slow, we estimated $T_{2\text{eff}}$ for the N-CH₃ groups to be 0.14 s by fitting the C-CH₃ intensities from the DEPT experiments on DMA at 323, 333 and 343 K to Eq. [2-34] with $\theta = 36^\circ$ and $k = 0$.

The data in Fig. 2-3 show that the DEPT intensities vary with the exchange rate. As in our study of CH...CH exchange, we have investigated the utility of DEPT measurements in the measurement of the exchange rate constant. k was varied at each temperature, with $T_{2\text{eff}}$ fixed at 0.14 s, and the values of k which gave the best fits of the experimental data were determined. The best fit lines and the corresponding values of k are given in Fig. 2-3. The intensities calculated with the values of k taken from studies of neat DMA-*d*₃ liquid (49,50) closely resemble the intensities calculated with the best fit values of k . The difference between the best fit values of k and the literature values reflect the sensitivity of the observed intensities to the value of k , and indicate that the exchange rate constant can be determined with a precision of 10-15% in the slow to moderate exchange region accessible to study with DMA.

In the range of temperatures studied, the CH₃...CH₃ exchange in DMA is in the slow exchange limit ($k \ll \Delta\omega_H, \Delta\omega_H + \Delta\omega_C, \Delta\omega_H - \Delta\omega_C, \Delta\omega_C$), and one might expect the DEPT intensities to follow Eq. [2-34]. We have therefore attempted to fit the DMA data to Eq. [2-34] using standard least squares procedures (74). The fits were much better than the corresponding fits in the acetylpyrrole case described above because k is small enough that the necessary inequalities are satisfied. We found that the values of k obtained by fitting the experimental data to Eq. [2-34] were equal, within the uncertainties given by the least squares procedure, to the literature values.

2.6 Summary

A theoretical description of the effects of chemical exchange in magnetic resonance experiments has been developed using product operators. The description of the DEPT magnetization transfer experiment on exchanging CH...CH and CH₃...CH₃ systems was developed in detail to demonstrate the application of the product operator description to experiments employing complicated pulse sequences. We have included relaxation effects in an *ad hoc* fashion by simply appending an $\exp[-3\tau/T_{2\text{eff}}]$ factor to the intensities in Eqs. [2-20] and [2-33].

We have shown that the ¹³C intensities from DEPT magnetization transfer experiments on N-acetylpyrrole and on N,N-dimethylacetamide are influenced by the rate of chemical exchange, and that the observed variations in intensity with the duration of the τ -delays agree quantitatively with the theoretical predictions. In the region of intermediate exchange (from the onset of significant exchange broadening, through coalescence, to exchange narrowing) the comparison of observed and calculated DEPT intensities affords the determination of the exchange rate to within 5-15%. Near the coalescence temperature, the DEPT magnetization transfer approach is expected to give a more precise determination of the exchange rate than the conventional lineshape fitting procedure because reliable peak intensities and integrals from DEPT experiments are more easily obtained than precise visual fitting of broad signals with low signal-to-noise. In the limits of very slow and very fast exchange, the τ -dependence of the DEPT intensities, like the NMR lineshape, is relatively insensitive to the exchange rate, and relaxation effects contribute significantly to the damping of the periodic τ -dependence of the intensities. In the region of intermediate exchange rates, relaxation effects are of negligible importance. We believe that the use of DEPT in the study of exchange processes may prove a useful adjunct to conventional lineshape analysis.

In section 2.5, we have investigated the utility of the approximate forms given in Eq. [2-21] for CH...CH exchange, and in Eq. [2-34] for CH₃...CH₃ exchange in the analysis of DEPT data for the slow exchange region. Provided that $k \ll \Delta\omega_H, \Delta\omega_C, \Delta\omega_H + \Delta\omega_C, |\Delta\omega_H - \Delta\omega_C|$, the observed and calculated intensities are well-described by the simpler forms. The analysis of the τ -dependence of the DEPT intensities by least squares fitting to these approximate forms provides a facile and precise method for determining exchange rates. In the theory section 2.3, the description of CH₂...CH₂ exchange was not discussed. It is useful however to point out here that the DEPT intensities for CH₂...CH₂ exchange are expected to be proportional to

$$\{2 \sin \beta [1 - \cos(4\pi J_{CH}\tau)] + \sin(2\beta) [3 - 2 \cos(2\pi J_{CH}\tau) + \cos(4\pi J_{CH}\tau)]\} \exp(-3k\tau)$$

when the final proton pulse has flip angle β .

CHAPTER 3

Development of Multisite Magnetization Transfer Experiments and Method of Data Analysis

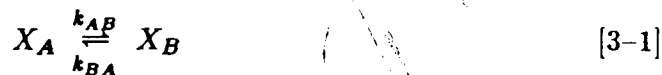
3.1 Introduction

Classical lineshape analysis is the most extensively used technique to determine exchange lifetimes or rate constants from NMR spectra (1,3). However, it is difficult to extend this technique to lifetimes longer than approximately one second due to the problem of insensitivity of the line shape to the exchange rate in very slow exchange situations (56). The lineshape method is inconvenient and sometimes practically impossible to apply successfully in complex exchange situations involving many exchange sites with several different mechanisms responsible for exchange behaviour. With the innovation of the homonuclear double resonance technique, Forsen and Hoffmann developed a simple dynamic method (55-57) for the study of nuclear exchange rates especially suitable for the determination of long exchange lifetimes. This multiple resonance method is similar to the non-equilibrium magnetization transfer method of McConnell and Thompson (75) and can be extended to delineate exchange mechanisms in complex systems. A non-equilibrium magnetization is first introduced selectively at one of the exchanging sites and rate constants and mechanisms are deduced by observing the transfer of this non-equilibrium magnetization to other exchanging sites. Selective perturbation can be achieved by applying a saturating rf field (55-57) or by selective pulses (58). A selective 180° pulse or a selective inversion gives the maximum perturbation and hence a larger dynamic range and better results (58-62). In this

chapter, the basic principles of magnetization transfer experiments are discussed using a simple two site chemical exchange problem. The modified Bloch equation description of this two site problem will be followed by a brief discussion of Forsen-Hoffmann saturation transfer experiments. Application of the selective inversion method in delineation of exchange mechanisms will be illustrated using the two site exchange case. The general N -site chemical exchange problem, involving different exchange mechanisms will then be developed, and the least squares method of data analysis used to obtain the values of the rate constants and estimates of the errors in the rate constants from experimental measurements is described in detail.

3.2 Basic concepts of magnetization transfer experiments

First consider a nucleus X which can reside in either of two nonequivalent magnetic environments; Site A and Site B , with resonance frequencies ν_A and ν_B respectively, which are connected by the exchange reaction



where,

k_{AB} is the rate constant for transfer of X spins from Site A to Site B ,

k_{BA} is the rate constant for transfer of spins from Site B to Site A .

The exchange of X nuclei between Sites A and B is described by,

$$\frac{d}{dt}[X_A] = -k_{AB}[X_A] + k_{BA}[X_B] \quad [3-2]$$

$$\frac{d}{dt}[X_B] = k_{AB}[X_A] - k_{BA}[X_B] \quad [3-3]$$

where $[X_l]$ denotes the concentration of X nuclei at site l ($l = A, B$). It is clear that any perturbation in the population at one site, would be detectable at the other

because of the exchange process. This is the basic idea behind all magnetization transfer experiments (56). In magnetization transfer experiments, one always perturbs the z - or longitudinal magnetization at one of the sites, and monitors the steady state or temporal response of the z -magnetization of one or both of the sites depending on the experimental procedure. In the experimental method which is to be described in more detail for the many-site case later in this chapter, the observation of the temporal response of the z -magnetizations at all sites is used. In all forms of the experiment, transverse magnetization is created only for the purpose of detecting and measuring the z -magnetizations, at the end of a certain evolutionary period following the initial perturbation. Hence the resonance frequencies ν_A, ν_B are not important in magnetization transfer experiments and only the behaviour of z -magnetizations are important. In the following section, the behaviour of the z -magnetization in magnetization transfer experiments is described, using the modified Bloch equations approach, for the simple two site exchange case.

3.3 Modified Bloch Equations for z -magnetization

When the nuclear spins X are placed in an external magnetic field, a longitudinal magnetization is established via the spin-lattice relaxation process (25). In the absence of chemical exchange effects, establishment of the longitudinal magnetizations at sites A and B are described by the phenomenological Bloch equations (25),

$$\frac{d}{dt} M_A^z = \frac{M_A^{eq} - M_A^z}{T_{1A}} \quad [3-4]$$

$$\frac{d}{dt} M_B^z = \frac{M_B^{eq} - M_B^z}{T_{1B}} \quad [3-5]$$

where T_{1A} and T_{1B} are the spin-lattice or longitudinal relaxation times of X nuclear spins at site A and site B respectively, M_A^z and M_B^z are the z -magnetization at sites A and B at time t , and M_A^{eq} and M_B^{eq} are the equilibrium z -magnetizations. If it is assumed that the spin states of nuclei do not change during the nuclear exchange and that rate constants for exchange are independent of the spin state of the nuclei, expressions for the flow of z -magnetization due to chemical exchange analogous to Eqs. [3-2] and [3-3], can be derived straightforwardly (76):

$$\frac{d}{dt}M_A^z = -k_{AB}M_A^z + k_{BA}M_B^z \quad [3-6]$$

$$\frac{d}{dt}M_B^z = +k_{AB}M_A^z - k_{BA}M_B^z \quad [3-7]$$

By combining Eqs. [3-6] and [3-7] with the phenomenological Bloch Eqs. [3-4] and [3-5], one obtains the Bloch equations modified for chemical exchange (76),

$$\frac{d}{dt}M_A^z = \frac{M_A^{eq} - M_A^z}{T_{1A}} - k_{AB}M_A^z + k_{BA}M_B^z \quad [3-8]$$

$$\frac{d}{dt}M_B^z = \frac{M_B^{eq} - M_B^z}{T_{1B}} + k_{AB}M_A^z - k_{BA}M_B^z \quad [3-9]$$

for the z - or longitudinal magnetization in the simple two site exchange. These equations are valid in the absence of any time dependent magnetic fields (rf fields), other than the external applied field. These equations describe the flow of z -magnetization between sites in a magnetization transfer experiment after the initial perturbation. Solution of these equations, using the appropriate boundary conditions, yield the temporal response of the z -magnetizations M_A^z , M_B^z , from which the rate constants for the two site exchange can be obtained, provided the relaxation rate is not too large compared to the exchange rate as will be shown later. The boundary conditions are determined by the type of perturbation employed.

When the selective perturbation is a saturating rf field, magnetization transfer experiments are referred to as saturation transfer experiments (55-57), and this method is discussed in the next section for the two site exchange case. Selective pulse perturbation will be discussed in section 3.5.

3.4 Saturation Transfer Experiments

In saturation transfer experiments, a saturating rf field is selectively applied to one of the resonances. Forsen and Hoffmann have described a set of four saturation transfer experiments (56) for the simple two site (A, B) case in which one monitors:

- (a) The decay of signal A upon saturation of signal B ,
- (b) The recovery of signal A upon removal of the saturation field at B ,
- (c) The recovery of signal A after prolonged saturation of A ,
- (d) The recovery of signal A after saturation of both A and B .

Method (a) is the simplest and most commonly employed, and is discussed in detail below. All the other experiments, cases (b) to (d), fall into a single class and only the general considerations and boundary conditions will be discussed.

3.4.1 Decay of signal A upon saturation of signal B

In the steady state saturation transfer experiment, a saturating rf field of sufficient magnitude H_1 is applied to one of the resonances - resonance B - for a time long enough to saturate the signal. The NMR spectrum at the end of the saturating period would correspond to the z -magnetization at each site in the state of equilibrium in the presence of the saturating rf field. Signal B has zero intensity because of saturation, and the intensity of signal A reflects the rate of transfer of saturation from B to A via the exchange process. When the conditions

for strong, selective saturation of the B resonance (77),

$$\gamma H_1 \ll 2\pi|\nu_A - \nu_B|$$

and

$$(\gamma H_1)^2 \gg (T_{1B}T_{2B})^{-1},$$

are met, $M_B^z = 0$ and M_A^z attains a steady state value $M_A^z(ss)$. From Eq. [3-8], it follows that

$$M_A^z(ss) = M_A^{cq} / (1 + k_{AB}T_{1A}). \quad [3-10]$$

Thus if $k_{AB} \ll 1/T_{1A}$, $M_A^z(ss) \approx M_A^{cq}$, i.e. M_A^z does not show any saturation transfer. As k_{AB} increases, $M_A^z(ss)$ is less than M_A^{cq} , i.e. saturation transfer occurs and the A signal decreases in intensity. The rate constant k_{AB} , can be determined from measurements of T_{1A} , M_A^{cq} and $M_A^z(ss)$:

$$k_{AB} = \frac{M_A^{cq} - M_A^z(ss)}{M_A^z(ss) T_{1A}}. \quad [3-11]$$

In the general case where the value of T_{1A} is not known, one can monitor M_A^z from the time the saturating field is applied to resonance B , and follow the temporal development of the new steady state. If the system is initially at thermal equilibrium, and the saturation of B is taken to be instantaneous ($M_B^z \equiv 0$), then

$$M_A^z(t) = M_A^z(ss) \left\{ 1 + k_{AB}T_{1A} \exp\left[-\frac{(1 + k_{AB}T_{1A})t}{T_{1A}}\right] \right\}, \quad [3-12]$$

and a plot of $\ln\{M_A^z(t) - M_A^z(ss)\}$ vs t is a straight line with slope $-(1 + k_{AB}T_{1A})/T_{1A}$. The measurement of $M_A^z(ss)$ and the slope of this plot affords k_{AB} and T_{1A} .

3.4.2 Cases (b) to (d) - Temporal Magnetization (Saturation) Transfer

In experiments (b), (c) and (d), Eq. [3 10] is no longer valid, and the rate constants cannot be obtained by solving only Eq. [3 8] as in the previous case, since the time dependence of z -magnetization at both sites has to be considered. For these cases the time dependence of M_A^z and M_B^z is determined by the complete solutions of the coupled differential equations, [3 8] and [3 9], subject to the boundary conditions appropriate for the experimental method. Since, in all experiments, the temporal behaviour of magnetization is monitored after turning off the saturating rf field, these experiments are classed as temporal magnetization transfer experiments.

The boundary conditions appropriate for the different experimental methods are:

case (b) $M_B^z = 0$ and $M_A^z = M_A^{eq}/(1 + k_{AB}T_{1A})$ at $t = 0$,

case (c) $M_A^z = 0$ and $M_B^z = M_B^{eq}/(1 + k_{BA}T_{1B})$ at $t = 0$ in symmetry with case (b),

case (d) $M_A^z = 0$ and $M_B^z = 0$ at time $t = 0$.

Although Forsen and Hoffmann described all cases in detail, the reviews of Faller (63) and Alger and Shulman (64) show that only the steady state saturation transfer method has been widely used.

3.5 Selective Pulse Experiments

In magnetization transfer experiments, the initial perturbation may be a selective pulse instead of a selective saturation (58). Maximum perturbation is achieved and hence the largest effects are observed when the selective pulse is a 180° pulse: i.e. a selective inversion of one of the exchanging resonances (61,62). The selective inversion experiment is a temporal magnetization transfer experiment in which a selective 180° pulse is applied to one of the resonances

and the temporal response of the z -magnetization at all the sites is then observed during an evolution period following the selective inversion, as a function of the duration of the evolution period. The sequence,

$$\left[\text{Relaxation Delay} \quad \begin{array}{c} \text{Selective} \\ \pi \text{ pulse} \end{array} \quad - \quad \tau \quad - \quad \begin{array}{c} \text{Non selective} \\ \pi/2 \text{ pulse} \end{array} \quad - \quad \text{Acquire} \right] \quad [3-13]$$

is repeated for a series of τ values such that, $0 \lesssim \tau \lesssim 5T_1$.

For the simple two site exchange, (see Eq. [3-1]), the evolution of the z -magnetization, following the selective inversion of one of the resonances, is again described by the modified Bloch equations [3-8] and [3-9]. It is useful to note that, when $\tau \rightarrow \infty$, both M_A^z and M_B^z will have reached their equilibrium values M_A^{eq} and M_B^{eq} respectively, and that

$$-k_{AB}M_A^{eq} + k_{BA}M_B^{eq} = 0. \quad [3-14]$$

The modified Bloch equations [3-8] and [3-9] can therefore be written as,

$$\frac{d}{dt}(M_A^z - M_A^{eq}) = \left(\frac{-1}{T_{1A}} - k_{AB} \right) (M_A^z - M_A^{eq}) + k_{BA}(M_B^z - M_B^{eq}) \quad [3-15]$$

and

$$\frac{d}{dt}(M_B^z - M_B^{eq}) = \left(\frac{-1}{T_{1B}} - k_{BA} \right) (M_B^z - M_B^{eq}) + k_{AB}(M_A^z - M_A^{eq}). \quad [3-16]$$

Equations [3-15] and [3-16] can be conveniently written in matrix form,

$$\frac{d}{dt}[\mathbf{M} - \mathbf{M}(\infty)] = \mathbf{A} [\mathbf{M} - \mathbf{M}(\infty)] \quad [3-17]$$

where

$$[\mathbf{M} - \mathbf{M}(\infty)] = \begin{pmatrix} M_A^z(\tau) - M_A^z(\infty) \\ M_B^z(\tau) - M_B^z(\infty) \end{pmatrix}$$

and

$$\mathbf{A} = \begin{pmatrix} -1/T_{1A} - k_{AB} & k_{BA} \\ k_{AB} & -1/T_{1B} - k_{BA} \end{pmatrix}$$

It is instructive here to separate the contributions from spin-lattice relaxation, forward exchange and reverse exchange processes to matrix \mathbf{A} as:

$$\mathbf{A} = \begin{pmatrix} -1/T_{1A} & 0 \\ 0 & -1/T_{1B} \end{pmatrix} + k^{(1)} \mathbf{\Pi}^{(1)} + k^{(2)} \mathbf{\Pi}^{(2)}, \quad [3-18]$$

where

$$k^{(1)} = k_{AB}, \quad \mathbf{\Pi}^{(1)} = \begin{pmatrix} -1 & 0 \\ 1 & 0 \end{pmatrix}$$

and

$$k^{(2)} = k_{BA}, \quad \mathbf{\Pi}^{(2)} = \begin{pmatrix} 0 & 1 \\ 0 & -1 \end{pmatrix}.$$

The matrices $\mathbf{\Pi}^{(\alpha)}$ ($\alpha = 1, 2$) in Eq. [3-18] are matrices of exchange coefficients. $\mathbf{\Pi}^{(1)}$ is the matrix of exchange coefficients which represents the forward exchange process and $k^{(1)}$ is the rate constant associated with the forward exchange process. Similarly $\mathbf{\Pi}^{(2)}$ represents the reverse exchange process and $k^{(2)} (= k_{BA})$ is the rate constant for reverse exchange. This representation which seems trivial and artificial in the simple two site exchange case, is very useful in the generalization to the many site exchange system where many complex exchange processes occur. In such a situation, each different exchange mechanism α , can be represented by a matrix of exchange coefficients $\mathbf{\Pi}^{(\alpha)}$, and the associated rate constant $k^{(\alpha)}$, for that exchange process. The behaviour of the z -magnetization during selective inversion experiments will be illustrated using the simplest two site case, before the discussion of general N -site case.

3.5.1 Simplest two site exchange

In the *simplest* two site exchange case possible in Eq. [3-1], $k_{AB} = k_{BA} = k$ and $T_{1A} = T_{1B} = T_1$. For this case, the matrix \mathbf{A} is given by

$$\mathbf{A} = \begin{pmatrix} -1/T_1 - k & k \\ k & -1/T_1 - k \end{pmatrix} \quad [3-19]$$

The behaviour of M_A^z , M_B^z during a selective inversion experiment assuming complete inversion of site A magnetization at time $t = 0$ ($M_A^z(0) = -M_A^{eq}$), is obtained by solution of Eq. [3-17], with the matrix \mathbf{A} given in Eq. [3-19]. The behaviour of M_A^z , M_B^z is shown in Fig. 3-1, as a function of the delay time τ in the selective inversion experiment, for $k = 10.0 \text{ s}^{-1}$ with $1/T_1 = 1 \text{ s}^{-1}$. In Fig. 3-2, the behaviour of M_B^z is shown for a series of values of k with $1/T_1 = 1 \text{ s}^{-1}$. The inverted signal recovers rapidly at short times due to the transfer of magnetization from the other site via the exchange process, and then slowly increases to its equilibrium value at long times through spin-lattice relaxation (see Fig. 3-1). At short times, M_B^z decreases in magnitude because of the transfer of magnetization to the inverted site by the exchange process, then M_B^z goes through a minimum and slowly increases to its equilibrium value through spin-lattice relaxation. The time required for M_B^z to reach its minimum intensity depends on the exchange rate k and $1/T_1$. When the exchange rate is slower, the initial decrease is slower and M_B^z reaches a minimum at longer times (see Fig. 3-2).

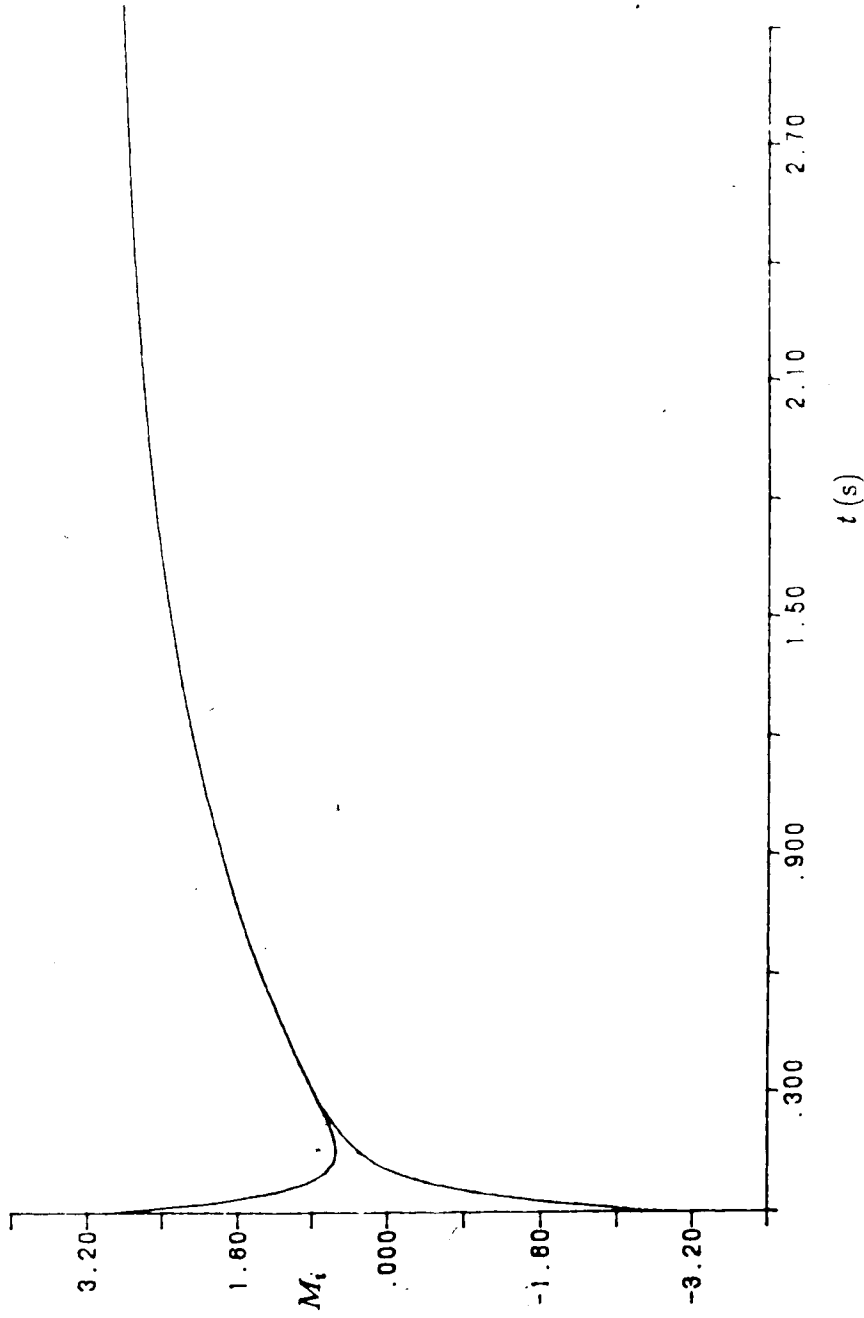


Fig. 3-1 Behaviour of the z -magnetizations in the simplest two site exchange case. Temporal responses of z -magnetizations at sites A and B following selective inversion of magnetization of site A for $k = 10.0 \text{ s}^{-1}$ and $1/T_1 = 1 \text{ s}^{-1}$.

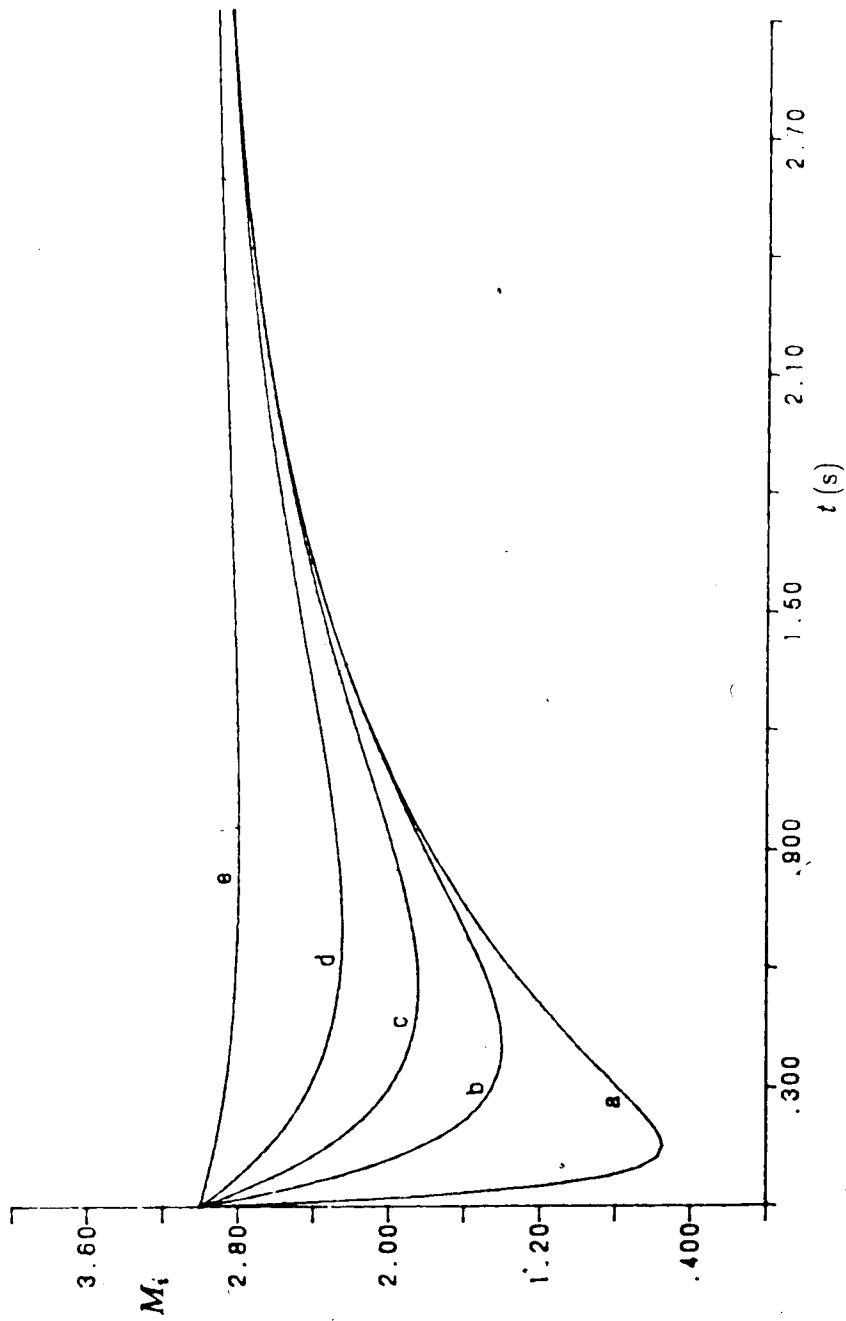


Fig. 3-2 Dependence of the temporal response of z -magnetization at site B_β on the exchange rate and relaxation rate. (a) $k = 10/T_1$, (b) $k = 2/T_1$, (c) $k = 1/T_1$, (d) $k = 0.5/T_1$ and (e) $k = 0.1/T_1$.

3.6 General N -Site Exchange – Selective Inversion Method

For a general exchange problem

$$X_i \xrightleftharpoons[k_{ji}]{k_{ij}} X_j$$

involving N nonequivalent sites with resonance frequencies ν_i ($i = 1, \dots, N$ and $\nu_i \neq \nu_j$ for $i \neq j$), the behaviour of the longitudinal magnetizations is again described by a set of modified Bloch equations. Extending the discussion of sections 2.3 and 2.5, to N -sites we find that Eq. [3-17] applies with, $[\mathbf{M} - \mathbf{M}(\infty)]$ an $N \times 1$ column matrix with elements $(M_i(\tau) - M_i^{eq})$, ($i = 1, \dots, N$), and \mathbf{A} an $N \times N$ square matrix with elements,

$$A_{ij} = \begin{cases} \sum_{\alpha} k^{(\alpha)} \Pi_{ji}^{(\alpha)} & i \neq j \\ -1/T_{1i} - \sum_{\alpha} \sum_l k^{(\alpha)} \Pi_{il}^{(\alpha)} & i = j, \end{cases} \quad [3-20]$$

where $k^{(\alpha)}$ is the rate constant for a particular exchange process α , and $\Pi^{(\alpha)}$ is the matrix of exchange coefficients which describes the α exchange process.

Solution of Eq. [3-17] with matrix \mathbf{A} given by Eq. [3-20] is obtained by direct diagonalization (78) of matrix \mathbf{A} and the solution can be written as,

$$M_l(t) = M_l(\infty) + \sum_{ij}^N \exp(\Delta_i t) U_{li} U_{ij}^{-1} [M_j(0) - M_j(\infty)], \quad (l = 1, \dots, N) \quad [3-21]$$

where Δ and \mathbf{U} are the eigenvalues and eigenvectors of \mathbf{A} and \mathbf{U}^{-1} is the inverse matrix of \mathbf{U} . i.e. $\mathbf{U}^{-1} \mathbf{A} \mathbf{U} = \Delta$. $M_l(t)$ is the z -magnetization at site l at time t following the selective inversion of one of the exchanging resonances at a site m at resonance frequency ν_m ($1 \leq m \leq N$). $M_j(0)$ is the z -magnetization at a site j ($j = 1, \dots, N$) at time $t = 0$ (just after the selective inversion of the m th resonance). Rate constants $k^{(\alpha)}$ are obtained by iterative least squares fitting of

the observed magnetizations $M_l^{obs}(t)$ from the selective inversion experiment to magnetizations $M_l(t)$ calculated using Eq. [3-21].

3.6.1 Least Squares Analysis of Selective Inversion-Magnetization transfer data

The non-linear least squares analysis of magnetization transfer data is an adaptation of the Marquardt algorithm (74) and uses analytic first derivatives of $M_l(t)$ with respect to each of the parameters $1/T_{1l}$, $M_l(\infty)$, $[M_l(0) - M_l(\infty)]$, and $k^{(\alpha)}$ to avoid excessive computation time required for numerical estimation of the derivatives. It is convenient, for the N -site exchange problem involving P independent exchange processes, to define a set of $3N + P$ parameters collectively designated β_Q such that,

$$\begin{aligned}\beta_l &= 1/T_{1l} , \\ \beta_{N+l} &= M_l(\infty) , \\ \beta_{2N+l} &= [M_l(0) - M_l(\infty)] , \\ \beta_{3N+\alpha} &= k^{(\alpha)}\end{aligned}\tag{3-22}$$

where $l = 1, 2, \dots, N$; $\alpha = 1, 2, \dots, P$; and $Q = 1, 2, \dots, 3N + P$. The least squares data analysis begins with the calculation of the $M_l(t)$'s using a set of initial parameters $\{\beta_Q^0\}$. Corrections to this set of parameters are determined, iterations are performed, and values of parameters are improved in successive iterations, until the corrections to parameters fall below a certain threshold value. The least squares method attempts to minimize the least squares sum,

$$S = \sum_n [M_l^{obs}(t_n) - M_l^{calc}(t_n)]^2 ,\tag{3-23}$$

where the sum over n includes all t_n at which experimental data are available, with respect to the corrections to parameters in order to obtain the best agreement between the observed and calculated magnetizations. This procedure is described in detail below.

For an initial set of parameters $\{\beta_Q^0 | Q = 1, \dots, (3N + P)\}$, the z -magnetization at each site l at time t_n is calculated by substituting the values $\{\beta_Q^0\}$ into Eq. [3-21]:

$$M_l^0(t_n) = M_l^0(\infty) + \sum_i U_{li} \exp(\Lambda_i^0 t_n) \sum_j U_{ij}^{-1} [M_j(0) - M_j(\infty)]^0. \quad [3-24]$$

The $M_l^{calc}(t_n)$, which correspond to magnetizations calculated using the "true" values of the parameters $\{\beta_Q\}$, are approximated by a Taylor series expansion about the initial parameters $\{\beta_Q^0\}$:

$$M_l^{calc}(t_n) \cong M_l^0(t_n) + \sum_Q D_Q^l(t_n) \delta\beta_Q, \quad Q = 1, \dots, (3N + P) \quad [3-25]$$

where

$$D_Q^l(t) = \left(\frac{\partial M_l(t)}{\partial \beta_Q} \right)_0 \quad \text{and} \quad \delta\beta_Q = \beta_Q - \beta_Q^0.$$

$D_Q^l(t)$ is the derivative of $M_l(t)$ with respect to the parameter β_Q , evaluated using the initial set of values $\{\beta_Q^0\}$.

The unknowns $\delta\beta_Q$ in Eq. [3-25] are determined by minimizing the least squares sum, Eq. [3-23], with respect to $\delta\beta_Q$'s. From equations [3-23] and [3-25], one obtains

$$S = \sum_l \sum_n [M_l^{obs}(t_n) - M_l^0(t_n) - \sum_Q (D_Q^l(t_n))_0 (\delta\beta_Q)]^2. \quad [3-26]$$

For S to be a minimum with respect to the corrections to parameters $\delta\beta_Q$,

$$\frac{\partial S}{\partial (\delta\beta_Q)} = 0 \quad \text{for all } Q = 1, \dots, (3N + P). \quad [3-27]$$

Hence

$$\begin{aligned} \frac{\partial S}{\partial(\delta\beta_\gamma)} &= -2(D_\gamma^l(t_i))_0 \sum_l \sum_i [M_i^{obs}(t_i) - M_i^0(t_i) - \sum_Q (D_Q^l(t_i))_0 (\delta\beta_Q)] \\ &= 0, \end{aligned} \quad [3-28]$$

for $\gamma = 1, \dots, 3N + P$.

Eq. [3-28] can be rearranged to give the normal equations

$$\sum_Q \left\{ \sum_n \sum_l D_Q^l(t_n) D_\gamma^l(t_n) \right\} \delta\beta_Q = \sum_n \sum_l [M_i^{obs}(t_n) - M_i^0(t_n)] D_\gamma^l(t_n), \quad [3-29]$$

or, in matrix form,

$$\mathbf{D} \vec{\delta\beta} = \vec{C} \quad [3-30]$$

where, \mathbf{D} is a symmetric square matrix of order equal to the total number of parameters ($3N + P$), with elements

$$D_{pq} = \sum_l \sum_n D_p^l(t_n) D_q^l(t_n), \quad [3-31]$$

and $\vec{\delta\beta}$ and \vec{C} are column vectors each having $(3N + P)$ rows with elements

$$(\vec{\delta\beta})_q = \delta\beta_q, \quad [3-32]$$

and

$$\vec{C}_q = \sum_l \sum_i [M_i^{obs}(t_i) - M_i^0(t_i)] D_q^l(t_i). \quad [3-33]$$

The corrections to the parameters, $\delta\beta_Q$, are obtained by inversion (79) of the matrix \mathbf{D} ,

$$\vec{\delta\beta} = \mathbf{D}^{-1} \vec{C} \quad [3-34]$$

where D^{-1} is the inverse matrix of D . Matrix D as well as the column vector \vec{C} are constructed using the analytic first derivatives of $M_l(t)$, with respect to each of the parameters.

3.6.2 Analytic First Derivatives of $M_l(t)$

Partial differentiation of Eq. [3-21], with respect to a general parameter β_Q yields,

$$\frac{\partial}{\partial \beta_Q} M_l(t_n) = \frac{\partial}{\partial \beta_Q} M_l(\infty) + \frac{\partial}{\partial \beta_Q} \left\{ \sum_m U_{lm} \exp(\Lambda_m t_n) \sum_j U_{mj}^{-1} [M_j(0) - M_j(\infty)] \right\}. \quad [3-35]$$

Using the standard methods of differentiation, Eq. [3-35] can be expanded to obtain,

$$\begin{aligned} \frac{\partial}{\partial \beta_Q} M_l(t_n) &= \frac{\partial M_l(\infty)}{\partial \beta_Q} + \sum_m \frac{\partial U_{lm}}{\partial \beta_Q} \exp(\Lambda_m t_n) \left(\sum_j U_{mj}^{-1} [M_j(0) - M_j(\infty)] \right) \\ &+ \sum_m U_{lm} t_n \exp(\Lambda_m t_n) \frac{\partial \Lambda_m}{\partial \beta_Q} \left(\sum_j U_{mj}^{-1} [M_j(0) - M_j(\infty)] \right) \\ &+ \sum_m U_{lm} \exp(\Lambda_m t_n) \sum_j \frac{\partial U_{mj}^{-1}}{\partial \beta_Q} [M_j(0) - M_j(\infty)] \\ &+ \sum_m U_{lm} \exp(\Lambda_m t_n) \sum_j U_{mj}^{-1} \frac{\partial}{\partial \beta_Q} [M_j(0) - M_j(\infty)]. \end{aligned} \quad [3-36]$$

In Eq. [3-36], derivatives with respect to the linear parameters $M_i(\infty)$ and $[M_i(0) - M_i(\infty)]$ are straightforward.

(a) Derivatives w.r.t. parameters $M_i(\infty)$:

$$\frac{\partial M_l(\infty)}{\partial M_i(\infty)} = \delta_{li}. \quad [3-37]$$

All other derivatives,

$$\frac{\partial U_{lm}}{\partial M_i(\infty)}, \frac{\partial U_{mj}^{-1}}{\partial M_i(\infty)}, \frac{\partial \Lambda_m}{\partial M_i(\infty)}, \text{ and } \frac{\partial [M_j(0) - M_j(\infty)]}{\partial M_i(\infty)}$$

are equal to zero.

(b) Derivatives w.r.t. parameters $[M_i(0) - M_i(\infty)]$:

$$\frac{\partial [M_i(0) - M_i(\infty)]}{\partial [M_i(0) - M_i(\infty)]} = \delta_{i,i} \quad [3-38]$$

and all others,

$$\frac{\partial M_i(\infty)}{\partial [M_i(0) - M_i(\infty)]}, \frac{\partial U_{lm}}{\partial [M_i(0) - M_i(\infty)]}, \frac{\partial U_{mj}^{-1}}{\partial [M_i(0) - M_i(\infty)]} \text{ and } \frac{\partial \Lambda_m}{\partial [M_i(0) - M_i(\infty)]}$$

are zero.

Derivatives with respect to the non-linear parameters, $1/T_{1i}$ and $k^{(a)}$ require further analysis because the eigenvalues Λ and eigenvectors U depend on these non-linear parameters.

(c) Derivatives w.r.t. $1/T_{1i}$ parameters:

Clearly,

$$\frac{\partial M_i(\infty)}{\partial (1/T_{1i})} = \frac{\partial [M_i(0) - M_i(\infty)]}{\partial (1/T_{1i})} = 0.$$

For Λ, U and U^{-1} , following the analysis of Wilkinson (80) we get,

$$\frac{\partial \Lambda_m}{\partial (1/T_{1i})} = U_{mi}^{-1} U_{im}, \quad [3-39]$$

$$\frac{\partial U_{lm}}{\partial (1/T_{1i})} = \sum_{k \neq m} \frac{(U_{lm} U_{mk} - U_{mm} U_{lk})}{U_{mm} (\Lambda_k - \Lambda_m)} U_{ki}^{-1} U_{im}, \quad [3-40]$$

and

$$\frac{\partial U_{mj}^{-1}}{\partial (1/T_{1i})} = - \sum_{k,p} U_{mk}^{-1} \left(\frac{\partial U_{kp}}{\partial (1/T_{1i})} \right) U_{pj}^{-1}. \quad [3-41]$$

(d) Derivatives w.r.t. $k^{(\alpha)}$ parameters:

Clearly,

$$\frac{\partial M_l(\infty)}{\partial k^{(\alpha)}} = \frac{\partial [M_l(0) - M_l(\infty)]}{\partial k^{(\alpha)}} = 0.$$

For Λ, U and U^{-1} , again following Wilkinson (80),

$$\frac{\partial \Lambda_m}{\partial k^{(\alpha)}} = \sum_{i,j} U_{mi}^{-1} \Pi_{ij}^{(\alpha)} U_{jm}, \quad [3-42]$$

$$\frac{\partial U_{lm}^0}{\partial k^{(\alpha)}} = \sum_{k \neq m} \frac{(U_{lm} U_{mk} - U_{mm} U_{lk})}{U_{mm} (\Lambda_k - \Lambda_m)} \sum_{i,j} U_{ki}^{-1} \Pi_{ij}^{(\alpha)} U_{jm}, \quad [3-43]$$

and

$$\frac{\partial U_{lm}^{-1}}{\partial k^{(\alpha)}} = - \sum_{k,p} U_{lk}^{-1} \left(\frac{\partial U_{kp}}{\partial k^{(\alpha)}} \right) U_{pm}^{-1}. \quad [3-44]$$

Thus the elements of the matrix D can be calculated using the analytic derivatives [3-37] to [3-44] in Eqs. [3-36] and [3-38]. The corrections $\delta\beta$, i.e. the elements of the vector $\vec{\delta\beta}$, are then easily obtained from Eq. [3-34] since the elements of the vector \vec{C} are also obtainable from the above derivatives (see Eq. [3-33]), and the difference between the observed magnetizations and the $M_l^0(t_n)$ calculated using the initial set of parameters $\{\beta_Q^0\}$.

3.6.3 New Parameters for Iteration and Convergence

Once the values of the $\delta\beta_Q$'s are determined from Eq. [3-34], a new set of parameters $\{\beta_Q^1\}$ can be obtained from the initial set of $\{\beta_Q^0\}$,

$$\beta_Q^1 = \beta_Q^0 + \delta\beta_Q \quad (Q = 1, \dots, (3N + P)). \quad [3-45]$$

This iterative procedure is repeated to obtain more refined corrections, until a convergence criterion,

$$|\delta\beta_Q^{n+1}| < \epsilon |\beta_Q^n| \text{ for all } Q, \quad [3-46]$$

where ϵ is a small real number such that $0 < \epsilon \ll 1$, is satisfied, at a certain $(n + 1)$ th iteration. Then, the parameters $\{\beta_Q^n\}$ at the end of the n th iteration are the most refined parameters, and the values which give best agreement between the observed and calculated magnetizations for all the sites. The values of the parameters $k^{(\alpha)}$ ($\beta_{3N+\alpha}^n$, $\alpha = 1, \dots, P$) at this point are the rate constants for different exchange processes α , as determined from the selective inversion experiment.

The variance (σ^2) of the least squares fit, i.e. the minimum variance with respect to the parameters, when the convergence is obtained is then given by,

$$\sigma^2 = \sum_{l=1}^N \sum_{n=1}^I (M_l^{obs}(t_n) - M_l^n(t_n))^2 / [NI - (3N + P)] \quad [3-47]$$

In Eq. [3-47], $M_l^n(t_n)$ is the calculated magnetization at site l using the best values of the parameters (β_Q^n , $Q = 1, \dots, (3N + P)$), I is the number of data points per site (i.e. the number of delay periods employed in the experiment) and $(3N + P)$ is the total number of parameters in the model.

The values of a selected number of parameters, c [$c < (3N + P)$], may be kept constant during iterations, by generating zero values for the corresponding corrections $\delta\beta_Q$ in Eq. [3-34]. This is achieved by assigning,

$$D_{L(p),j} = D_{j,L(p)} = \delta_{L(p),j} \quad [3-48]$$

and,

$$C_{L(p)} = 0, \quad [3-49]$$

where $L(p)$, $p = 1, \dots, c$ are the indices of the parameters which are to be kept constant and $j = 1, \dots, (3N + P)$. The variance of the least squares fit in this

case is given by,

$$\sigma^2 = \sum_{l=1}^N \sum_{n=1}^I (M_l^{obs}(t_n) - M_l^n(t_n))^2 / [N I + c - (3N + P)] \quad [3-50]$$

Usually the values of parameters $1/T_{1l}$ ($l = 1, \dots, N$) are fixed in this manner during the least squares iterations since the $1/T_{1l}$ s are measured using an independent experiment.

3.6.4 Estimation of Errors in Rate Constants

Once convergence is attained, the variance of the least squares fit, Eq. [3-50], is used to obtain the standard deviation of each of the parameters,

$$\sigma_{(\beta_Q)} = \sqrt{\sigma^2 D_{qq}^{-1}}, \quad [3-51]$$

where $\sigma_{(\beta_Q)}$ is the standard deviation of the β_Q th parameter. These standard deviations are then used to obtain the 95% confidence intervals on all parameters based on the F(Variance-Ratio) distribution function (81). These confidence limits are expressed as linear and non-linear errors of the parameter β_Q by defining (81),

$$\text{Linear error in } \beta_Q = \sigma_{(\beta_Q)} T \quad [3-52]$$

$$\text{Non - linear error in } \beta_Q = \sigma_{(\beta_Q)} F \quad [3-53]$$

In Eq. [3-52], $T = \sqrt{F(\nu_1, \nu_2)}$, where $F(\nu_1, \nu_2)$ is the value of the F-distribution function for $\nu_1 = 1$ and $\nu_2 = N I + c - (3N + P)$.

In Eq. [3-53], $F = \sqrt{[(3N + P) - c] F(\nu_1, \nu_2)}$, where $F(\nu_1, \nu_2)$ is the value of the F-distribution function for $\nu_1 = [(3N + P) - c]$ and $\nu_2 = N I + c - (3N + P)$.

The appropriate values of the F-distribution function are calculated numerically using the series expansion for the F-distribution function (82). The confidence limits in Eq. [3-53], may overestimate the errors in the value of the parameter, β_i , when some of the correlation coefficients, $D_{ij}^{-1} / \sqrt{D_{ii}^{-1} D_{jj}^{-1}}$, between β_i and other parameters β_j , are small. The non-linear error does, however, provide consistent reliable estimates of errors in the least squares parameters.

3.7 Summary

The basic principles of magnetization transfer experiments were illustrated using the modified Bloch equation description of the simple two site exchange problem for the Forsen and Hoffmann steady state saturation transfer experiment. The development of the selective inversion method, and the method of data analysis to obtain rate constants from multisite exchanging systems was discussed in detail. In the method described here, the parameters $k^{(a)}$, $1/T_{1i}$, $M_i(\infty)$ and $[M_i(0) - M_i(\infty)]$ are variables in the least squares procedure, and the method of fixing some of these variables at constant values was described. Estimation of the errors in the rate constants was described using the F-distribution function. In the next chapter, the application of the multisite magnetization transfer method to delineate exchange mechanisms and rate constants in some complex systems will be discussed.

It should be mentioned that this multisite problem had been addressed independently by two other groups (83,84). One major difference between these approaches and the method developed here is the way in which the exchange process is incorporated into the theory, and therefore the method by which the rate constants are to be extracted from the experimental data. The rate constants k_{ji} used by other workers (83,84) describe the transfer of magnetization from site j

to site i , and may contain contributions from a number of distinct mechanisms. In the method developed here $k^{(\alpha)}$ is the rate constant for a particular exchange process, and not the rate constant for transfer of magnetization from one site to another. Use of matrices of exchange coefficients $\Pi^{(\alpha)}$ allows the determination of the contributions from each of the different exchange processes in a clear, concise fashion.

CHAPTER 4

Details of Selective Inversion Experiment and Evaluation of the Method

4.1 Introduction

In this chapter, the application of the selective inversion multisite magnetization transfer method to delineate exchange mechanisms and to determine rate constants for these exchange processes is illustrated fully using the fluxional behaviour of the transition metal organometallic complex $(\eta^3\text{-C}_7\text{H}_7)\text{-Os}(\text{CO})_3\text{-SnPh}_3$, as a test case. The method of selective inversion and the experimental procedure is discussed. Results of selective inversion experiments on the test compound are described in detail in order to illustrate the general applicability and the power of the technique in analysing complex multisite exchange systems. The limitations of the method and the effects of imperfect experimental conditions on the values of rate constants will also be discussed.

4.2 Experimental Details

Magnetization transfer experiments were performed using the sequence shown in Eq. [3-13]. Selective inversion of the magnetization at the desired site was achieved using the DANTE sequence (61). DANTE is a selective excitation technique in which a train of hard pulses of small flip angle α ($\alpha \ll \pi/2$), each of duration t_α is applied with a very short delay δt between the pulses (see Fig. 4-1). The pulse train has the effect of selective pulses of cumulative flip angle $m\alpha$, at the transmitter frequency and at frequencies $1/\Delta t$ separated from the transmitter.

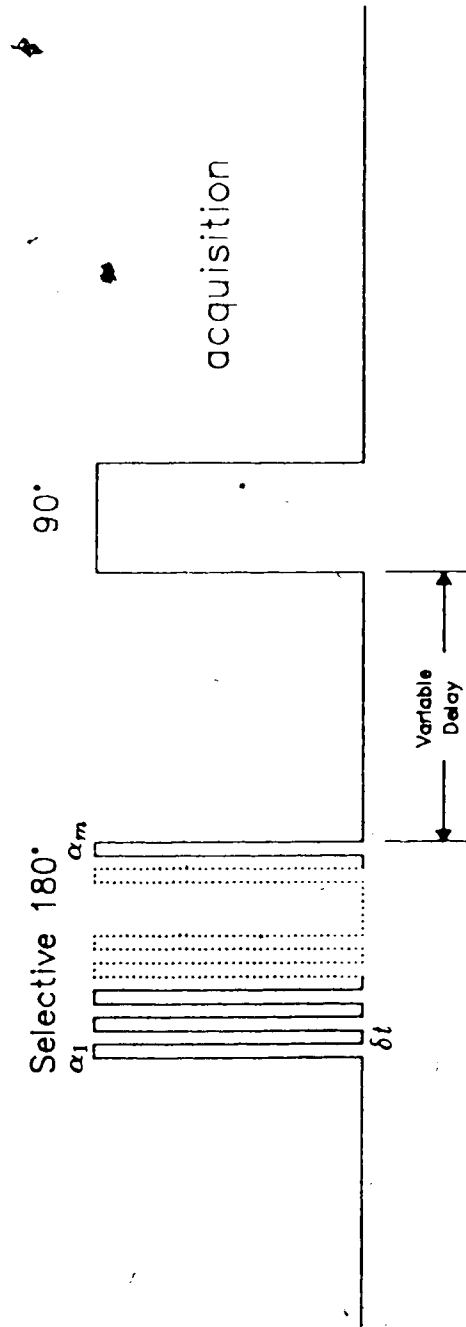


Fig. 4-1 DANTE selective inversion recovery pulse sequence.

Here m is the number of small pulses of flip angle α and $\Delta t = (\delta t + t_\alpha)$. If the transmitter frequency is ν_0 , then selective excitation occur at frequencies,

$$\nu_0, \nu_0 \pm 1/\Delta t, \nu_0 \pm 2/\Delta t, \dots$$

For selective inversion,

$$m\alpha = \pi \quad [4-1]$$

and the DANTE sequence is usually applied, on resonance with the magnetization to be inverted or using the first side band frequency $\nu_0 \pm 1/\Delta t$. Selective excitation is effective over a small frequency band width $\delta\nu$,

$$\delta\nu = 1/(\Delta t m) \quad [4-2]$$

at these frequencies, $\nu_0 \pm n/\Delta t$, where n is a non-negative integer. Thus for a pulse train of one second duration, a selectivity of the order of 1 Hz is attained in principle, neglecting the effects of relaxation. In all the experiments that are to be discussed here, the DANTE sequence was applied on resonance with the magnetization to be inverted, and the delay time δt between pulses was chosen so that the first side band frequency $\nu_0 \pm 1/\Delta t$, fell outside the spectral region of interest. The values of t_α , m and δt were adjusted to obtain optimum selectivity and maximum inversion.

The complete pulse sequence used in experiments, corresponding to Eq. [3-13] in chapter 3, with the DANTE sequence included for the selective inversion, is shown in Fig. 4-1. For the test compound, ^1H spectra were recorded on an unmodified Bruker WH-400 spectrometer, and the typical values used for the DANTE selective inversion were $m = 18-20$, $\delta t = 400-500 \mu\text{s}$. The non-selective 90° pulse width for ^1H was $22 \mu\text{s}$. However, maximum inversion ($\sim 70-80\%$) was

achieved, when t_a was slightly larger than $(44/m)\mu\text{s}$, (See Eq. [4-1]). A series of fid's, corresponding to variable delay time τ , ranging from 0.00005 s to 10 s, following the selective inversion, was collected. The fid's were transformed without using any linebroadening or zero filling, and all spectra were normalized with respect to the spectrum which corresponds to the longest variable delay time.

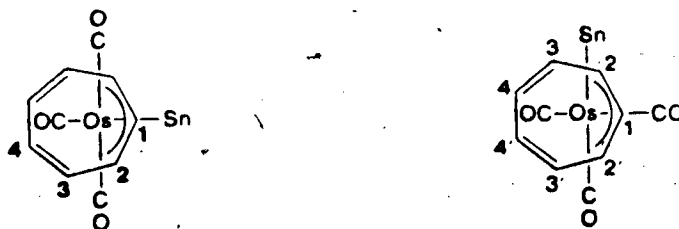
Non-selective inversion recovery experiments were also performed in order to measure the relaxation time T_1 , using the sequence (85),

$$[\text{RelaxationDelay} - \pi - \tau - \pi/2 - \text{Acquire}] , \quad [4-3]$$

where the pulses π , $\pi/2$ are non-selective and τ is the variable delay time ($0 \leq \tau \leq 5T_1$).

4.3 Application of the selective inversion method to a study of the fluxional behaviour of $(\eta^3\text{-C}_7\text{H}_7)\text{-Os}(\text{CO})_3\text{-SnPh}_3$

The Selective inversion method was applied to the $(\eta^3\text{-C}_7\text{H}_7)\text{-Os}(\text{CO})_3\text{-SnPh}_3$ complex, as a test case. It has been established (65), that this complex exists in solution as a mixture of non-interconverting symmetric and



asymmetric isomers, and in the low temperature limit (below $\sim 198\text{ K}$), only the asymmetric isomer is fluxional. By virtue of the asymmetry, all protons and carbons in the C_7H_7 moiety of the asymmetric isomer are non equivalent, and this isomer therefore provides a case involving a seven site exchange problem. The seven resonances due to the asymmetric isomer are shown in the ^1H NMR spectrum of the mixture at 188 K (Fig. 4-2). The fluxional nature of the bonding

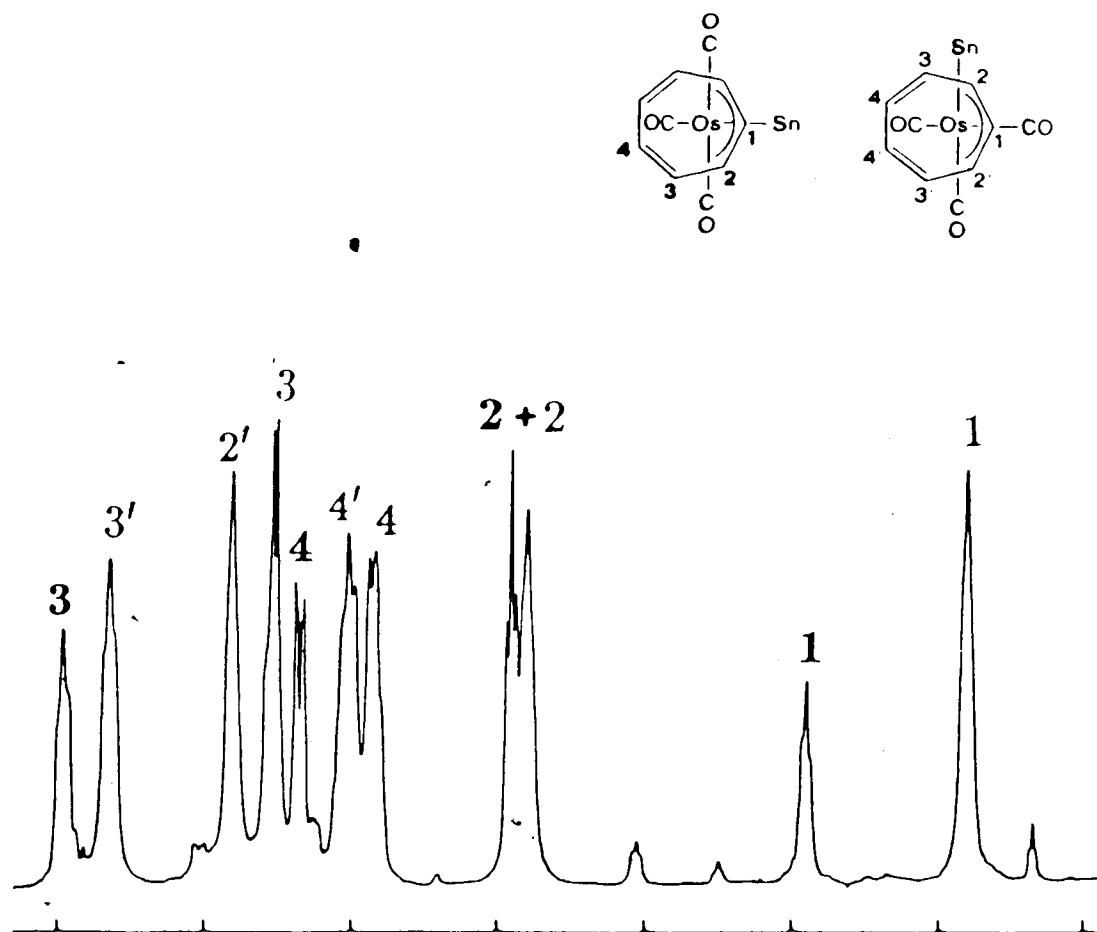
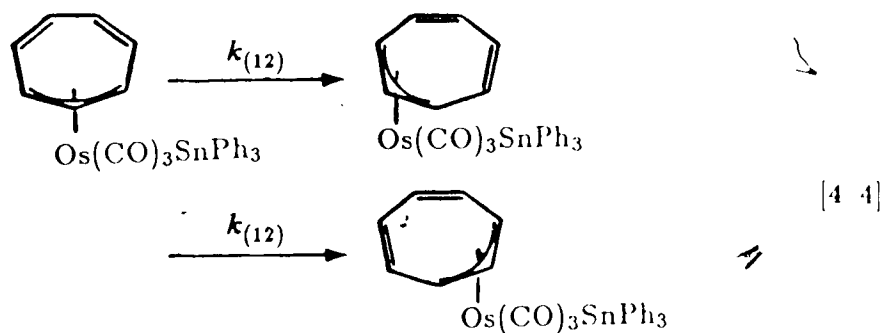
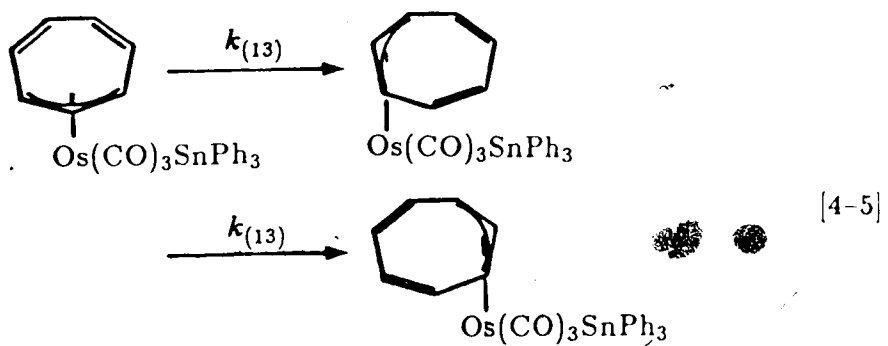


Fig. 4-2 ^1H NMR spectrum (400 MHz) of the C_7H_7 region for $(\eta^3\text{-C}_7\text{H}_7)\text{-Os(CO)}_3\text{-SnPh}_3$ in CD_2Cl_2 at 188 K (200 Hz/division). Peaks labelled 1, 1', 2, 2', 3, 3', 4 and 4' arise from the asymmetric isomer, and peaks 1, 2, 3 and 4 are due to the symmetric isomer.

between the Os atom and the cycloheptatriene ring is believed to arise from a "1-2" exchange process (65),



and possibly from a "1-3" exchange process,



The delineation of the exchange mechanism, and the determination of the rate constants $k_{(12)}$, $k_{(13)}$ for the asymmetric isomer is discussed below. Fluxional behaviour of the symmetric isomer at higher temperatures will be discussed in section 4.4

For the asymmetric isomer, the "1-2" exchange process (Eq. [4-4]) is described in the model by rate constant $k^{(1)} = k_{(12)}$ and matrix of exchange

coefficients $\Pi^{(1)}$,

$$\Pi^{(1)} = \begin{pmatrix} -2 & 1 & 0 & 0 & 0 & 0 & 1 \\ 1 & -2 & 1 & 0 & 0 & 0 & 0 \\ 0 & 1 & -2 & 1 & 0 & 0 & 0 \\ 0 & 0 & 1 & -2 & 1 & 0 & 0 \\ 0 & 0 & 0 & 1 & -2 & 1 & 0 \\ 0 & 0 & 0 & 0 & 1 & -2 & 1 \\ 1 & 0 & 0 & 0 & 0 & 1 & -2 \end{pmatrix} \quad [4-6]$$

and the "1-3" exchange process is described by rate constant $k^{(2)} = k_{(13)}$, and exchange coefficient matrix $\Pi^{(2)}$,

$$\Pi^{(2)} = \begin{pmatrix} -2 & 0 & 1 & 0 & 0 & 1 & 0 \\ 0 & -2 & 0 & 1 & 0 & 0 & 1 \\ 1 & 0 & -2 & 0 & 1 & 0 & 0 \\ 0 & 1 & 0 & -2 & 0 & 1 & 0 \\ 0 & 0 & 1 & 0 & -2 & 0 & 1 \\ 1 & 0 & 0 & 1 & 0 & -2 & 0 \\ 0 & 1 & 0 & 0 & 1 & 0 & -2 \end{pmatrix} \quad [4-7]$$

The matrices $\Pi^{(1)}, \Pi^{(2)}$ are then used to construct the matrix \mathbf{A} in Eq. [3-17], which is a 7 by 7 matrix for this case.

4.3.1 Qualitative determination of exchange mechanism

Behaviour of the magnetization in a selective inversion experiment performed at 188 K, by selectively inverting the site 2' magnetization, is shown in Fig. 4-3 as a function of the variable delay time τ . Examination of the observed data shows that the inverted site 2' magnetization recovers rapidly at short times, because of the transfer of magnetization from other sites via exchange processes, and at long times slowly increases towards its equilibrium value by spin-lattice relaxation. Magnetizations at all other sites decrease to a minimum at short times because of the exchange process, and then slowly increase to their equilibrium values through magnetic relaxation. The most rapid initial decreases occur at site 1 and site 3'. The decreases in the magnetization at sites 2 and 4' are slower and the

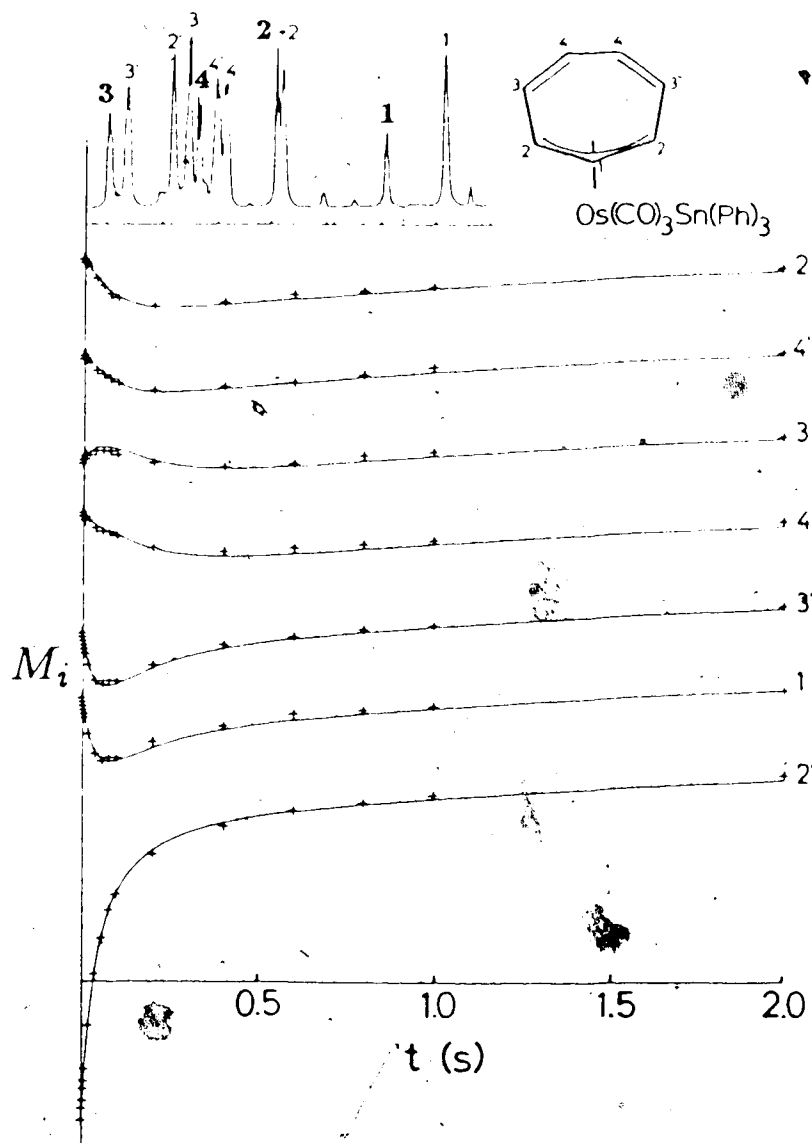


Fig. 4-3 Comparison of the observed and calculated magnetizations for the asymmetric isomer at 188 K. + - Magnetizations $M_i(t)$ (arbitrary units) at the seven sites of the asymmetric isomer following the selective inversion of the site 2' magnetization. Curves represent least squares fit for $k_{(12)} = 8.5 \text{ s}^{-1}$ and $k_{(13)} = 0$.

slowest decreases occur at sites 3 and 4. Since sites 1 and 3' are the sites adjacent to the inverted site, this behaviour indicates that the transfer of magnetization rapidly occurs by "1-2" exchange process. First, the equilibrium magnetization at sites 1 and 3' rapidly decreases by transferring magnetization to the inverted site 2'. The magnetizations at the next nearest pair of sites 2 and 4', decrease slowly by "1-2" magnetization transfer to site 1 and 3' respectively, and at longer times the magnetizations at sites 3 and 4 decrease by "1-2" transfer to sites 2 and 4'. Thus, by visual inspection of the observed data, one can qualitatively determine that the "1-2" exchange process is the predominant exchange mechanism responsible for the fluxional behaviour of this isomer.

It should be mentioned here that the time dependence of site 3 magnetization shows a slight increase initially, in contrast to the above description, but this has no adverse effect on the overall description given above. This complicated behaviour of the site 3 magnetization is a result of the imperfect selectivity of the DANTE sequence, and it will be discussed later in more detail.

4.3.2 Quantitative determination of rate constants

In the least squares analysis of this data set, the values of parameters $1/T_{1l}$ ($l = 1, \dots, 7$) were fixed at values which were independently determined from a non-selective inversion recovery experiment (Eq. [4-3]), at the same temperature. All values of $1/T_{1l}$ were found to be equal to 0.6 s^{-1} within experimental uncertainties. The calculated curves in Fig. 4-3, were obtained from a least squares fit in which $k^{(2)} \equiv k_{(13)}$ was fixed at zero — i.e. assuming no "1-3" shifts, and values of $k^{(1)} \equiv k_{(12)}$, $M_l(\infty)$ and $(M_l(0) - M_l(\infty))$ were varied to minimize the variance. The rate constant $k^{(1)} \equiv k_{(12)}$, has a value of $8.5 \pm 0.9 \text{ s}^{-1}$ for this fit, and the agreement between the calculated and observed magnetization is extremely good.

4.3.3 Importance of the "1-3" exchange process

To investigate the importance of the "1-3" shift mechanism, a second least squares analysis was performed using the same set of experimental data. In this fit, $k^{(2)} \equiv k_{(13)}$ was allowed to vary freely along with $k^{(1)}$, $M_l(\infty)$ and $(M_l(0) - M_l(\infty))$ and the resulting rate constants were $k^{(1)} = 7.8 \pm 1.5 \text{ s}^{-1}$ and $k^{(2)} = 0.4 \pm 0.8 \text{ s}^{-1}$. The variance of the second fit was no better than that in the original analysis where $k^{(2)}$ was fixed at zero. A third least squares fitting where $k^{(1)}$ was fixed at 8.5 and $k^{(2)}$ was allowed to vary freely, produced a value of $0.1 \pm 0.4 \text{ s}^{-1}$ for $k^{(2)} = k_{(13)}$. Clearly one must conclude that the "1-3" shifts are not important in the fluxionality of this organometallic complex.

4.3.4 Clockwise vs Anticlockwise Metal Migration

It should be mentioned here that in the asymmetric isomer, it is possible to determine whether the rates of metal migration in the clockwise sense and anticlockwise sense are equal or not. The two processes can be distinguished by associating the rate constant $k_{(12)}^c$ for clockwise rotation with the matrix of exchange coefficients $\Pi_c^{(1')}$,

$$\Pi_c^{(1')} = \begin{pmatrix} -1 & 0 & 0 & 0 & 0 & 0 & 1 \\ 1 & -1 & 0 & 0 & 0 & 0 & 0 \\ 0 & 1 & -1 & 0 & 0 & 0 & 0 \\ 0 & 0 & 1 & -1 & 0 & 0 & 0 \\ 0 & 0 & 0 & 1 & -1 & 0 & 0 \\ 0 & 0 & 0 & 0 & 1 & -1 & 0 \\ 1 & 0 & 0 & 0 & 0 & 1 & -1 \end{pmatrix}, \quad [4-8]$$

and the rate constants for 1,2 shifts in the anticlockwise sense $k_{(12)}^{ac}$ with the exchange coefficient matrix $\Pi_{ac}^{(2')}$,

$$\Pi_{ac}^{(2')} = \begin{pmatrix} -1 & 1 & 0 & 0 & 0 & 0 & 1 \\ 0 & -1 & 1 & 0 & 0 & 0 & 0 \\ 0 & 0 & -1 & 1 & 0 & 0 & 0 \\ 0 & 0 & 0 & -1 & 1 & 0 & 0 \\ 0 & 0 & 0 & 0 & -1 & 1 & 0 \\ 0 & 0 & 0 & 0 & 0 & -1 & 1 \\ 1 & 0 & 0 & 0 & 0 & 0 & -1 \end{pmatrix}. \quad [4-9]$$

Least squares analysis of the magnetization transfer data shown in Fig. 4-3 (see section 4.3.2) with both $k_{(12)}^c$ and $k_{(12)}^{ac}$ allowed to vary independently yielded, $k_{(12)}^c = 8.5 \pm 0.9 \text{ s}^{-1}$ and $k_{(12)}^{ac} = 8.5 \pm 0.8 \text{ s}^{-1}$, which are essentially identical to the result $k_{(12)} = 8.5 \pm 0.9 \text{ s}^{-1}$ obtained earlier for this data set using the matrix of exchange coefficients $\Pi^{(1)}$ given in Eq. [4-6]. Since the rates of metal migration in both clockwise and anticlockwise sense are identical, we have used the rate constant $k_{(12)}$, which is associated with the matrix of exchange coefficients given in Eq. [4-6], in the analysis of magnetization transfer data.

4.3.5 Reliability of rate constants

To assess the reliability of the rate constants obtained from this method, other experiments were performed in which the magnetization at site 1, and at site 3, were selectively inverted and the temporal responses of the system monitored. Least squares analysis of these data sets, assuming that there are no "1-3" shifts, yielded $k_{(12)} = 7.8 \pm 0.7 \text{ s}^{-1}$ for selective inversion of site 1 and $k_{(12)} = 8.3 \pm 1.3 \text{ s}^{-1}$ for selective inversion of site 3. The three independent determinations of $k_{(12)}$, 8.5 ± 0.9 , 7.8 ± 0.7 and $8.3 \pm 1.3 \text{ s}^{-1}$ are equal within the error limits estimated by the least squares analysis. The agreement of the results of the three experiments demonstrates the reliability of selective inversion experiments in the measurement of rate constants.

4.3.6 Effects of imperfect selectivity of inversion

It is important to note that the DANTE inversion of the site 2' magnetization, shown in Fig. 4-3 significantly perturbed the site 3 magnetization. Thus the time dependence of $M_3(t)$ is more complicated than the time dependence of $M_4(t)$. Since magnetization at site 4 is unperturbed by inversion, it decreases

slowly at short times due to magnetization transfer to site 3, which has been slightly depleted by the DANTE sequence, and to site 4' which becomes depleted by the successive "1-2" magnetization transfers $3' \rightarrow 2'$ and $4' \rightarrow 3'$ as discussed earlier. At longer times, site 4 magnetization relaxes back to its equilibrium value. The site 3 magnetization is smaller than its equilibrium value initially due to the imperfect selectivity of the DANTE sequence, and increases in the initial time period due to $4 \rightarrow 3$ and $2 \rightarrow 3$ magnetization transfers. However, at times ~ 0.06 s after the inversion, the magnetization at site 2 has become so depleted by the successive $1 \rightarrow 2'$, $2 \rightarrow 1$, transfers, that $3 \rightarrow 2$ magnetization transfer begins and site 3 magnetization decreases just as site 4 magnetization does in this time period. Finally, the site 3 magnetization increases to its equilibrium value, via magnetic relaxation. It is most satisfying that both the experimental and calculated magnetizations show the time dependence discussed here.

The presence of imperfect selectivity does not affect the data analysis adversely and fits for the inversion recovery data for both sites 2 and 3 are as good as the fits of the data for other sites.

4.3.7 Effect of absence of data from one site on the rate constant

It is instructive to investigate the effects on the value of the rate constant, when the data from site 2 magnetization (which is significantly overlapped with a peak from the symmetric isomer) are not included in the least squares analysis. The exchange problem is still analysed as a seven site problem, but observed data from only six of the sites are now used in the data analysis.

In a general case, where the magnetization data from a certain site m is not available, it is necessary to keep the values for parameters $1/T_{1m}$, $M_m(\infty)$ and $(M_m(0) - M_m(\infty))$ fixed during iterations. In a case where all the T_1 values

are not equal, it is sufficient to use an approximate T_1 value, estimated by taking the average of the known values, since the accuracy of $1/T_1$ values is not critical for the determination of rate constants as will be shown in section 4.5.2. A good approximation is obtained for $M_m(\infty)$, by taking the weighted average of equilibrium magnetizations of other sites, which are estimated from a conventional spectrum. Since, in principle, $(M_l(0) - M_l(\infty))$ should be zero for an unperturbed site, $(M_m(0) - M_m(\infty))$ is usually fixed at zero during iterations.

For the selective inversion of site 2' magnetization, least squares analysis using only the data from six sites, excluding site 2 data, and fixing the values of $M_2(\infty)$ and $(M_2(0) - M_2(\infty))$ as stated above, in addition to fixing $1/T_1$ for all sites at 0.6 s^{-1} , yielded $k_{(12)} = 7.8 \pm 1.6$, $k_{(13)} = 0.4 \pm 0.8 \text{ s}^{-1}$ when both $k_{(12)}$ and $k_{(13)}$ were allowed to vary freely. This is essentially identical to the result obtained from the analysis using data from all the seven sites. Results obtained for selective inversion of sites 2', 1 and 3, and allowing only $k_{(12)}$ to vary ($k_{(13)} = 0$ fixed) are shown in Table 4.1.

Table 4.1

Inverted site	Site 2-data Excluded Variance	$k_{(12)} \text{ s}^{-1}$	Site 2-data Included Variance	$k_{(12)} \text{ s}^{-1}$
1	0.00129	7.7 ± 0.9	0.00116	7.8 ± 0.7
2'	0.00029	8.5 ± 0.9	0.00027	8.5 ± 0.9
3	0.00050	7.9 ± 1.2	0.00045	8.3 ± 1.3

For these cases, the calculated and observed magnetizations for sites from which the data are available are in good agreement and the calculated magnetization for site 2, shows the expected temporal response. The absence of data from site 2 did not hinder the delineation of the correct mechanism and the values of the rate constants obtained are very close to the values obtained with the full set of data as

shown in Table 4.1. Larger variances and hence larger errors in the rate constants are to be expected here, due to the decrease of the number of data points used in the analysis.

The capability of determining the rate constants, even in the absence of data from one of the sites, is very useful in situations where a resonance from an exchanging site is obscured by other signals or is so broad that it cannot be measured precisely.

4.4 Application of the method to the study of the fluxional behaviour of the symmetric isomer, in the presence of rapidly exchanging asymmetric isomer

The symmetric isomer is not fluxional in the low temperature range below 196 K. Above 203 K, the resonances from the asymmetric isomer broaden considerably, and approach coalescence above 213 K. The symmetric isomer begins to show fluxional behaviour above 203 K. Since the symmetric isomer is still in the slow exchange limit in the temperature range 203 K to 233 K, the fluxional behaviour of the symmetric isomer can be studied by the selective inversion method, even in the presence of the now rapidly exchanging asymmetric isomer. Selective inversion experiments were performed by inverting the site 1 magnetization, which is the only resonance that is free of overlap (See Fig. 4-4). Since this resonance is not overlapped with any signal from the asymmetric isomer, selective inversion would not perturb any resonances from the asymmetric isomer significantly and hence those broad signals do not show any temporal response during the experiment. Thus the intensities of the peaks due to the symmetric isomer, are governed only by the magnetization transfer occurring in the symmetric isomer. It is clear that it may be difficult to obtain precise peak intensities of the resonances

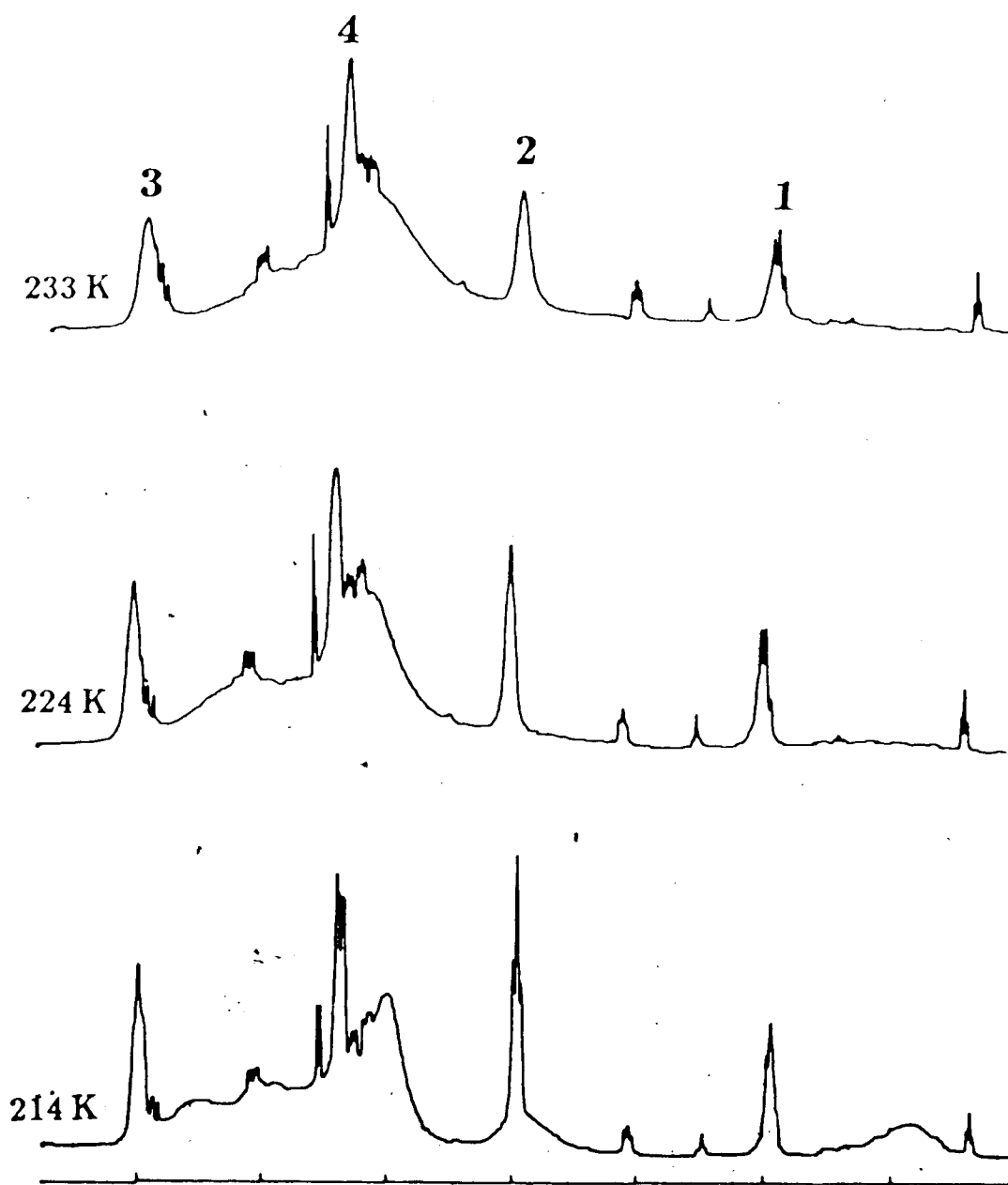


Fig. 4-4 ^1H NMR spectra (400 MHz) of the C_7H_7 region for $(\eta^3\text{-C}_7\text{H}_7)\text{-Os(CO)}_3\text{-SnPh}_3$ in CD_2Cl_2 at 214, 224 and 233 K (200 Hz/division). Peaks labelled 1, 2, 3 and 4 are due to the symmetric isomer.

from sites 2,3 and 4 of the symmetric isomer which appear as sharp resonances superimposed on the broad asymmetric peaks which essentially form a distorted baseline.

For this four site exchange problem, the "1-2" exchange mechanism is described in the model by a matrix of exchange coefficients $\Pi^{(1)}$,

$$\Pi^{(1)} = \begin{pmatrix} -2 & 1 & 0 & 0 \\ 2 & -2 & 1 & 0 \\ 0 & 1 & -2 & 1 \\ 0 & 0 & 1 & -1 \end{pmatrix} \quad [4-10]$$

and the "1-3" exchange mechanism is described by an exchange coefficient matrix $\Pi^{(2)}$,

$$\Pi^{(2)} = \begin{pmatrix} -2 & 0 & 1 & 0 \\ 0 & -1 & 0 & 1 \\ 2 & 0 & -2 & 1 \\ 0 & 1 & 1 & -2 \end{pmatrix} \quad [4-11]$$

The results of a selective inversion experiment at 214 K, are shown in Fig. 4-5. The observed magnetization at site 2 rapidly decreases to a minimum at short times, and then slowly increases to its equilibrium value at long times, following the selective inversion of magnetization at site 1. The decrease in magnetization at site 3 is considerably slower than that at site 2, and the decrease at site 4 is the slowest. The rapid decrease of magnetization at site 2 following the selective inversion of magnetization at site 1, indicates rapid transfer of magnetization due to a "1-2" exchange process. The slower decrease at sites 3 and 4 occur by successive 3 → 2 and 4 → 3 transfers. This temporal behaviour of the magnetizations indicate qualitatively that again the "1-2" exchange process is the predominant exchange mechanism in the symmetric isomer as well. Least squares analysis of this set of data, with both $k_{(12)}$ and $k_{(13)}$ allowed to vary freely, yielded $k_{(12)} = 2.8 \pm 0.8 \text{ s}^{-1}$ and $k_{(13)} = -0.2 \pm 0.4 \text{ s}^{-1}$. A second least squares analysis with only $k_{(12)}$ allowed to vary and $k_{(13)}$ fixed at zero yielded, $k_{(12)} = 2.5 \pm 0.6 \text{ s}^{-1}$. The calculated

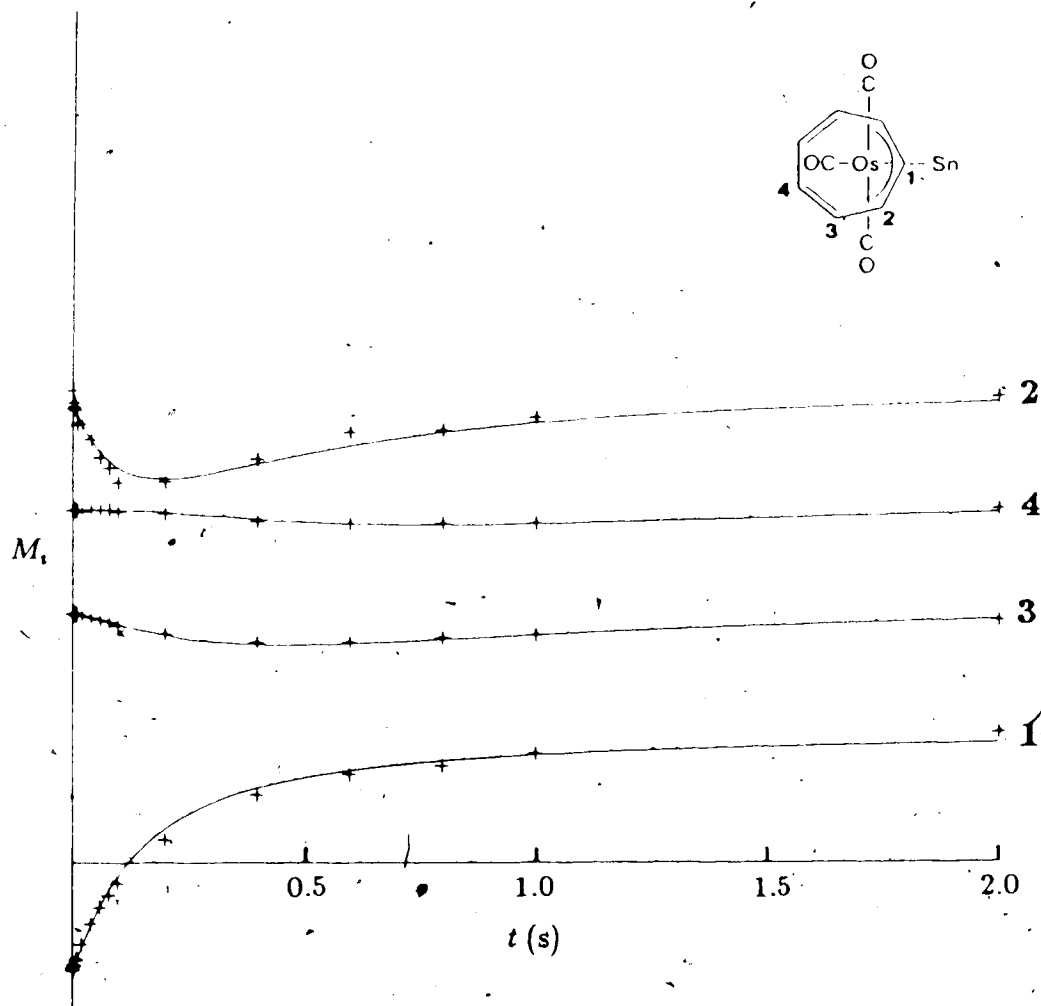


Fig. 4-5' Comparison of the observed and calculated magnetizations for the symmetric isomer at 214 K. + - Magnetizations $M_i(t)$ (arbitrary units) at the four sites of the symmetric isomer following the selective inversion of the site 1 magnetization. Curves represent least squares fit for $k_{(12)} = 2.5 \text{ s}^{-1}$ and $k_{(13)} = 0$.

magnetizations in Fig. 4-5, correspond to the second fit and the agreement between the calculated and observed magnetizations is extremely good, confirming that the "1-3" shifts are not important. Error estimates of the rate constants are expected to be higher in this case, since precise peak integrals are more difficult to obtain due to the distorted baseline. Even under such unfavourable conditions with severe baseline distortions, and the presence of another fast exchanging isomer, it was possible to delineate the definite exchange mechanism, and to obtain reliable rate constants for the "1-2" exchange process, using the selective inversion method. It is clear that any other method, like classical line shape analysis, would be practically impossible to use, in such cases.

The application of the selective inversion method to this organometallic complex clearly demonstrates the power and usefulness of the multisite magnetization transfer method in the investigation of complex exchange systems. The limitations of this method and other factors which affect the values of rate constants obtainable from this method will be illustrated in the next section.

4.5 Limitations of the multisite magnetization transfer method

The selective inversion method has been shown above to be a very powerful technique in the delineation of exchange mechanisms in complex systems. It is important to investigate the limitations of the method and the effects of imperfect data on the values of rate constants obtained. In this section, the effects of inefficient inversion, inaccurate T_1 values, and the neglect of cross relaxation effects in the analysis on the rate constants will be discussed.

4.5.1 Inefficient selective inversion

Although the DANTE sequence is very efficient in selectively inverting narrow resonances, difficulties may be encountered in inverting resonances which

are considerably broadened by exchange. Since it is practically impossible to achieve complete inversion even for a narrow resonance, the amount of inversion achievable in the case of a broad line could be considerably smaller. This reduces the extent of selective perturbation. The inverted signal would be of weak intensity and hence the time period following the inversion in which the magnetization recovers primarily, due to the exchange process, will be very short. This results in reducing the number of reliable data points that are obtainable at short times where the exchange effects are important. This decrease in the number of data points at higher exchange rates, relative to that at slower exchange rates, results in higher error estimates for rate constants that are derived from signals which are considerably broadened by exchange.

4.5.2 Effect of inaccurate T_1 values

In the least squares analysis of multisite magnetization transfer data, the parameters $1/T_{1i}$ are fixed at values which are independently determined from a non-selective inversion recovery experiment. In principle this is not required and the values of parameters $1/T_{1i}$ are also obtainable from the least squares analysis of selective inversion data. In practice, these parameters are not well determined when there is a large number of sites since there are too many variable parameters. For the selective inversion of site 2' magnetization in the asymmetric isomer of $(\eta^3\text{-C}_7\text{H}_7)\text{-Os}(\text{CO})_3\text{-SnPh}_3$, least squares analysis of the data shown in Fig. 4-3, with parameters $1/T_{1i}$ allowed to vary freely, gave $k_{(12)} = 9.1 \pm 1.3 \text{ s}^{-1}$, but negative unrealistic values were obtained for the relaxation times.

$1/T_{1i}$ are determined from non-selective inversion recovery experiments (see Eq. [4-3]), by fitting the data from each site to the equation,

$$M(\tau) = M(\infty) - (M(\infty) - M(0)) \exp(-\tau/T_1) \quad [4-12]$$

where, $M(\infty)$, $(M(\infty) - M(0))$ and $1/T_1$ are variable parameters. However, in the case of an exchanging system, the $1/T_1$ values obtained from the three parameter Eq. [4-12], contain contributions due to the exchange processes, and hence should be considered effective relaxation times, not the true relaxation times (86). The true relaxation times could only be obtained by a multiparameter analysis, including the exchange effects on the non-selective inversion recovery experiment (86). According to reference (86) in the limit of slow exchange,

$$1/T_{1\text{eff}} = 1/T_{1\text{true}}, \quad [4-13]$$

but the effective and true relaxation times may be different in the intermediate exchange range. Analysis of the non-selective inversion recovery data from the asymmetric isomer at 188 K, using the non-linear least squares method described earlier, failed to yield reliable relaxation rates for the seven sites, when the rate constant $k_{(12)}$ was allowed to vary freely with all the other parameters, or when it was fixed at 8.5 s^{-1} . In both cases very large or negative unrealistic values were obtained for the $1/T_1$ parameters. When the non-selective inversion recovery data from the simpler four site system of the symmetric isomer were analysed with fixed $k_{(12)}$, relaxation rates which are very close to values obtained from three parameter fits are obtained: at 214 K, relaxation rates for the four sites from multiparameter analysis with $k_{(12)}$ fixed at 2.6 s^{-1} are 1.0 ± 0.4 , 1.2 ± 0.3 , 0.8 ± 0.2 and $0.9 \pm 0.1\text{ s}^{-1}$ whereas the corresponding values from the three parameter fits are 1.0 ± 0.05 , 0.9 ± 0.02 , 1.1 ± 0.03 , and $1.1 \pm 0.03\text{ s}^{-1}$ respectively. Since, in the intermediate exchange region, the rate of exchange is much faster than the relaxation rate, the accuracy of the T_1 values is not found to be critical in the determination of rate constants. The results of least squares analyses of the magnetization transfer data following selective inversion of site 2' magnetization, of the asymmetric isomer of

$(\eta^3\text{-C}_7\text{H}_7)\text{-Os}(\text{CO})_3\text{-SnPh}_3$ for various $1/T_1$ values are shown in Table 4.2.

Table 4.2

$1/T_1 \text{ s}^{-1}$	$k_{(12)} \text{ s}^{-1}$
0.3	8.7 ± 1.6
0.6	8.5 ± 0.9
1.2	8.0 ± 1.4

These results clearly show that the rate constant obtained is relatively insensitive to the value of $1/T_1$ used, and that it is sufficient to use the values of $1/T_1$ which are obtainable from the three parameter fit of the non-selective inversion recovery data to Eq. [4-12].

4.5.3 Effects of Cross Relaxation

Cross relaxation effects have been neglected in the description of the multisite magnetization transfer method given in Chapter 3, and hence it is important to investigate the situations where these effects could be significant. It can be shown that, when the dipolar relaxation mechanisms are important, the cross relaxation rate is about half the spin lattice relaxation rate (87). Hence, especially when the exchange rate is smaller than or comparable to the proton spin-lattice relaxation rate, rate constants for "1-2" shifts estimated from this method may contain some contributions due to cross-relaxation. Since the dipolar relaxation is inversely dependent on the sixth power of the distance between relaxing spins, cross relaxation effects will not be significant in "1-3" shifts. The effect of cross relaxation on the slow $k_{(12)}$ rate constants can be examined by investigating a system where $k_{(12)} \leq 1/T_1$ for protons, using ^{13}C NMR, where the cross relaxation effects are not significant. Results of such an investigation are given in Chapter 6.

4.6 Summary

Experimental aspects of the DANTE selective inversion in multisite magnetization transfer experiments has been briefly discussed. The application of the selective inversion method to delineate the exchange mechanism was demonstrated using the test compound $(\eta^3\text{-C}_7\text{H}_7)\text{-Os}(\text{CO})_3\text{-SnPh}_3$. Results of selective inversion experiments were shown to give reliable, quantitative values for exchange rate constants. It was demonstrated that the method can be successfully applied to delineate mechanisms and to determine reliable rate constants, even under non-ideal conditions such as imperfect selectivity of inversion, baseline distortions and absence of data from one of the sites. The power of the technique was clearly shown in this particular example of a mixture of fluxional, but noninterconverting, symmetric and asymmetric isomers, since it was possible to quantitatively investigate the symmetric isomer, in the presence of interfering signals due to the rapidly fluxional asymmetric isomer, where a method like classical lineshape analysis would be inapplicable. Effects of the imperfect conditions such as the use of fixed effective relaxation rates instead of true relaxation rates in the least-squares analysis and not considering the cross relaxation effects were also discussed. The accuracy of relaxation rates was not found to be very critical for the determination of rate constants. Values of the rate constants for "1-2" shifts, may be overestimated due to cross relaxation effects when $k_{(12)} \leq 1/T_{1s}$.

The activation parameters obtained from the results of selective inversion experiments at different temperatures, for the "1-2" exchange process in this organometallic complex, will be discussed in the next chapter.

Fluxionality of $(\eta^3\text{-C}_7\text{H}_7)\text{-Os}(\text{CO})_3\text{-SnPh}_3$

5.1 Introduction

Fluxional molecules are defined as molecules which have several interconvertible configurations of the nuclei which are equivalent in structure and bonding and hence are of equal free energy (66). Interconversion of configurations occur by intramolecular degenerate rearrangements, and in many fluxional compounds, atoms of a given chemical species pass among several different chemical environments within the molecule, thus leading to a "site exchange" process, which is detectable by NMR spectroscopy. Thus, the study of fluxional behaviour is closely associated with the development of suitable NMR techniques. The power of the multisite magnetization transfer method, in the delineation of rearrangement mechanisms, and in the determination of exchange rate constants for these rearrangements has been clearly demonstrated in the previous chapter, using the fluxional organometallic complex, $(\eta^3\text{-C}_7\text{H}_7)\text{-Os}(\text{CO})_3\text{-SnPh}_3$ as a test case. In this chapter the results of a detailed investigation of the fluxional behaviour of this complex are presented. This complex belongs to the class of fluxional organometallic molecules in which a cyclic polyolefin is π -bonded to a metal atom. Fluxional behaviour of such organometallic complexes has been explained by Mingos (71), using the Woodward-Hoffmann orbital symmetry rules (72), based on a valence bond description of the bonding in the polyene and polyenyl complexes of transition metals. However, the predictive validity of these symmetry rules seems to be violated by the C_7H_7 ring system. For example, the metal migration in the

monohapto cycloheptatrienyl complex of the main group element Sn, $(\eta^1\text{-C}_7\text{H}_7)\text{-SnPh}_3$, was found to proceed via the "allowed" [1,5] sigmatropic shifts ("1-4" metal shifts) (88,89) whereas, the transition metal organometallic complex, $(\eta^1\text{-C}_7\text{H}_7)\text{-Re}(\text{CO})_5$ manifested its fluxionality via "forbidden" [1,7] sigmatropic shifts ("1-2" metal shifts) (90,91): $(\eta^2\text{-C}_7\text{H}_7)$ systems had been found to be highly fluxional, but $(\eta^5\text{-C}_7\text{H}_7)$ systems, which should be static according to the rules, have been found to be fluxional also (69,70,92). In earlier studies on $(\eta^3\text{-C}_7\text{H}_7)$ systems, the rearrangement mechanism was qualitatively established as "1-2" metal shifts, by observing the broadening of exchanging resonances at different temperatures (69,93-96). In the reviews by Mann (69,70) and the work of Reuvers (54,97) and Heinekey (91) activation parameters were obtained from the rate constants which were determined by fitting the ^1H or ^{13}C NMR lineshape, assuming a "1-2" shift mechanism, or sometimes only the approximate ΔG^\ddagger values, which are calculated from the coalescence temperature using approximate formulae, were reported.

The $(\eta^3\text{-C}_7\text{H}_7)\text{-Os}(\text{CO})_3\text{-SnPh}_3$ complex exists in solution as a mixture of distinct, non-interconverting, asymmetric/meridional ($\eta^3\text{-AO}_3$) and symmetric/facial ($\eta^3\text{-SO}_3$) geometrical isomers (65), which have distinctly different fluxionality (see appendix A for perspective drawings). Application of the selective inversion method enabled the study of the fluxional behaviour of both the asymmetric and symmetric isomers. The asymmetric isomer was studied in the low temperature range where only this isomer is fluxional, while the symmetric isomer was studied in the temperature range where both isomers are fluxional. The results of these experiments will be discussed in section 5.3. This will be followed by a comparison of the results obtained for these molecules, with the analogous Fe complex which had been studied by Reuvers (54,97). Finally the fluxional behaviour of the $(\eta^3\text{-C}_7\text{H}_7)\text{-Os}(\text{CO})_3\text{-SnPh}_3$ complex will be compared with the behaviour

of some related ($\eta^3\text{-C}_7\text{H}_7$) systems reported in the literature (91). The fluxional behaviour of some ($\eta^5\text{-C}_7\text{H}_7$) systems will be discussed in the next chapter.

5.2 Experimental

^1H NMR spectra of ($\eta^3\text{-C}_7\text{H}_7$)-Os(CO)₃-SnPh₃ in CD₂Cl₂ were recorded, at different temperatures, on a Bruker WH-400 spectrometer. The pulse sequence shown in Fig. 4-1 was used for the selective inversion experiments. In both asymmetric ($\eta^3\text{-A}_{\text{Os}}$) and symmetric ($\eta^3\text{-S}_{\text{Os}}$) isomers, site 1 magnetization was selectively inverted (see Figs. 4-2 and 4-4) and the experimental parameters were as described in section 4.2. Non-selective inversion recovery experiments [4-3] were also performed at each temperature. Temperatures were measured using a copper-constantan thermocouple inserted in a 5 mm NMR tube containing CD₂Cl₂, before and after each experiment. The uncertainty in the temperature measurement is about ± 1 K.

5.3 Results of Selective Inversion Experiments on ($\eta^3\text{-C}_7\text{H}_7$)-Os(CO)₃-SnPh₃

5.3.1 Rate Constants and Activation parameters for the Asymmetric isomer

It has been established that ($\eta^3\text{-C}_7\text{H}_7$)-Os(CO)₃-SnPh₃ exists as a mixture of two fluxional, but non-interconverting, symmetric and asymmetric isomers, and that only the asymmetric isomer is fluxional in the low temperature region below ~ 198 K (65). The fluxional nature of bonding between the Os atom, and the cycloheptatrienyl ring was believed to arise from a "1-2" metal shift (65). This was confirmed by the selective inversion experiments as discussed in section 4.3.2, and the presence of a "1-3" shift mechanism was quantitatively ruled out.

In the low temperature range, 180 K to 196 K, selective inversion data following the inversion of magnetization of site 1 of the asymmetric isomer, were analysed, using the least squares method described earlier, by fixing $k_{(13)} = 0$, and allowing $k_{(12)}$ to vary freely. It should be recalled here that rates of migration in both clockwise and anticlockwise senses were found to be identical, and that the rate constant $k_{(12)}$ which we use here is associated with the matrix of exchange coefficients $\Pi^{(1)}$ given in Eq. [4-6]. During the iterations $1/T_1$ values for each of the seven sites were fixed at the average of the $1/T_1$ values determined from the non-selective inversion recovery experiment at that temperature, since the $1/T_1$ values for individual sites were found to be equal within experimental error. The dependence of the rate constant $k_{(12)}$ on temperature is shown in Table 5.1.

Table 5.1 Rate constants for exchange in asymmetric $(\eta^3\text{-C}_7\text{H}_7)\text{-Os}(\text{CO})_3\text{-SnPh}_3$

T (K)	$k_{(12)}$ (s^{-1})	$1/T_1$ (s^{-1})
180.0	3.98 ± 0.62	0.40
186.5	5.85 ± 0.80	0.47
191.0	11.07 ± 1.14	0.56
196.0	16.07 ± 1.91	0.65

The activation energy for the "1-2" exchange process was obtained by a linear least squares fitting of the data shown in Table 5.1 to a linearized Arrhenius equation, and other activation parameters are similarly obtained by linear regression, using the Eyring equation. Values obtained for the activation parameters E_a , ΔH^\ddagger and ΔS^\ddagger are given in Table 5.3, together with activation parameters obtained for the symmetric isomer.

5.3.2 Rate constants and activation parameters for the symmetric isomer

The symmetric isomer was found to be fluxional in the temperature range above ~ 198 K only (65). Above 198 K, the asymmetric isomer approaches the rapid exchange region, and resonances due to the sites 2,3 and 4 of the symmetric isomer are superimposed on the broad peaks from the asymmetric isomer, as shown in Fig. 4-4. Selective inversion experiments were performed at several different temperatures in the range 203 K to 233 K, by inverting the unobstructed site 1 magnetization of the symmetric isomer. Fluxional behaviour of this isomer was also found to arise from a "1-2" shift mechanism, as shown earlier in section 4.4. Thus magnetization transfer data at different temperatures were analysed to obtain $k_{(12)}$, by fixing $k_{(13)}$ at zero during iterations, and the values of rate constant $k_{(12)}$ are tabulated in Table 5.2.

Table 5.2 Rate constants for the symmetric isomer

T (K)	$k_{(12)}$ (s^{-1})	$\overline{1/T_1}$ (s^{-1})
203.0	0.97 ± 0.38	0.80
214.0	2.56 ± 0.58	1.00
224.0	6.26 ± 1.89	1.10
233.0	21.71 ± 10.70	1.13

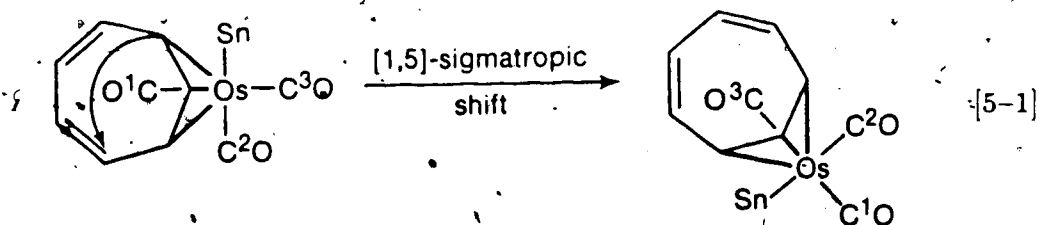
It should be mentioned that the errors in rate constants were larger for the symmetric isomer than for the asymmetric isomer. These larger errors are primarily due to the difficulties in obtaining precise integrals, owing to the severe distortion of the baseline as discussed in section 4.4. The error in the rate constant at 233 K is further increased by the short dynamic range at this particular temperature due to rather broad and less intense resonances which yield only a few

data points in the short times where the exchange effects are dominant. For the symmetric isomer, a higher activation energy was obtained than for the asymmetric isomer as expected, and the values of activation parameters are given in Table 5.3.

Table 5.3 Activation parameters for $(\eta^3\text{-C}_7\text{H}_7)\text{-Os}(\text{CO})_3\text{-SnPh}_3$

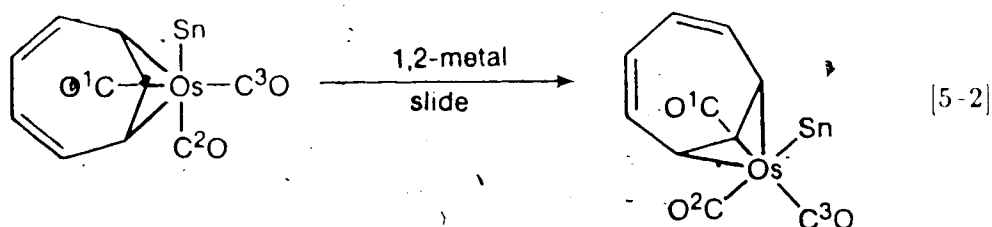
	E_a (kcal/mol)	ΔH^\ddagger (kcal/mol)	ΔS^\ddagger (cal/mol K)
Asymmetric isomer	6.35 ± 0.81	5.98 ± 0.81	-21.7 ± 4.3
Symmetric isomer	9.50 ± 1.01	9.07 ± 1.01	-13.4 ± 4.6

According to the predictions based on the Woodward-Hoffmann symmetry rules as formulated by Mingos and others (69-71), "1-2" metal migrations in $(\eta^3\text{-C}_7\text{H}_7)$ complexes are expected to occur by "allowed" [1,5] sigmatropic shifts. However, an "allowed" [1,5] sigmatropic shift would interconvert enantiomeric asymmetric isomers in one step, and this process should occur with the simultaneous averaging of the two axial carbonyl groups:



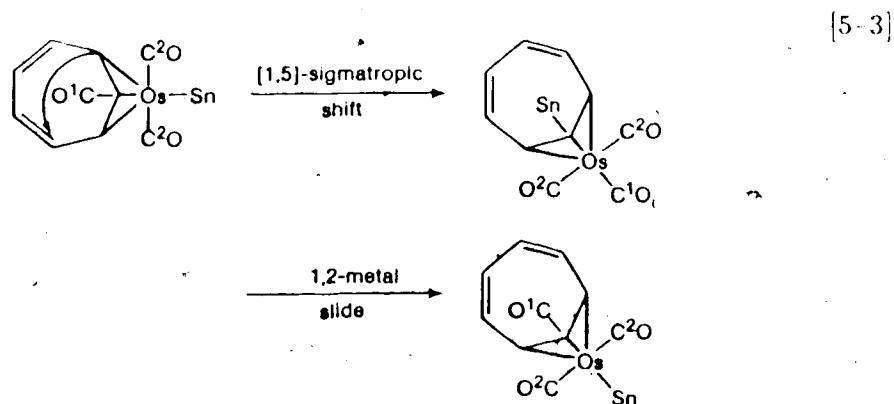
By the examination of the ^{13}C resonances in both the cycloheptatrienyl region and the carbonyl region, Kiel and Takats (65) have shown that, contrary to the requirements of the [1,5] sigmatropic shifts, the ring whizzing process and the carbonyl

exchange process are not coupled: the CO resonances had shown little broadening at a temperature where the C_7H_7 resonances are virtually collapsed, and Kiel and Takats (98) have determined the ΔG^\ddagger for the axial carbonyl ligand exchange to be 13.1 kcal/mol at the coalescence temperature (284 K). Thus they have postulated that the low temperature ring whizzing may occur via a simple slide of the rigid $Os(CO)_3-SnPh_3$ moiety over the π -surface of the cycloheptatrienyl ring(65):



Results of the selective inversion experiments show that the activation barrier for the low temperature "1-2" metal migration process (see Table 5.3) is smaller than the activation barrier for the exchange of axial carbonyl ligands ($\Delta G^\ddagger = 13.1$ kcal/mol), thus strongly supporting the suggestion of Kiel and Takats (65) that, at low temperature, "1-2" metal shifts and the exchange of carbonyl ligands occur by different mechanisms.

Kiel and Takats (65) have also shown that an "allowed" [1,5] sigmatropic shift would produce an alternate higher energy symmetric isomer, and return to the original symmetric isomer would occur after two consecutive steps giving rise to an overall "1-3" metal shift in the symmetric isomer. However, by observing the exchange broadening of the ^{13}C resonances of the C_7H_7 ring, they have speculated that "1-2", not overall "1-3", metal shifts operate in this isomer as well (65).



The results of the selective inversion experiments reported in this chapter confirm that "1-2" metal shifts occur in the symmetric isomer, but this "1-2" shift has a higher activation energy than the "1-2" process in the asymmetric isomer. This confirmation of the presence of "1-2" shifts in the symmetric isomer gives strong support to the simple metal sliding mechanism in this isomer as well, instead of a "1-3" metal shift as predicted by the Woodward-Hoffmann symmetry rules.

5.3.3 Comparison of Fluxional behaviour of $(\eta^3\text{-C}_7\text{H}_7)\text{-M}(\text{CO})_3\text{-SnPh}_3$ ($\text{M}=\text{Fe}, \text{Os}$) systems

It is instructive to compare the fluxional behaviour of $(\eta^3\text{-C}_7\text{H}_7)\text{-Os}(\text{CO})_3\text{-SnPh}_3$ with analogous $(\eta^3\text{-C}_7\text{H}_7)\text{-M}(\text{CO})_3\text{-SnPh}_3$ systems. Unfortunately, no direct analogue of the $(\eta^3\text{-C}_7\text{H}_7)\text{-Os}(\text{CO})_3\text{-SnPh}_3$ asymmetric isomer has been reported. The Fe analogue of the symmetric isomer had been studied by Reuvers using ^1H NMR (54), and by Reuvers and Takats (97) using ^{13}C NMR. In the case of $(\eta^3\text{-C}_7\text{H}_7)\text{-Fe}(\text{CO})_3\text{-SnPh}_3$ only the symmetric isomer was present, and the fluxional behaviour of this isomer was qualitatively attributed to "1-2" metal shifts by observing the temperature dependent exchange broadening of the four ^1H resonances of the C_7H_7 moiety. Reuvers and Takats (97) have reported the

activation parameters, ΔH^\ddagger , ΔS^\ddagger calculated using the rate constants which had been obtained by ^{13}C NMR lineshape fitting in the temperature range 170–213 K. These activation parameters and the activation energy for the “1 2” shifts for this complex are compared with those obtained for $(\eta^3\text{-C}_7\text{H}_7)\text{-Os}(\text{CO})_3\text{-SnPh}_3$ symmetric isomer in Table 5.4.

Table 5.4 Activation parameters for $(\eta^3\text{-C}_7\text{H}_7)\text{-M}(\text{CO})_3\text{-SnPh}_3$ symmetric isomer

M	E_a (kcal/mol)	ΔH^\ddagger (kcal/mol)	ΔS^\ddagger (cal/mol K)	Ref
Fe	8.0 ± 0.2	7.6 ± 0.2	8.4 ± 1.0	97
Os	9.5 ± 1.0	9.1 ± 1.0	13.4 ± 4.6	This work

Although the differences between the activation parameters of the two complexes are small, they follow the normal trend that the activation energy for metal migration increases in descending a transition metal group; i.e. activation energy for migration is in the order $\text{Fe} < \text{Ru} < \text{Os}$ (99–101). However, in contrast to the absence of carbonyl group scrambling in the symmetric isomer of $(\eta^3\text{-C}_7\text{H}_7)\text{-Os}(\text{CO})_3\text{-SnPh}_3$, the two CO signals observed in the $(\eta^3\text{-C}_7\text{H}_7)\text{-Fe}$ analogue were broad at low temperature and coalesced as the temperature was raised (54,97). Reuvers and Takats (97) have reported the activation parameters, $E_a = 8.4 \pm 0.1$ (kcal/mol), $\Delta H^\ddagger = 8.5 \pm 0.1$ (kcal/mol) and $\Delta S^\ddagger = -8.6 \pm 0.6$ (kcal/mol) for this carbonyl exchange process, by fitting the ^{13}C NMR lineshape but it is not certain whether the metal migration and the CO exchange are independent or coupled together and proceed by the same mechanism.

5.4 Comparison of fluxional behaviour of $(\eta^3\text{-C}_7\text{H}_7)\text{-Os}(\text{CO})_3\text{-SnPh}_3$ with other fluxional $(\eta^3\text{-C}_7\text{H}_7)$ systems with symmetric and asymmetric isomers

Only a few $(\eta^3\text{-C}_7\text{H}_7)$ complexes which exist as a mixture of fluxional symmetric and asymmetric isomers, similar to the $(\eta^3\text{-C}_7\text{H}_7)\text{-Os}$ case studied, have been reported. It has been shown by Heinekey (91) that $(\eta^3\text{-C}_7\text{H}_7)\text{-Re}(\text{CO})_3\text{-P}(\text{CH}_3)_3$ exists as a mixture of symmetric and asymmetric isomers, and that the exchange broadening of ^1H NMR resonances (400 MHz) observed in the temperature range, 233 K to \sim 298 K indicates qualitatively that Re migration occurs by "1-2" shifts. Below 303 K the PMe_3 group was seen as two distinct doublets in the ^1H NMR spectrum, indicating that there is little isomer interconversion below ambient temperature. This was also considered as evidence of the absence of axial-equatorial carbonyl scrambling. Heinekey (91) has noted that this was consistent with the absence of carbonyl scrambling accompanying Re migration in the complex $(\eta^3\text{-C}_7\text{H}_7)\text{-Re}(\text{CO})_4$, for which he has reported the activation parameters, $\Delta H^\ddagger = 14.6 \pm 0.2$ kcal/mol, $\Delta S^\ddagger = 7.4 \pm 0.8$ cal/mol K and $\Delta G^\ddagger_{300} = 12.4 \pm 0.3$ kcal/mol, for "1-2" metal shifts, based on a ^{13}C NMR line-shape analysis. However, there is no quantitative information available for the isomers of the $(\eta^3\text{-C}_7\text{H}_7)\text{-Re}(\text{CO})_3\text{-P}(\text{CH}_3)_3$ complex. Heinekey (91) has concluded that, in both $(\eta^3\text{-C}_7\text{H}_7)\text{-Re}(\text{CO})_4$ and $(\eta^3\text{-C}_7\text{H}_7)\text{-Re}(\text{CO})_3\text{-P}(\text{CH}_3)_3$, Re migration apparently occurs via a mechanism which does not scramble other ligands attached to the metal. It should be mentioned here that the observations of Heinekey can be explained by considering the simple slide of the metal over the cycloheptatrienyl ring as suggested by Kiel and Takats (65) for the $(\eta^3\text{-C}_7\text{H}_7)\text{-Os}(\text{CO})_3\text{-SnPh}_3$ complex.

Heinekey (91) has also reported the fluxional behaviour of the analogous Mn complex, $(\eta^3\text{-C}_7\text{H}_7)\text{-Mn}(\text{CO})_3\text{-P}(\text{CH}_3)_3$, which was again qualitatively

established to exhibit "1 2" metal shifts. This complex also exists as a mixture of symmetric and asymmetric isomers, but they were found to be interconverting in this case. From the observed spectral changes in the PMe_3 region, quantitative information about the interconversion rate has been obtained, but it is not mentioned whether any ligand scrambling independent of this interconversion is occurring or not, similar to the observation of carbonyl scrambling in the $(\eta^3\text{-C}_7\text{H}_7)\text{-Os}(\text{CO})_3\text{-SnPh}_3$ asymmetric isomer (65) or the $(\eta^3\text{-C}_7\text{H}_7)\text{-Fe}(\text{CO})_3\text{-SnPh}_3$ symmetric isomer (54,97).

5.5 Summary

The multisite magnetization transfer method was successfully applied to the study of the fluxional behaviour of a noninterconverting mixture of asymmetric/meridional and symmetric/facial isomers of $(\eta^3\text{-C}_7\text{H}_7)\text{-Os}(\text{CO})_3\text{-SnPh}_3$ and the rate constants and activation parameters were determined for metal migration in both isomers. The symmetric isomer was shown to have a significantly higher activation energy for "1-2" metal shifts than that of the asymmetric isomer. It was not possible to make any generalizations from a comparison of the fluxional behaviour of other similar $(\eta^3\text{-C}_7\text{H}_7)$, symmetric and asymmetric systems. The comparisons themselves were difficult due to the lack of reliable quantitative information from other studies. This seems to be the first detailed study of the fluxionality of such a mixture of $(\eta^3\text{-C}_7\text{H}_7)$ isomers which provides quantitative information about the fluxionality of both symmetric and asymmetric isomers in the mixture. Quantitative results obtained in this study support the simple metal sliding mechanism, suggested by Kiel and Takats (65), for the metal migration in both isomers, and not the [1,5] sigmatropic shift mechanism as predicted by the Woodward-Hoffman symmetry rules.

The fluxional behaviour of the related pentahapto complexes $(\eta^5\text{-C}_7\text{H}_7)\text{-M}(\text{CO})_2\text{-SnPh}_3$, (M=Fe, Ru, Os), which are of special interest regarding the predictive validity of the Woodward-Hoffmann symmetry rules in the description of the fluxionality of metal cycloheptatrienyl complexes, will be discussed in the next chapter.

CHAPTER 6

Fluxionality of $(\eta^5\text{-C}_7\text{H}_7)\text{-M}(\text{CO})_2\text{-SnPh}_3$, $\text{M}=\text{Fe}, \text{Ru}, \text{Os}$

6.1 Introduction

The fluxional behaviour of an isomeric mixture of η^3 -cycloheptatrienyl complexes of the transition metal Os was described in detail in the previous chapter. "1-2" metal shifts were found to be responsible for the fluxional behaviour in both isomers, as had been predicted and observed for $\eta^3\text{-C}_7\text{H}_7$ complexes of transition metal organometallic compounds (69,70). The multisite magnetization transfer method has also been applied to study the fluxional behaviour of some η^5 -cycloheptatrienyl complexes of group 8B transition metals and the results of these investigations are discussed in this chapter.

Although fluxional behaviour of transition metal organometallic compounds has been studied by many workers (66-70,92), only a very few $\eta^5\text{-C}_7\text{H}_7$ compounds have been reported, as presented in recent reviews by Mann (69,70). Fluxional behaviour of $\eta^5\text{-C}_7\text{H}_7$ -systems is of special interest since attempts to use the Woodward-Hoffmann symmetry rules to explain their fluxionality have been largely unsuccessful. According to these rules, $\eta^5\text{-C}_7\text{H}_7$ systems are predicted to be rigid (69,70), but most of the known systems exhibited fluxional behaviour (54,92-105). In most cases, the mechanism was qualitatively established to be a "1-2" metal shift, but in the case of $(\eta^5\text{-C}_7\text{H}_7)\text{-Fe}(\text{CO})_2\text{-SnPh}_3$ attempts to fit variable temperature ^1H NMR lineshape assuming a "1-2" shift mechanism were reported to be unsuccessful and did not unambiguously ascertain whether "1-2", "1-3" or "1-4" shifts were responsible (54). Although saturation transfer

experiments on this complex indicated the presence of a "1-3" shift mechanism, no quantitative information is available (106). The selective inversion method provides an unambiguous way of establishing these mechanisms, and the results of the application of this method to the study of the fluxional behaviour of this complex are described in section 6.3. This will be followed by the description of the results of experiments on analogous complexes of Os and Ru. The Ru complex exists as a mixture of interconverting symmetric and asymmetric isomers (98) and in this complex the isomer interconversion process was also studied using the selective inversion method. The results of the isomer interconversion study are presented in section 6.5 before the results for the migration process. The results obtained for the fluxional behaviour of the complexes $(\eta^5\text{-C}_7\text{H}_7)\text{-M}(\text{CO})_2\text{-SnPh}_3$, $\text{M}=\text{Fe}$, Ru , Os , will be compared with each other in section 6.6 and with other $\eta^5\text{-C}_7\text{H}_7$ systems reported in the literature (91,102-105) in section 6.7.

6.2 Experimental

^1H NMR spectra of the complexes $(\eta^5\text{-C}_7\text{H}_7)\text{-M}(\text{CO})_2\text{-SnPh}_3$, $\text{M}=\text{Fe}$, Ru , were recorded on a Bruker WH-400 spectrometer and ^1H NMR of the analogous complex of Os were recorded on a Bruker WH-200 spectrometer. The pulse sequence shown in Fig. 4-1 was used for the experiments, with parameters for the DANTE selective inversion chosen as described in section 4.2

The iron complex was studied using $\text{THF-}d_8$ as solvent. Two sets of selective inversion experiments were performed at each of six different temperatures in the range 258 K to 283 K. In the first set the magnetization at site 2 was inverted, and in the second set the magnetization at site 4 was inverted (see Fig. 6-1).

^1H NMR spectra of $(\eta^5\text{-C}_7\text{H}_7)\text{-Os}(\text{CO})_2\text{-SnPh}_3$ in $\text{toluene-}d_8$ were recorded at five different temperatures in the range 268 K to 298 K. The site 1 magnetization

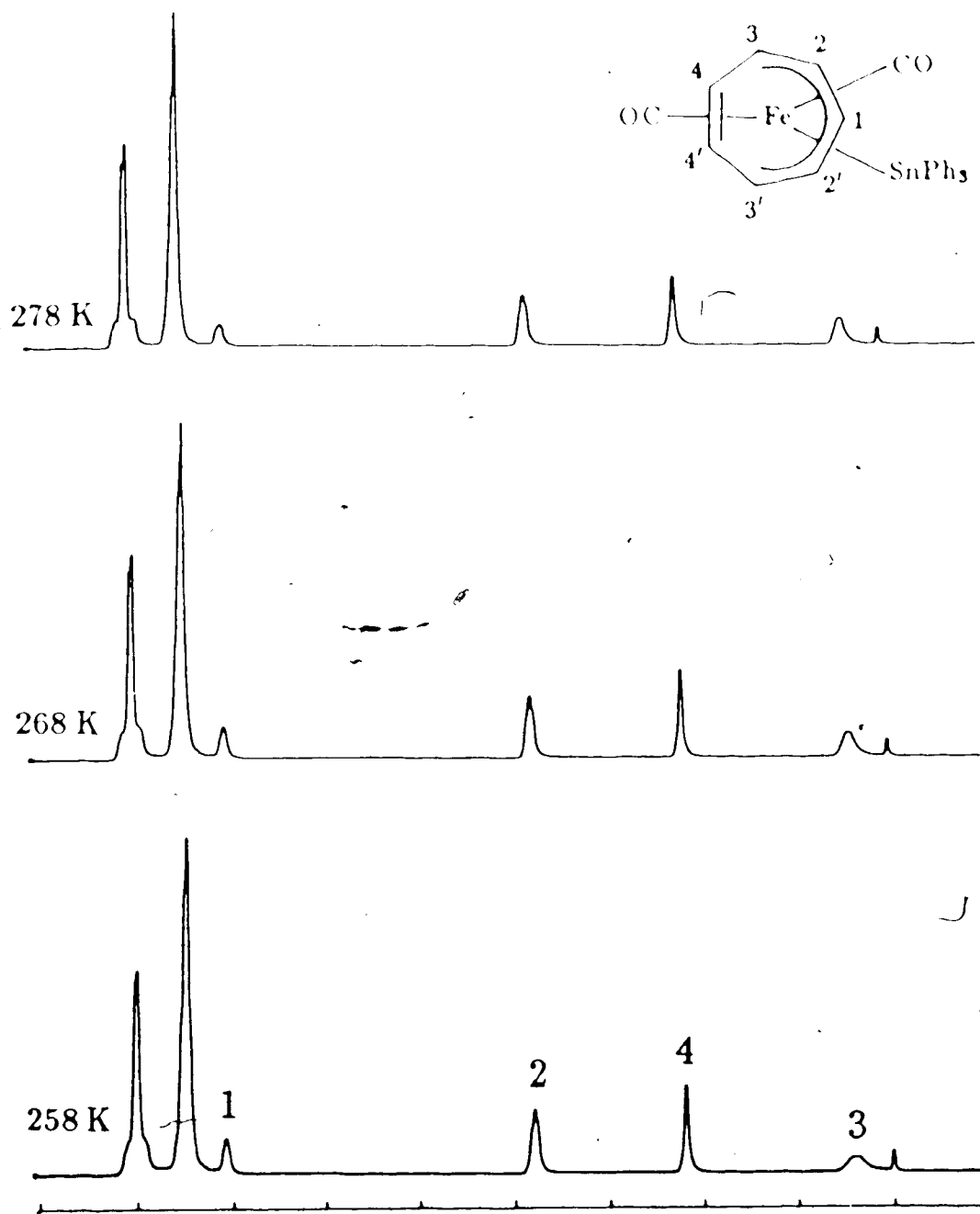


Fig. 6-1. ^1H NMR spectra (400 MHz) of the C_7H_7 region for $(\eta^5\text{-C}_7\text{H}_7)\text{-Fe}(\text{CO})_2\text{-SnPh}_3$ in $\text{THF-}d_8$ at 258, 268 and 278 K (200 Hz/division). Peaks labelled 1, 2, 3 and 4 arise from the time averaging of $\{\text{H}_1\}$, $\{\text{H}_2, \text{H}_2'\}$, $\{\text{H}_3, \text{H}_3'\}$ and $\{\text{H}_4, \text{H}_4'\}$ of asymmetric enantiomers.

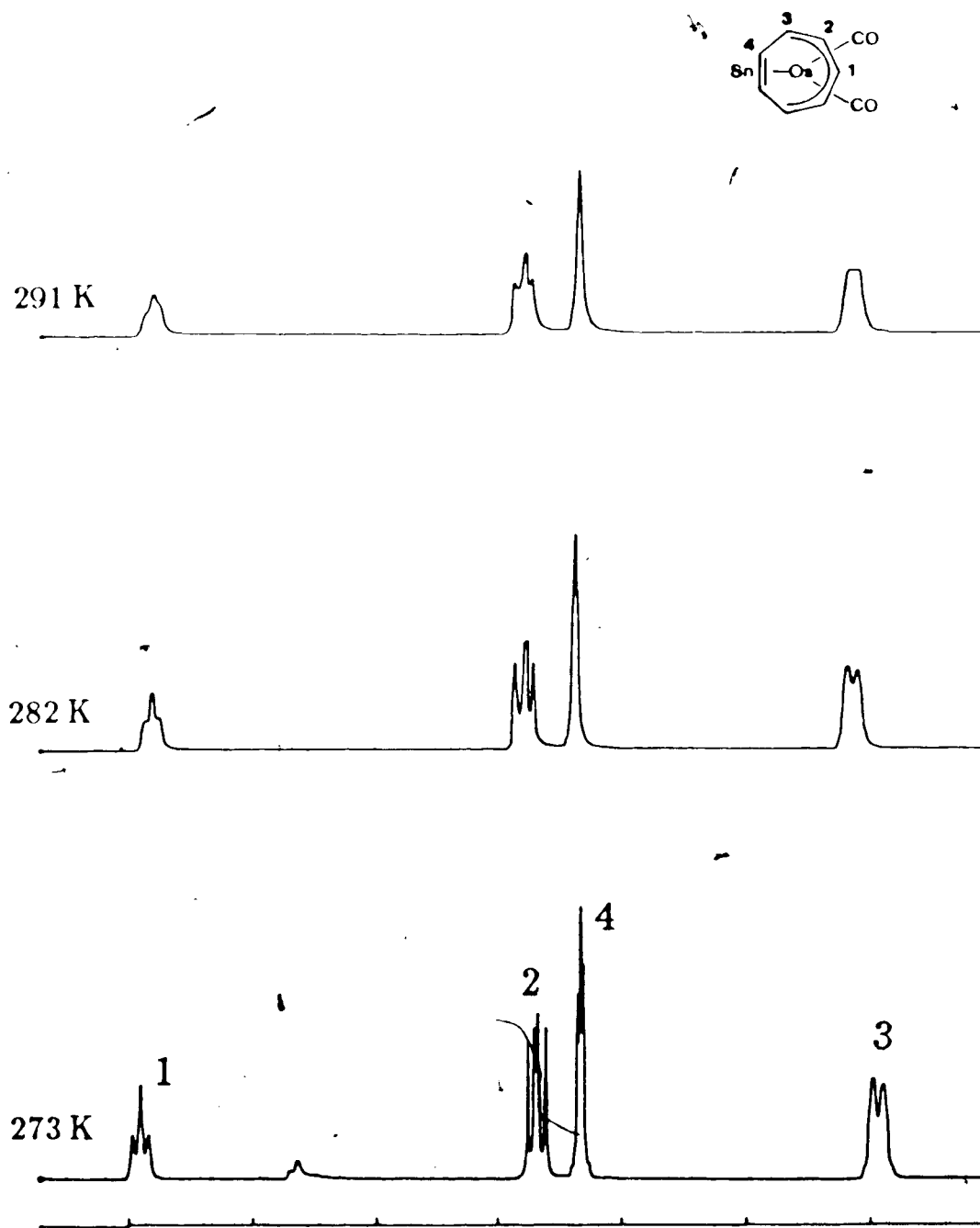


Fig. 6-2 ^1H NMR spectra (200 MHz) of the C_7H_7 region for $(\eta^5\text{-C}_7\text{H}_7)\text{-Os}(\text{CO})_2\text{-SnPh}_3$ in $\text{toluene-}d_8$ at 273, 282 and 291 K (100 Hz/division). Peaks labelled 1, 2, 3 and 4 are due to the symmetric isomer.

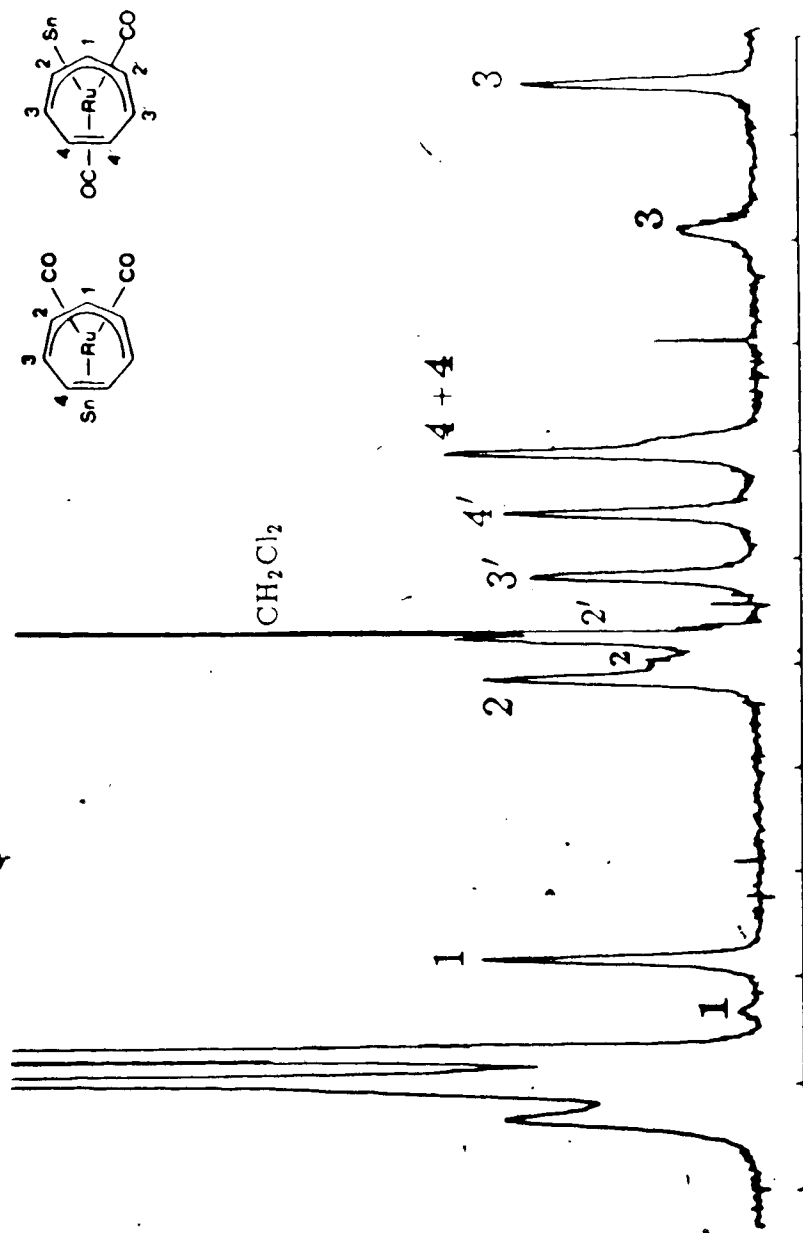


Fig. 6-3 ^1H NMR spectrum (400 MHz) of the C_7H_7 region for $(\eta^5\text{-C}_7\text{H}_7)\text{-Ru}(\text{CO})_2\text{-SnPh}_3$ in CD_2Cl_2 at 183 K (200 Hz/division). Peaks labelled 1, 1', 2, 2',

3, 3', 4 and 4' arise from the asymmetric isomer, and peaks 1, 2, 3 and

4 are due to the symmetric isomer.

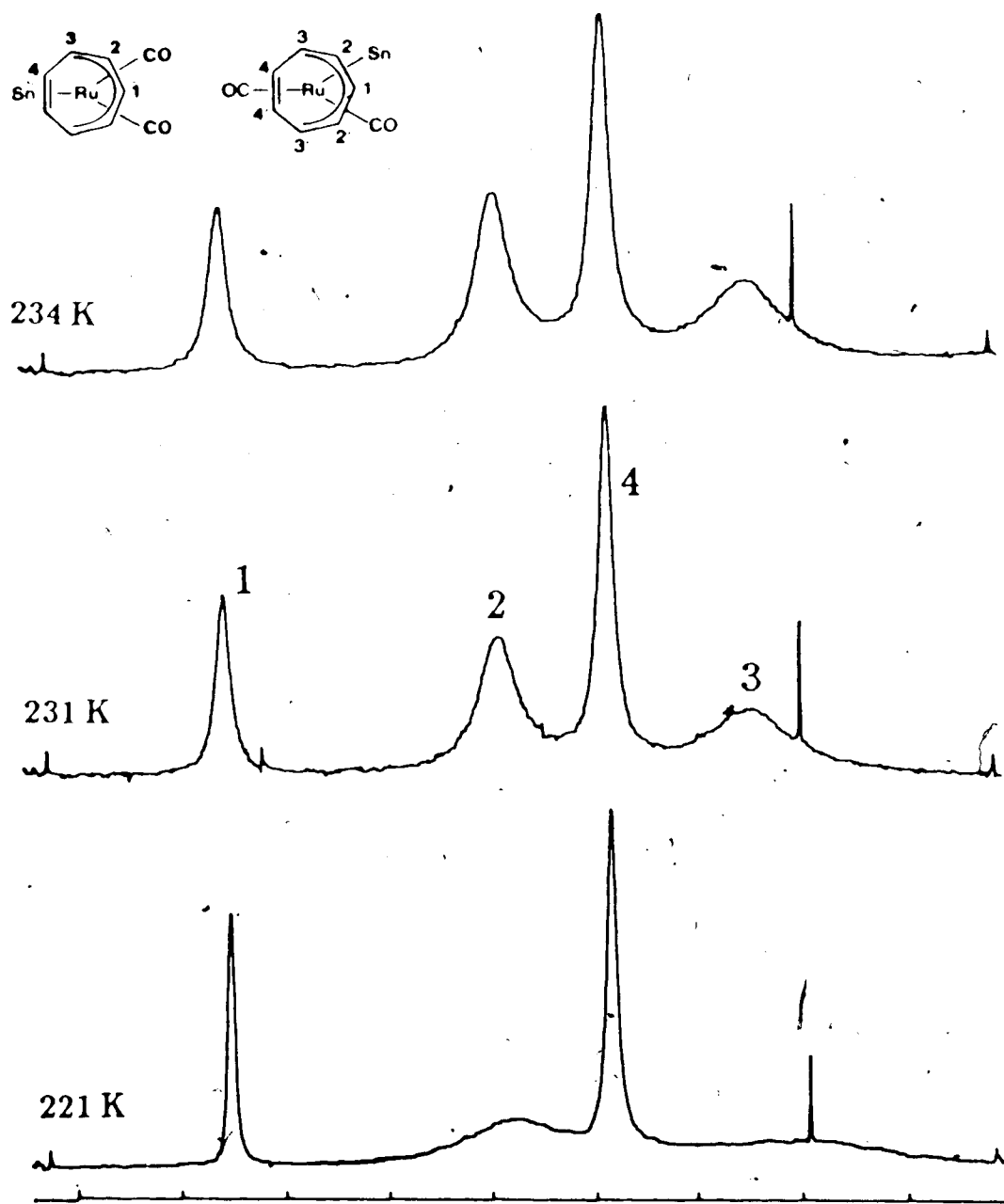


Fig. 6-4 ^1H NMR spectra (400 MHz) of the C_7H_7 region for $(\eta^5\text{-C}_7\text{H}_7)\text{-Ru}(\text{CO})_2\text{-SnPh}_3$ in $\text{toluene-}d_8$ at 221, 231, and 234 K (200 Hz/division). Peaks labelled 1, 2, 3 and 4 arise from the time averaging of $\{\text{H}_1, \text{H}_1\}$, $\{\text{H}_2, \text{H}_2', \text{H}_2\}$, $\{\text{H}_3, \text{H}_3', \text{H}_3\}$ and $\{\text{H}_4, \text{H}_4', \text{H}_4\}$.

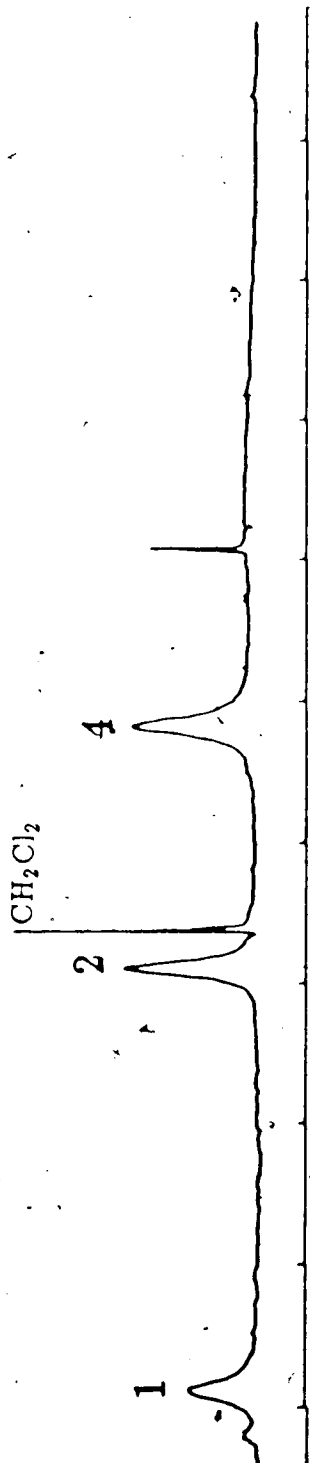
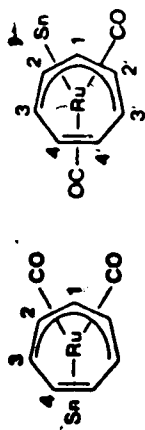


Fig. 6-5 ^1H NMR spectrum (400 MHz) of the C_7H_7 region for $(\eta^5\text{-C}_7\text{H}_7)\text{-Ru(CO)}_2\text{-SnPh}_3$ in CD_2Cl_2 at 232 K (200 Hz/division). Peaks labelled 1, 2 and 4 arise from the time averaging of $\{\text{H}_1, \text{H}_1\}$, $\{\text{H}_2, \text{H}_2, \text{H}_2\}$ and $\{\text{H}_4, \text{H}_4, \text{H}_4\}$.

was inverted at each of the five temperatures and measurements were also taken at temperatures 273 K and 291 K in which site 3 magnetization was selectively inverted (Fig. 6-2). For these experiments performed on the WH-200 spectrometer, the non-selective 90° ^1H pulse width was $5.2\ \mu\text{s}$. Only 18-20 pulses of small flip angle were used for the DANTE selective inversion, with DANTE pulse delays in the range of 0.700-1.390 ms. A ^{13}C NMR selective inversion experiment (at 100.6 MHz, on the WH-400 spectrometer) was also performed on this complex, at 273 K, using the same sample as used for ^1H NMR experiments. ^{13}C magnetization at site 2 was inverted using the DANTE sequence, and the maximum inversion was obtained with 20 pulses of $1.2\ \mu\text{s}$ duration with $455\ \mu\text{s}$ delays between them. The ^{13}C 90° non-selective pulse was $11.2\ \mu\text{s}$. In this case, two of the DANTE sidebands were allowed to fall within the spectral region of interest, but they were sufficiently removed from the other resonances of interest. Broadband ^1H decoupling was employed throughout the experiment.

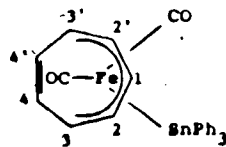
In the case of the Ru complex, isomer interconversion was studied using CD_2Cl_2 as the solvent. The ^1H NMR assignment of the C_7H_7 moiety was confirmed by selective decoupling experiments, at a temperature just below 178 K. Isomer interconversion was studied by inverting the site 3 magnetization of the asymmetric isomer in the temperature range 178 K to 189 K (see Fig. 6-3). At 178 K, a second experiment was also performed by inverting the magnetization of site 3 of the symmetric isomer (see Fig. 6-3). The mechanism of metal migration around the C_7H_7 ring was studied by selective inversion experiments in the temperature range 221 to 233 K using samples of this complex in CD_2Cl_2 and toluene- d_8 solvents. In these experiments, magnetization at either site 1 or 2 was inverted (Figs. 6-4 and 6-5).

In order to determine ^1H relaxation times, non-selective inversion-recovery experiments were performed at each temperature using the pulse sequence [4-3].

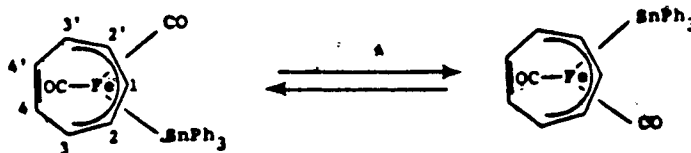
In order to obtain the ^{13}C relaxation times for the complex, the same sequence was used with continuous broadband proton decoupling during the experiment. All proton fid's were transformed without any linebroadening or zero filling, but ^{13}C fid's were transformed with 3 Hz linebroadening and no zero filling. All temperatures were measured using a copper-constantan thermocouple inserted in a 5 mm NMR tube containing the solvent before and after the experiment. The uncertainty in the temperature measurement is about $\pm 1\text{ K}$ for ^1H NMR experiments, but was estimated to be about $\pm 2\text{ K}$ over the long duration of the ^{13}C NMR experiment.

6.3 Fluxional Behaviour of $(\eta^5\text{-C}_7\text{H}_7)\text{-Fe}(\text{CO})_2\text{-SnPh}_3$

It has been established that $(\eta^5\text{-C}_7\text{H}_7)\text{-Fe}(\text{CO})_2\text{-SnPh}_3$ exists as an asymmetric isomer, with known solid state structure



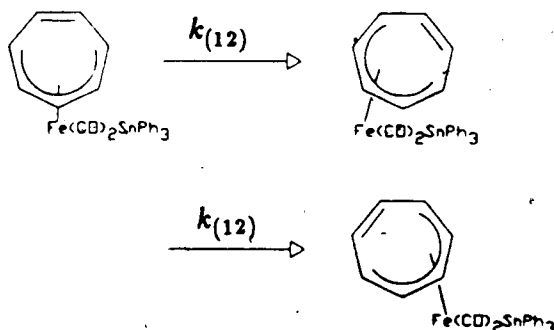
and, because of the asymmetry, all seven protons and carbons in the C_7H_7 ring are chemically non equivalent (54). It has been also shown that in addition to the migration of the Fe atom around the C_7H_7 ring which occurs at temperatures above 258 K, there is a second exchange process due to the enantiomeric interconversion of the asymmetric isomer at lower temperature (54):



This enantiomer interconversion induces a plane of symmetry in the seven membered ring with a resulting averaging of the chemical shift differences at sites 2 and 2', 3 and 3' and 4 and 4'. For the enantiomer interconversion at lower temperatures, an activation barrier of ~ 9.5 kcal/mol has been estimated by Reuvers (54) from the coalescence of the ^{13}C resonance of the carbonyl groups. Qualitative determination of the mechanism of migration of the Fe atom around the C_7H_7 ring has been difficult due to the significantly large proton spin-spin coupling which gives rise to multiplets and differences in linewidths observed at temperatures just above 258 K, where the four resonances due to protons 1, (2,2'), (3,3') and (4,4') are still resolved (54). Attempts to simulate the spectra by assuming "1-2" shifts has failed, and an unambiguous assignment of the mechanism has not been made (54). Thus the fluxional behaviour of this complex was studied in the temperature range 258 K to 283 K where the four resonances are resolved, using the selective inversion method. In order to avoid any ambiguities, the magnetization corresponding to sites 2(2,2') and 4(4,4') were selectively inverted in separate experiments. Delineation of the exchange mechanism is described in the following section and the rate constant and activation parameters are given in 6.3.2.

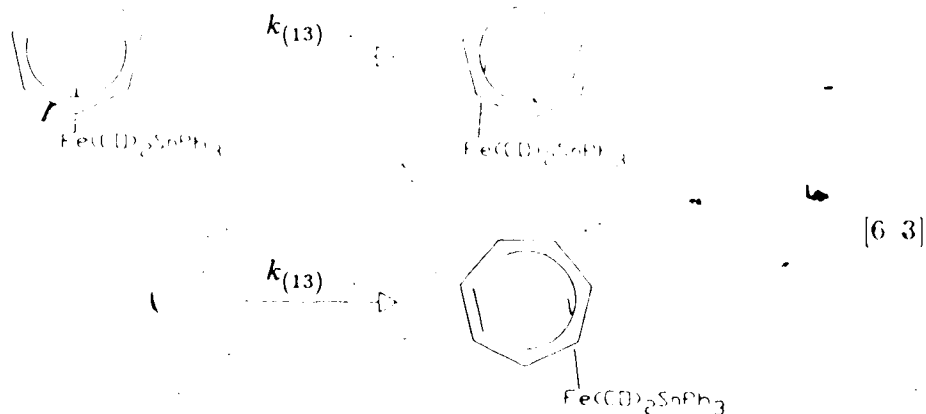
6.3.1 Delineation of the exchange mechanism of $(\eta^5\text{-C}_7\text{H}_7)\text{-Fe(CO)}_2\text{-SnPh}_3$

In order to establish the exchange mechanism in the $(\eta^5\text{-C}_7\text{H}_7)\text{-Fe(CO)}_2\text{-SnPh}_3$ systems, a "1-2" shift mechanism

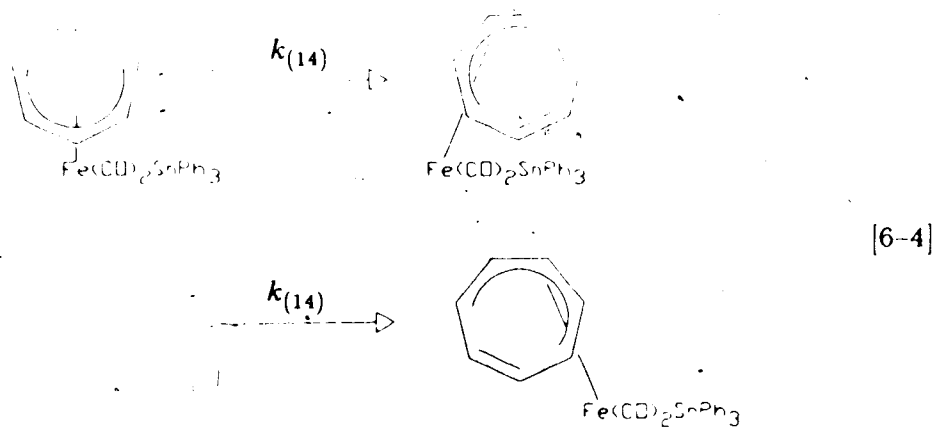


[6-2]

a "1-3" process



described by the matrices of exchange coefficients $\Pi^{(1)}$ and $\Pi^{(2)}$ given in Eqs. [4-10] and [4-11] respectively, and the "1-4" process,



described by a rate constant $k_{(14)}$ and a matrix of exchange coefficients $\Pi^{(3)}$

$$\Pi^{(3)} = \begin{pmatrix} -2 & 0 & 0 & 1 \\ 0 & -2 & 1 & 1 \\ 0 & 1 & -1 & 0 \\ 2 & 1 & 0 & -2 \end{pmatrix} \quad [6-5]$$

were considered.

Results of a selective inversion experiment at 263 K, following the inversion of magnetization at site 2, are shown in Fig. 6-6. Qualitative examination

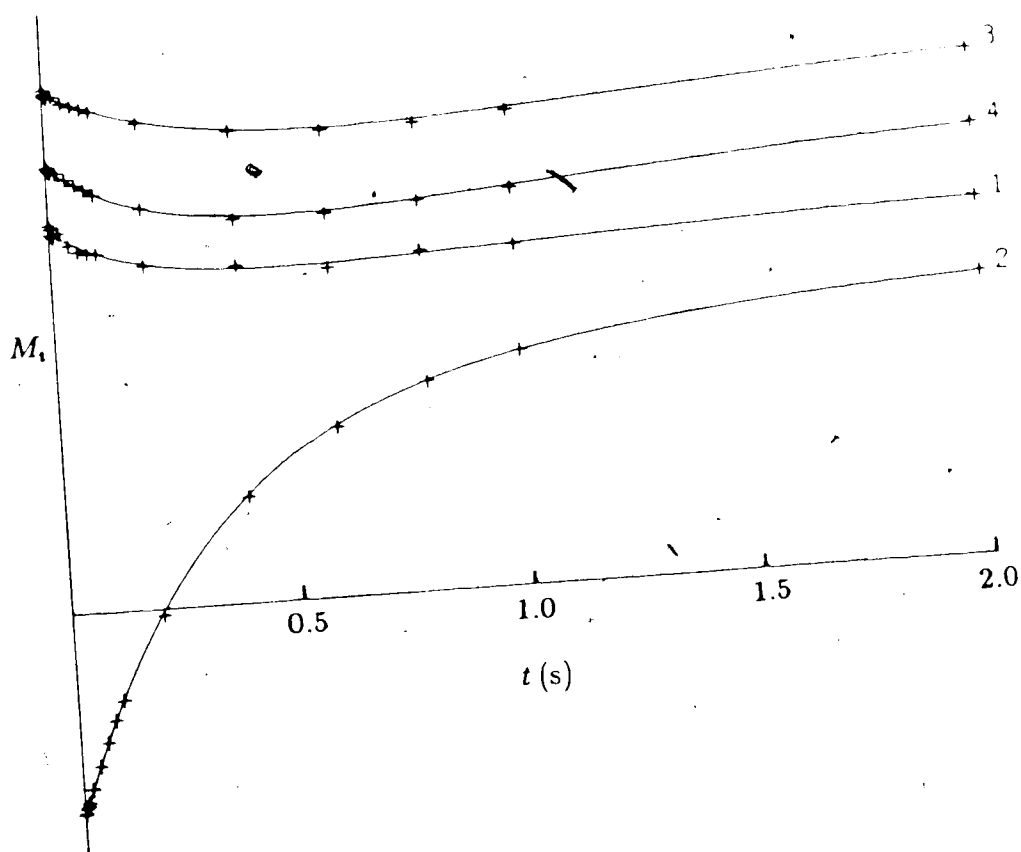


Fig. 6-6 Comparison of the observed and calculated magnetizations including both "1-2" and "1-3" shifts for $(\eta^5\text{-C}_7\text{H}_7)\text{-Fe}(\text{CO})_2\text{-SnPh}_3$. + - Magnetizations $M_i(t)$ (arbitrary units) at the four sites following the selective inversion of the site 2 magnetization at 262.5 K. Curves represent least squares fit for $k_{(12)} = 0.49\text{ s}^{-1}$, $k_{(13)} = 0.73\text{ s}^{-1}$, and $k_{(14)} = 0$.

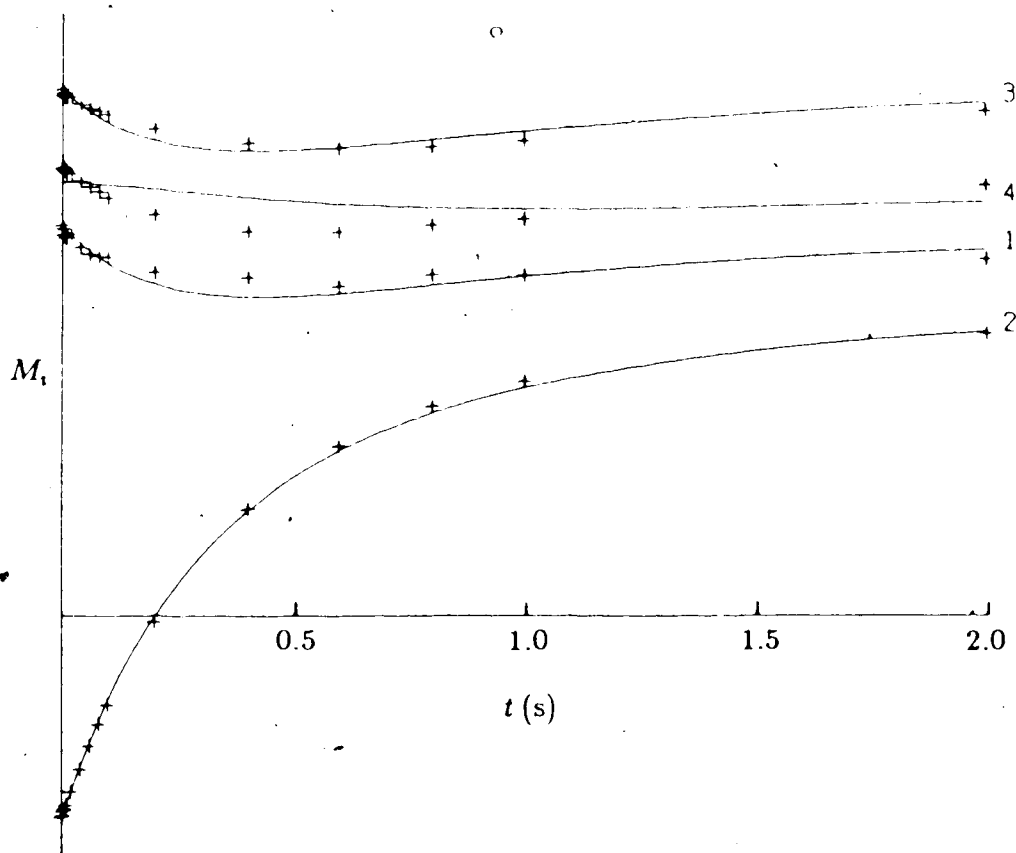


Fig. 6-7 Comparison of the observed and calculated magnetizations including only "1-2" shifts for $(\eta^5\text{-C}_7\text{H}_7)\text{-Fe}(\text{CO})_2\text{-SnPh}_3$. + - Magnetizations $M_i(t)$ (arbitrary units) at the four sites following the selective inversion of the site 2 magnetization at 262.5 K. Curves represent least squares fit for $k_{(12)} = 0.90 \text{ s}^{-1}$, $k_{(13)} = k_{(14)} = 0$.

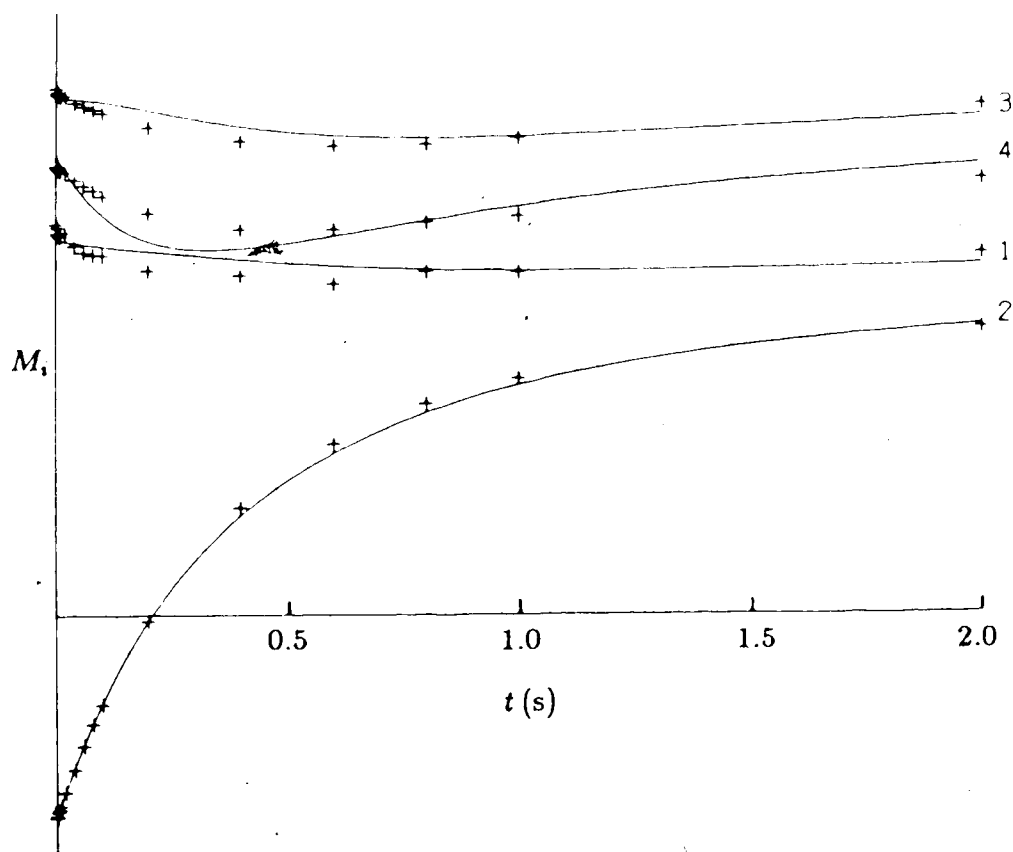


Fig. 6-8 Comparison of the observed and calculated magnetizations including only "1-3" shifts for $(\eta^5\text{-C}_7\text{H}_7)\text{-Fe(CO)}_2\text{-SnPh}_3$. + - Magnetizations $M_i(t)$ (arbitrary units) at the four sites following the selective inversion of the site 2 magnetization at 262.5 K. Curves represent least squares fit for $k_{(13)} = 1.80\text{s}^{-1}$, $k_{(12)} = k_{(14)} = 0$.

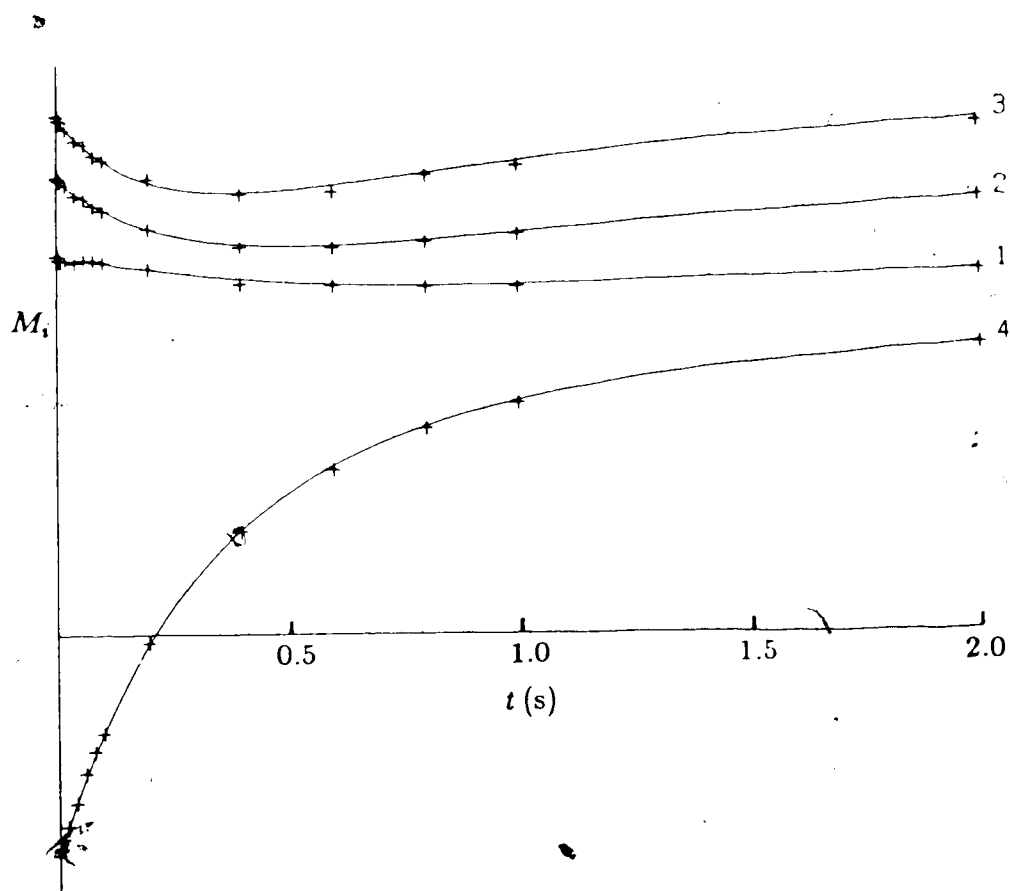


Fig. 6-9 Comparison of the observed and calculated magnetizations including both "1-2" and "1-3" shifts for $(\eta^5\text{-C}_7\text{H}_7)\text{-Fe}(\text{CO})_2\text{-SnPh}_3$. + - Magnetizations $M_i(t)$ (arbitrary units) at the four sites following the selective inversion of the site 4 magnetization at 262.5 K. Curves represent least squares fit for $k_{(12)} = 0.50 \text{ s}^{-1}$, $k_{(13)} = 0.74 \text{ s}^{-1}$, and $k_{(14)} = 0$.

of the data shows that, following the inversion of magnetization at site 2, site 4 magnetization decreases to a minimum at short times, slightly faster than magnetization at sites 3 and 1, which indicates the presence of a "1-3" metal shift process. It cannot be determined at this point whether only this mechanism is present or whether this is operative in combination with any other mechanisms. Hence least squares analysis of the data was performed, using all three rate constants, $k_{(12)}$, $k_{(13)}$ and $k_{(14)}$ as variables and allowing them to vary freely during iterations. $1/T_1$ values for the four sites were fixed at values determined from a non-selective inversion experiment at this temperature, and the values obtained for the three rate constants were $k_{(12)} = 0.46 \pm 0.19 \text{ s}^{-1}$, $k_{(13)} = 0.68 \pm 0.42 \text{ s}^{-1}$ and $k_{(14)} = 0.05 \pm 0.34 \text{ s}^{-1}$. These results indicate that the 1,4 process is not important and hence a second least squares fitting was performed in which $k_{(14)}$ was fixed at zero and both $k_{(12)}$ and $k_{(13)}$ were allowed to vary freely. This yielded $k_{(12)} = 0.49 \pm 0.10 \text{ s}^{-1}$ and $k_{(13)} = 0.73 \pm 0.18 \text{ s}^{-1}$. The variance of this fit was slightly smaller than in the earlier fit. In Fig. 6-6, the curves corresponding to the calculated magnetization for this fit are shown and the agreement between the calculated and observed magnetizations is extremely good. This shows clearly that "1-4" shifts are not important in the fluxionality of this complex. In order to firmly establish the presence¹ of both "1-2" and "1-3" shifts, two other least squares fittings were performed using the same set of experimental data: (i) allowing only $k_{(12)}$ to vary freely with $k_{(13)} = k_{(14)} = 0$ fixed in one case, and (ii) allowing only $k_{(13)}$ to vary freely with $k_{(12)} = k_{(14)} = 0$ fixed in the other. In both cases, the variance of the fit increased by a factor of approximately 10 compared to the fit when both $k_{(12)}$ and $k_{(13)}$ were allowed to vary with $k_{(14)} = 0$ fixed. The poor agreement between the calculated and observed magnetizations is clearly shown graphically in Fig. 6-7 for only "1-2" shifts and Fig. 6-8 for only "1-3" shifts.

Following the selective inversion of the site 4 magnetization at this temperature, magnetization at site 2 decreased rapidly to a minimum (see Fig. 6.9), and least squares analysis of the data with $k_{(12)}$ and $k_{(13)}$ allowed to vary freely and $k_{(14)}$ fixed at zero yielded $k_{(12)} = 0.50 \pm 0.28 \text{ s}^{-1}$ and $k_{(13)} = 0.74 \pm 0.14 \text{ s}^{-1}$. Again the agreement between the calculated and observed magnetizations is very good as shown in Fig. 6.9. The excellent agreement between the values of the rate constants obtained from the two independent determinations show unambiguously that both "1 2" and "1 3" metal shifts are operative in the fluxional behaviour of the $(\eta^5\text{-C}_7\text{H}_7)\text{-Fe}(\text{CO})_2\text{-SnPh}_3$ complex.

6.3.2 Rate constants and Activation Parameters for $(\eta^5\text{-C}_7\text{H}_7)\text{-Fe}(\text{CO})_2\text{-SnPh}_3$

In order to obtain the activation parameters for the "1 2" and "1 3" metal shifts in the Fe complex, selective inversion experiments were performed at six different temperatures in the range of 258 K to 283 K where four distinct resonances are observed for the C_7H_7 ring protons. Magnetization transfer data at each temperature were analysed using the least squares procedure with $k_{(12)}$ and $k_{(13)}$ both allowed to vary freely and $k_{(14)}$ fixed at zero, since "1 4" metal shifts have been shown to be unimportant. Two sets of experiments were performed at each temperature, with inversion of magnetization at site 2 or at site 4, and the results obtained are summarized in Table 6.1. It should be mentioned here that, in obtaining the rate constants shown in Table 6.1, $1/T_1$ values for the four sites were fixed at individual values determined from non-selective inversion recovery experiments, since at the lowest temperature, values of $1/T_1$ showed differences of $\geq 10\%$ for some resonances. But a subsequent analysis, using the mean relaxation rates at each temperature gave essentially the same values for the rate constants $k_{(12)}$ and $k_{(13)}$.

Table 6.1 Rate constants for "1-2" and "1-3" shifts in $(\eta^5\text{-C}_7\text{H}_7)\text{-Fe}(\text{CO})_2\text{-SnPh}_3$

T (K)	Inverted Site	$k_{(12)}(\text{s}^{-1})$	$k_{(13)}(\text{s}^{-1})$	$\overline{1/T_1}(\text{s}^{-1})$
258.0	2	0.19 ± 0.07	0.38 ± 0.13	0.94
	4	0.22 ± 0.15	0.38 ± 0.08	
262.5	2	0.49 ± 0.10	0.73 ± 0.18	0.89
	4	0.50 ± 0.28	0.74 ± 0.14	
268.0	2	0.93 ± 0.20	1.35 ± 0.34	0.84
	4	1.02 ± 0.41	1.38 ± 0.20	
272.0	2	1.49 ± 0.18	2.40 ± 0.31	0.80
	4	1.65 ± 0.63	2.23 ± 0.31	
277.5	2	2.90 ± 0.46	4.40 ± 0.82	0.74
	4	2.59 ± 1.37	4.42 ± 0.71	
283.0	2	5.26 ± 0.87	7.77 ± 1.48	0.68
	4	6.02 ± 2.06	7.20 ± 0.95	

The data in Table 6.1 show that rate constants obtained from independent experiments involving inversion of magnetization at site 2 and at site 4 are equal within the error limits at all temperatures. However, experiments in which site 2 magnetization was inverted consistently yielded rate constants $k_{(12)}$ with smaller errors at all temperatures, and experiments with inversion of magnetization of site 4 yielded rate constants $k_{(13)}$ with consistently smaller errors at all temperatures. Thus, in calculating the activation parameters, the set of $k_{(12)}$ values determined from inversion of site 2 magnetization, and the set of $k_{(13)}$ values determined from inversion of site 4 magnetization were used. Plots of $\ln k$ against $1/T$ for these data are shown in Fig. 6-10. The value of the rate constant $k_{(12)}$ obtained at the lowest temperature seems to be underestimated and hence this point was neglected in evaluating the activation parameters which are summarized in

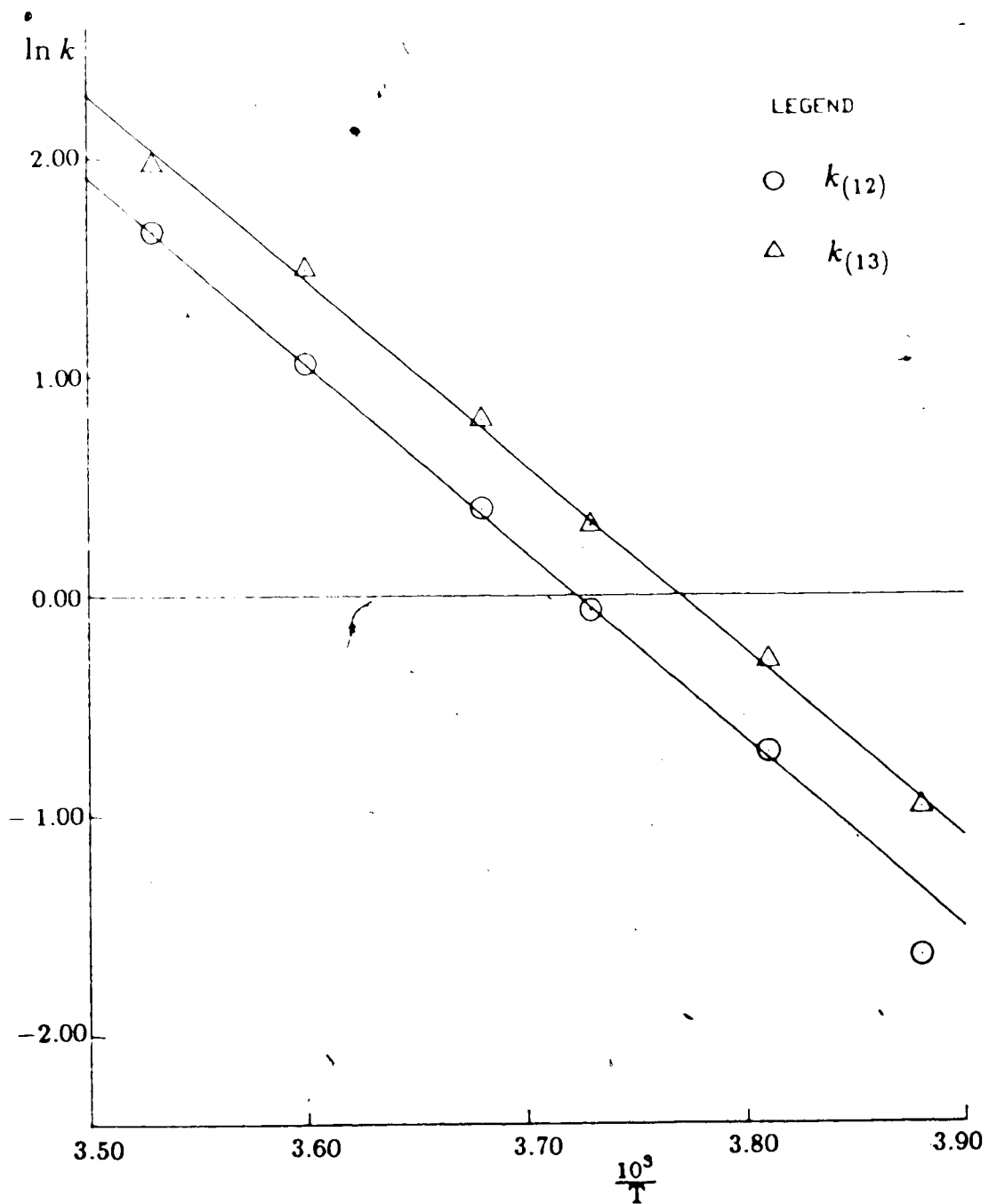


Fig. 6-10 Arrhenius plot for $(\eta^5\text{-C}_7\text{H}_7)\text{-Fe(CO)}_2\text{-SnPh}_3$.

Table 6.2.

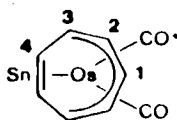
Table 6.2 Activation parameters for $(\eta^5\text{-C}_7\text{H}_7)\text{-Fe(CO)}_2\text{-SnPh}_3$

	E_a (kcal/mol)	ΔH^\ddagger (kcal/mol)	ΔS^\ddagger (cal/mol K)
"1-2" Shifts	17.20 ± 0.19	16.66 ± 0.19	3.73 ± 0.70
"1-3" Shifts	16.70 ± 0.42	16.16 ± 0.42	2.65 ± 1.55

These results show that although the rates "1-3" shifts are faster than the rates of "1-2" shifts by a factor of ~ 1.5 , both processes occur with essentially the same activation energy. It should be mentioned here that the expectation of Reuvers (54), that only "1-2" shifts were occurring in this complex, was found to be incorrect but his approximate activation energy of ~ 15 kcal/mol for "1-2" shifts is reasonably close to the value obtained here.

6.4 Fluxional Behaviour of $(\eta^5\text{-C}_7\text{H}_7)\text{-Os}(\text{CO})_2\text{-SnPh}_3$

In contrast to the Fe complex, the Os complex $(\eta^5\text{-C}_7\text{H}_7)\text{-Os}(\text{CO})_2\text{-SnPh}_3$ exists only as the symmetric isomer $\eta^5\text{-Os}$ (98);



It has been observed that ^{13}C NMR spectra (100.6 MHz) showed only a single resonance for the carbonyl groups in the temperature range 179 K to 380 K (98). Four resonances due to the C_7H_7 ring carbon atoms showed broadening in the range 298 K to 318 K, and the four signals were very broad and collapsed to the baseline at 380 K. These observations indicated that this isomer is fluxional by metal migration around the C_7H_7 ring (98), but no further quantitative or qualitative information about the fluxionality was available. Fluxional behaviour of this complex was studied using the magnetization transfer method, by selectively inverting the proton magnetization at site 1 (see Fig. 6-2) at several temperatures in the range of 268 K to 298 K (200 MHz, ^1H). Experiments in which the proton magnetization at site 3 was inverted were performed at two temperatures. Delineation of the metal migration mechanism is described in the following section, and the activation parameters are given in section 6.4.2.

6.4.1 Delineation of the Exchange Mechanism of $(\eta^5\text{-C}_7\text{H}_7)\text{-Os}(\text{CO})_2\text{-SnPh}_3$

The results of a selective inversion experiment at 282 K, following the inversion of site 1 magnetization, are shown in Fig. 6-11. Following the inversion of magnetization at site 1, the observed magnetization at site 2 decreases to a

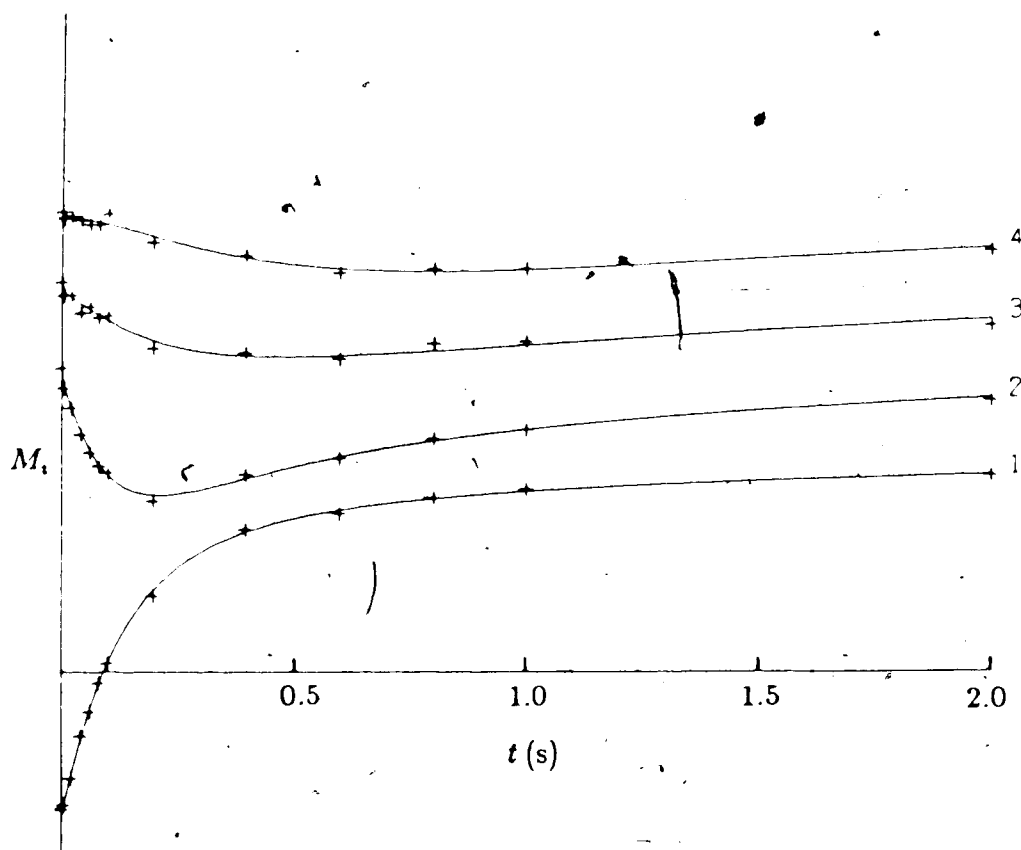


Fig. 6-11 Comparison of the observed and calculated magnetizations including both "1-2" and "1-3" shifts for $(\eta^5\text{-C}_7\text{H}_7)\text{-Os}(\text{CO})_2\text{-SnPh}_3$ - Magnetizations $M_i(t)$ (arbitrary units) at the four sites following the selective inversion of the site 1 magnetization at 282 K. Curves represent least squares fit for $k_{(12)} = 2.52 \text{ s}^{-1}$, $k_{(13)} = 0.43 \text{ s}^{-1}$, and $k_{(14)} = 0$.

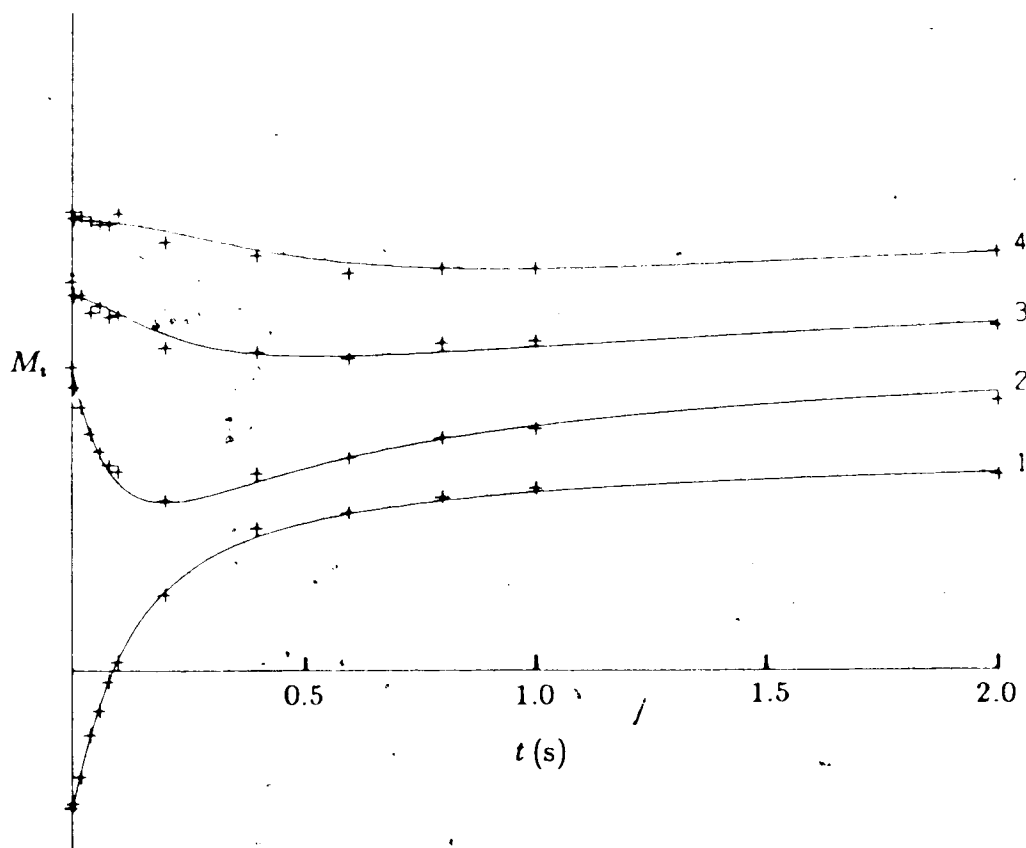


Fig. 6-12 Comparison of the observed and calculated magnetizations including only "1-2" for $(\eta^5\text{-C}_7\text{H}_7)\text{-Os}(\text{CO})_2\text{-SnPh}_3$. + - Magnetizations $M_i(t)$ (arbitrary units) at the four sites following the selective inversion of the site 1 magnetization at 282 K. Curves represent least squares fit for $k_{(12)} = 3.07 \text{ s}^{-1}$, $k_{(13)} = k_{(14)} = 0$.

minimum at short times, faster than the magnetizations at site 3 or at site 4. In this case, the decrease of magnetization at site 4 is very slight. These observations indicate the presence of a dominant "1-2" process, but this does not rule out the presence of other mechanisms, especially the "1-3" metal shifts, of smaller magnitude. Least squares analysis of the data, in which all three rates constants $k_{(12)}$, $k_{(13)}$ and $k_{(14)}$ were allowed to vary freely, yielded $k_{(12)} = 2.52 \pm 0.49 \text{ s}^{-1}$, $k_{(13)} = 0.44 \pm 0.46 \text{ s}^{-1}$ and $k_{(14)} = -0.02 \pm 0.31 \text{ s}^{-1}$, clearly indicating the absence of "1-4" metal shifts. Fitting the data with $k_{(14)}$ fixed at 0 and allowing $k_{(12)}$ and $k_{(13)}$ to vary freely, gave $k_{(12)} = 2.52 \pm 0.47 \text{ s}^{-1}$ and $k_{(13)} = 0.43 \pm 0.28 \text{ s}^{-1}$. Analysis of this set of data with only $k_{(12)}$ allowed to vary freely with both $k_{(13)}$ and $k_{(14)}$ fixed at zero, yielded $k_{(12)} = 3.07 \pm 0.50 \text{ s}^{-1}$, but the variance 0.0220, obtained for this fit was almost twice as large as the variance, 0.0113, obtained for the fit $k_{(12)} = 2.52 \pm 0.47 \text{ s}^{-1}$, $k_{(13)} = 0.43 \pm 0.28 \text{ s}^{-1}$ with $k_{(14)} = 0$. The agreement between the observed and calculated magnetization considerably improved when both "1-2" and "1-3" shifts were included, as indicated by the smaller variance of the least squares fit. The differences in the two fits are rather difficult to show graphically due to the smaller magnitude of the rate constant for "1-3" shifts compared to $k_{(12)}$. However a close examination of the fits for only "1-2" shifts (Fig. 6-12) and for both "1-2" and "1-3" shifts (Fig 6-11) shows that the fit is better, particularly for the magnetization at site 4, when both processes are included. Least squares analysis of the data were performed with only $k_{(12)}$ allowed to vary and both $k_{(12)}$ and $k_{(13)}$ allowed to vary at two other temperatures, and the results obtained are shown in Table 6.3

Table 6.3

T (K)	Inverted Site	Only "1-2" shifts		Both "1-2" & "1-3" shifts		
		variance	$k_{(12)}(s^{-1})$	variance	$k_{(12)}(s^{-1})$	$k_{(13)}(s^{-1})$
273.0	1	0.0040	0.78 ± 0.13	0.0017	0.64 ± 0.10	0.12 ± 0.07
	3	0.0025	0.80 ± 0.12	0.0017	0.62 ± 0.21	0.17 ± 0.20
282.0	1	0.0220	3.07 ± 0.50	0.0013	2.52 ± 0.47	0.43 ± 0.28
291.0	1	0.0106	7.01 ± 1.60	0.0041	4.73 ± 1.17	1.41 ± 0.68
	3	0.0038	6.44 ± 0.54	0.0024	5.39 ± 0.90	0.94 ± 0.77

The data in Table 6.3 show that the agreement between the calculated and observed magnetization considerably improves when both "1-2" and "1-3" shifts are allowed, as shown numerically in the smaller variances of the least squares fits. Thus one must conclude that "1-2" metal shifts are the predominant exchange mechanism in the $(\eta^5\text{-C}_7\text{H}_7)\text{-Os}(\text{CO})_2\text{-SnPh}_3$ complex, but "1-3" metal shift are also present to a smaller but non-negligible extent. The data in Table 6.3 also shows that experiments involving the inversion of magnetization at site 3 give $k_{(13)}$ with larger estimated errors than experiments in which site 1 magnetization is inverted, but any such pattern was not shown for $k_{(12)}$ values. Thus experiments in which the magnetization at site 1 was inverted were performed at other temperatures, and the activation parameters obtained for the two processes from these experiments are given below.

6.4.2 Rate constants and Activation Parameters for $(\eta^5\text{-C}_7\text{H}_7)\text{-Os}(\text{CO})_2\text{-SnPh}_3$

Since "1-3" metal shifts of non-negligible magnitude are found to occur, together with dominant "1-2" metal shifts, magnetization transfer data at

all temperatures were analysed with both $k_{(12)}$ and $k_{(13)}$ allowed to vary freely during least squares iterations with $k_{(14)}$ fixed at zero. $1/T_1$ values were fixed at the average values for the four sites, since the individual values, as determined from non-selective inversion recovery experiments, were found to be equal within the experimental errors. Rate constants obtained for all five temperatures are tabulated in Table 6.4.

Table 6.4 Rate constants for $(\eta^5\text{-C}_7\text{H}_7)\text{-Os}(\text{CO})_2\text{-SnPh}_3$

T (K)	Inverted Site	$k_{(12)}(\text{s}^{-1})$	$k_{(13)}(\text{s}^{-1})$	$\overline{1/T_1}(\text{s}^{-1})$
268.0	1	0.21 ± 0.09	0.04 ± 0.07	0.74
273.0	1	0.64 ± 0.10	0.12 ± 0.07	0.62
	3	0.62 ± 0.21	0.17 ± 0.20	
282.0	1	2.52 ± 0.47	0.43 ± 0.28	0.52
291.0	1	4.72 ± 1.17	1.41 ± 0.69	0.43
	3	5.38 ± 0.90	0.95 ± 0.77	
298.0	1	9.19 ± 6.23	2.26 ± 3.09	0.39

The larger errors in the rate constants at higher temperatures are due to the increased broadening of the resonances at the higher exchange rates, making the selective inversion difficult, and due to the decreased number of data points at short times where the exchange effects are predominant. In evaluating the activation parameters, average rate constants were used for temperatures at which duplicate values are available. Plots of $\ln k$ against $1/T$ are shown in Fig. 6-13. Since the values of the rate constants obtained at the lowest temperature, 268K are considerably removed from the linear regions observed for values of $\ln k_{(12)}$ and $\ln k_{(13)}$ at other temperatures, the data at 268 K were neglected in calculating the activation parameters which are shown in Table 6.5.

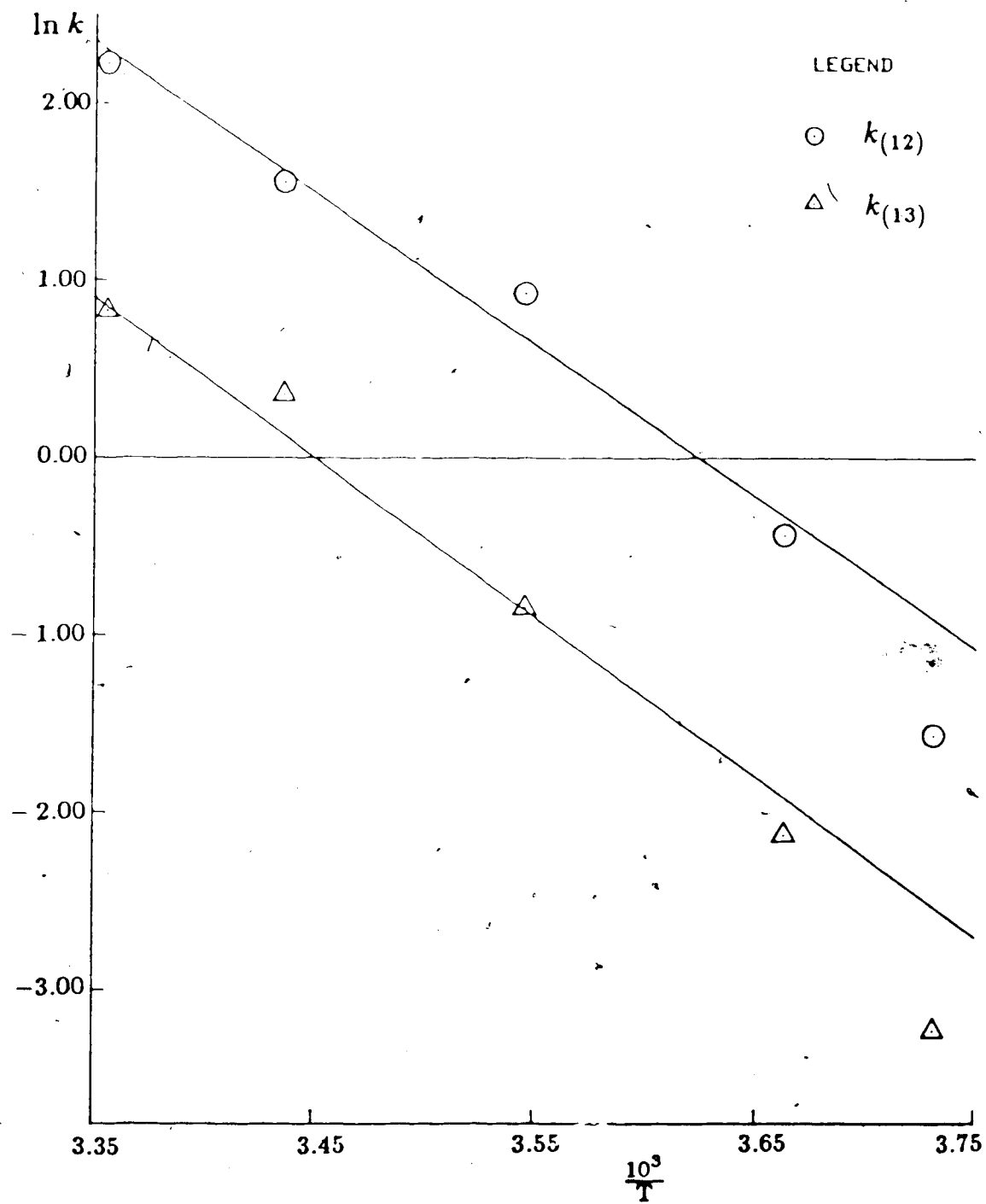


Fig. 6-13 Arrhenius plot for $(\eta^5\text{-C}_7\text{H}_7)\text{-Os}(\text{CO})_2\text{-SnPh}_3$.

Table 6.5 Activation Parameters for $(\eta^5\text{-C}_7\text{H}_7)\text{-Os}(\text{CO})_2\text{-SnPh}_3$

	E_a (kcal/mol)	ΔH^\ddagger (kcal/mol)	ΔS^\ddagger (cal/mol K)
"1-2" Shifts	16.96 ± 1.80	16.39 ± 1.81	1.06 ± 6.32
"1-3" Shifts	18.07 ± 0.44	17.50 ± 0.45	1.90 ± 1.56

Activation parameters obtained for the two processes clearly show that both processes occur with similar activation energies, although the "1-2" process is faster than the "1-3" process, by a factor of more than four.

At this point it is important to establish that the rate constants obtained for the "1-2" shifts at low temperatures, where the ^1H relaxation rates are either larger than or comparable to $k_{(12)}$, are not overestimated because of the non-inclusion of cross-relaxation effects in the model. A ^{13}C selective inversion experiment at 273 K, in which the carbon magnetization at site 2 was inverted, was performed. A least squares fit of the ^{13}C data with $k_{(13)}$ fixed at 0.15 s^{-1} (from Table 6.4), $k_{(14)}$ fixed at zero, and $k_{(12)}$ allowed to vary freely resulted in a value of $0.91 \pm 0.50\text{ s}^{-1}$ for $k_{(12)}$. This value of $k_{(12)}$, 0.91 s^{-1} , is slightly larger than the value, 0.63 s^{-1} , obtained in the proton NMR experiments (Table 6.4), but the values are equal within the estimated errors. If nearest neighbour proton-proton cross-relaxation were an important mechanism for magnetization transfer in the proton selective inversion experiments, one would expect the value of $k_{(12)}$ obtained in the corresponding carbon inversion experiment to be substantially smaller in the latter. The fact that the values of $k_{(12)}$ obtained from carbon and proton inversion experiments are equal within experimental error indicates that cross-relaxation does not contribute significantly to the dynamics of proton magnetizations. The higher errors in $k_{(12)}$ obtained in the ^{13}C inversion experiment

reflect the poorer signal-to-noise ratio in these experiments, and the absence of reliable intensities for site 1.

6.5 Fluxional Behaviour of $(\eta^5\text{-C}_7\text{H}_7)\text{-Ru}(\text{CO})_2\text{-SnPh}_3$

Unlike the previously discussed Fe and Os complexes, where only one isomeric form was present, the analogous complex of Ru, $(\eta^5\text{-C}_7\text{H}_7)\text{-Ru}(\text{CO})_2\text{-SnPh}_3$, was found to exist as a mixture of symmetric $\eta^5\text{-S}_{\text{Ru}}$ and asymmetric $\eta^5\text{-A}_{\text{Ru}}$ isomers at low temperatures (98).



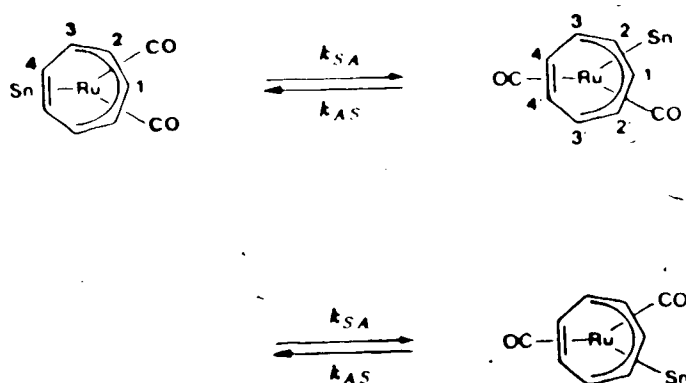
It has been observed in ^{13}C NMR spectra (100.6 MHz) at temperatures near $\sim 183\text{ K}$ that the intensity ratio of corresponding signals due to the asymmetric and symmetric isomers changes with temperature, indicating that the two isomers are interconverting even at such low temperatures (98). This isomer interconversion was studied quantitatively using the ^1H magnetization transfer experiments, and the results are described in the following section, before the investigation of the Ru metal migration around the C_7H_7 ring, which was studied at the higher temperature range $\sim 223\text{ K}$ to $\sim 233\text{ K}$. At these higher temperatures, the proton NMR spectrum of the C_7H_7 moiety corresponds to that of a time-averaged symmetric isomer, hence the metal migration was studied as a four site exchange problem. The results of this investigation are given in sections 6.5.2 and 6.5.3.

6.5.1 Isomer interconversion in $(\eta^5\text{-C}_7\text{H}_7)\text{-Ru}(\text{CO})_2\text{-SnPh}_3$

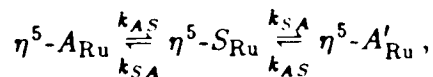
From observations of ^{13}C NMR spectra in the low temperature range of 175 K to 183 K , it was inferred that the symmetric and asymmetric isomers of this

complex are interconverting, and that the Ru metal migration around the C_7H_7 ring is not of importance at these temperatures (98). The isomer interconversion process was investigated at 178 K using the magnetization transfer method, by selectively inverting the 1H magnetization at one of the sites in the asymmetric isomer in one set of experiments and at the corresponding site in the symmetric isomer in another set of experiments. The 1H NMR spectrum of the isomeric mixture is shown in Fig. 6-3. Selective inversion experiments were performed by inverting the magnetization at site 3 of the asymmetric isomer η^5-A_{Ru} , and at site 3 of the symmetric isomer η^5-S_{Ru} , and the temporal responses of all the observable resonances due to the C_7H_7 rings from both isomers were monitored. Following the selective inversion of the magnetization at site 3 of the asymmetric isomer, the magnetization at site 3' of the asymmetric isomer and at site 3 of the symmetric isomer decreased to a minimum at short times and then recovered to their equilibrium values at longer times, in the well defined manner normally observed in selective inversion experiments on exchanging systems. The observed magnetizations at all other sites stayed more or less constant and did not show such temporal responses. Similarly, following the selective inversion of site 3 magnetization of the symmetric isomer η^5-S_{Ru} , only the magnetization at sites 3 and 3' of the asymmetric isomer showed the characteristic temporal response shown by exchanging resonances, and the other resonances remained constant during the delay times following selective inversion. These observations clearly show that magnetization transfer is occurring only between the corresponding sites of the two isomers, and that there is no magnetization transfer between the non-equivalent sites of the same isomer, as observed in systems with metal migration. This confirms that, at this temperature, the complex is not fluxional by Ru metal migration, but only isomer interconversion is occurring.

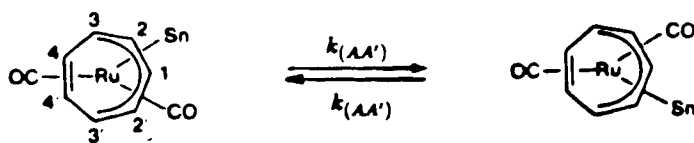
In order to obtain quantitative information about the isomer interconversion, it is instructive to consider the possible interconversion pathways consistent with the above observations. The decrease in the magnetization of sites 3 and 3' of the asymmetric isomer, following the selective inversion of site 3 of the symmetric isomer, indicates that there is direct intermolecular exchange between the symmetric isomer, and the enantiomers of the asymmetric isomer:



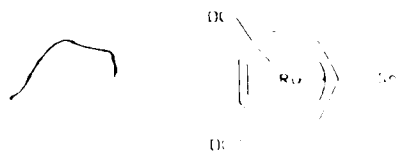
The decrease in the magnetization at site 3' of the asymmetric isomer $\eta^5-A'_{Ru}$ following the inversion of the magnetization at site 3 of the asymmetric isomer η^5-A_{Ru} , could occur by successive magnetization transfers through the symmetric isomer:



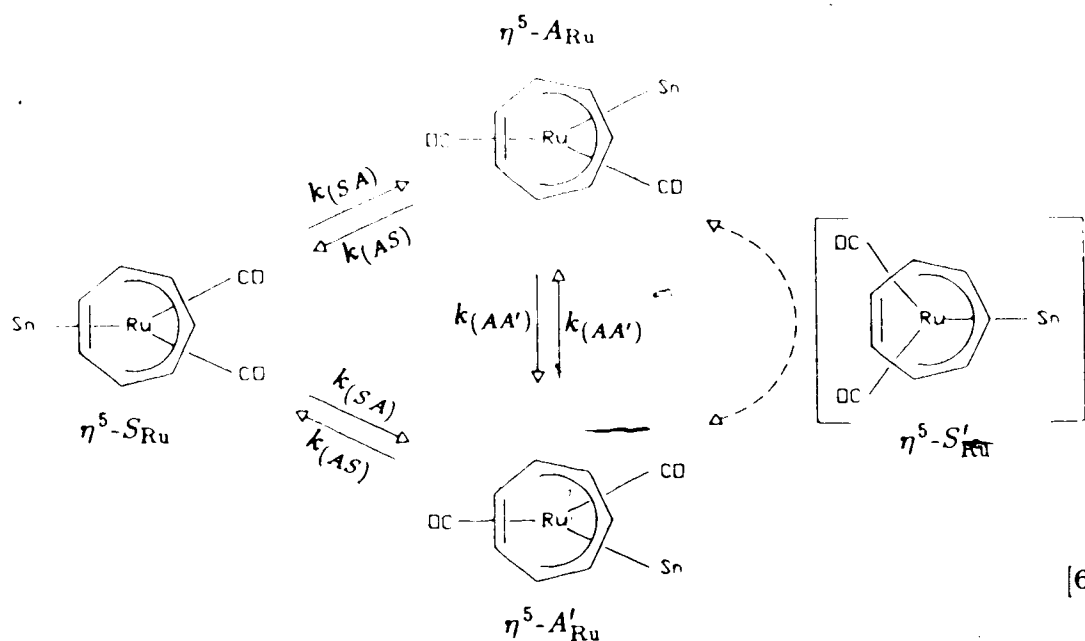
or by transfer of magnetization $3 \rightarrow 3'$, via the direct intramolecular exchange:



which should occur via the symmetric intermediate ($\eta^5-S'_{Ru}$),



It is convenient to represent the above exchange processes, in a single scheme;



[6-8]

Since, following the selective inversion of magnetization at one of the sites (e.g. 3 of the asymmetric isomer), magnetization is transferred to only two other sites, (e.g. 3' of the asymmetric and 3 of the symmetric), this isomer interconversion can be treated as a three site exchange problem. In the least squares analysis of the selective inversion recovery data, following the inversion of site 3 of the symmetric isomer or the site 3 magnetization of the asymmetric isomer η^5-A_{Ru} , site 3 magnetization of the asymmetric isomer $\eta^5-A'_{Ru}$ is designated as the first site, the site 3 magnetization of the symmetric isomer η^5-S_{Ru} is the second site, and site 3' magnetization of the asymmetric isomer $\eta^5-A'_{Ru}$ is the third site. In

the model, the intramolecular asymmetric enantiomer interconversion is described by rate constant $k_{(AA')}$ with matrix of exchange coefficients $\Pi^{(1)}$,

$$\Pi^{(1)} = \begin{pmatrix} -1 & 0 & 1 \\ 0 & 0 & 0 \\ 1 & 0 & 1 \end{pmatrix}; \quad [6-9]$$

symmetric to asymmetric conversion is described by rate constant $k_{(SA)}$ with matrix of exchange coefficients $\Pi^{(2)}$,

$$\Pi^{(2)} = \begin{pmatrix} 0 & 0.5 & 0 \\ 0 & -1 & 0 \\ 0 & 0.5 & 0 \end{pmatrix}; \quad [6-10]$$

and the asymmetric to symmetric conversion by, rate constant $k_{(AS)}$ with exchange coefficient matrix $\Pi^{(3)}$,

$$\Pi^{(3)} = \begin{pmatrix} -1 & 0 & 0 \\ 1 & 0 & 1 \\ 0 & 0 & -1 \end{pmatrix}. \quad [6-11]$$

Alternatively, the number of independent rate constants can be reduced by measuring the equilibrium concentrations, $[S]$ of the symmetric isomer and $[A]$ and $[A']$ of the asymmetric one. Since,

$$k_{(SA)} = k_{(AS)}K_{eq}, \quad [6-12]$$

where $K_{eq} = \{[A] + [A']\}/[S]$ and K_{eq} can be obtained from the ratio of the corresponding signal intensities in a conventional ^1H NMR spectrum at the relevant temperatures, only two independent rate constants, $k_{(AA')}$ and $k_{(AS)}$, are needed. In this approach the rate constant $k_{(AA')}$ is associated with the exchange coefficient matrix $\Pi^{(1)}$ given in Eq. [6-9] as before, but the rate constant $k_{(AS)}$ is now associated with exchange coefficient matrix $\Pi^{(2')}$,

$$\Pi^{(2')} = \begin{pmatrix} -1 & 3.50 & 0 \\ 1 & -7.00 & 1 \\ 0 & 3.50 & -1 \end{pmatrix}. \quad [6-13]$$

In the least squares analysis of the magnetization transfer data, the first approach is used, but it will be shown later that consistent rate constants are also obtained from the second approach.

In the analysis of magnetization transfer data following the inversion of magnetization at site 3 of the symmetric isomer $\eta^5\text{-SRu}$ at 178 K, all three rate constants $k_{(AA')}$, $k_{(AS)}$ and $k_{(SA)}$ were allowed to vary freely, and the values obtained for the rate constants were, $k_{(SA)} = 15.54 \pm 10.43 \text{ s}^{-1}$, $k_{(AS)} = 49.18 \pm 21.33 \text{ s}^{-1}$, unexpectedly, $k_{(AA')} = 185.4 \pm 6223.8 \text{ s}^{-1}$. Thus a second least squares analysis, with $k_{(AA')}$ fixed at zero, was performed and it yielded $k_{(SA)} = 15.52 \pm 9.86 \text{ s}^{-1}$ and $k_{(AS)} = 49.14 \pm 20.17 \text{ s}^{-1}$. The rapid convergence of both analyses and the small, similar variances of the two fits: 0.00554 when all $k_{(AA')}$, $k_{(AS)}$ and $k_{(SA)}$ were allowed to vary, and 0.00543 when $k_{(AA')}$ was fixed at zero, indicated that the observed time-dependent magnetizations and the values obtained for $k_{(SA)}$ and $k_{(AS)}$ from analysis of the time-dependence of the magnetizations were insensitive to the values of $k_{(AA')}$. Subsequent analyses with $k_{(AA')}$ fixed at 0.5, 5, 10 and 100 s^{-1} , resulted in values of $k_{(AS)}$ in the range $15.55\text{--}15.54 \text{ s}^{-1}$ and $k_{(SA)}$ in the range of $49.18\text{--}49.19 \text{ s}^{-1}$ with no changes in the estimated errors. This confirms that the analysis of the data from the experiment where the symmetric resonance was inverted are insensitive to the value of $k_{(AA')}$.

In the least squares analysis of the selective inversion data following the inversion of magnetization of site 3 of the asymmetric isomer $\eta^5\text{-ARu}$, it was impossible to attain convergence when all three rate constants were allowed to vary freely. When $k_{(AA')}$ was fixed at zero, rapid convergence was obtained, with values of $k_{(AS)} = 18.06 \pm 6.32 \text{ s}^{-1}$ and $k_{(SA)} = 59.64 \pm 32.38 \text{ s}^{-1}$. Convergence was not attained when iterations were performed for a series of fixed non zero values of $k_{(AA')}$, with both $k_{(AS)}$ and $k_{(SA)}$ allowed to vary freely. Thus in order to

ascertain the effect of $k_{(AA')}$ on the agreement between the observed and calculated magnetizations, least squares analyses were performed for a series of fixed values of $k_{(AA')}$ with values of $k_{(AS)}$ and $k_{(SA)}$ fixed at 18.06 and 59.64 respectively, and allowing only the linear parameters to vary during iterations. The effect of the magnitude of $k_{(AA')}$ on the variance of such fits are shown below in Table 6.6.

Table 6.6

$k_{(AA')} \text{ s}^{-1}$	variance
0	0.16553
10	0.43881
25	0.91671
50	1.54602
100	2.59559
500	4.10931

The variances in the Table 6.6 show that estimated errors increase considerably with the value of $k_{(AA')}$, and that the best agreement between the calculated and observed magnetizations is obtained when the value of $k_{(AA')}$ is zero. The values of $k_{(AS)}$ and $k_{(SA)}$ obtained with $k_{(AA')}$ fixed at zero from the two independent experiments are equal within the error limits estimated by the least squares procedure, and in both cases, the agreement between the calculated and the observed magnetizations is quite good (see Figs. 6-14 and 6-15). These results indicate that interconversion of the two asymmetric enantiomers occurs predominantly via the symmetric isomer $\eta^5\text{-S}_{\text{Ru}}$ rather than through the symmetric intermediate, $\eta^5\text{-S}'_{\text{Ru}}$.

Least squares analysis of the selective inversion data following inversion of site 3 magnetization of $\eta^5\text{-A}_{\text{Ru}}$, using $K_{eq} \approx 3.5$ estimated from the conventional

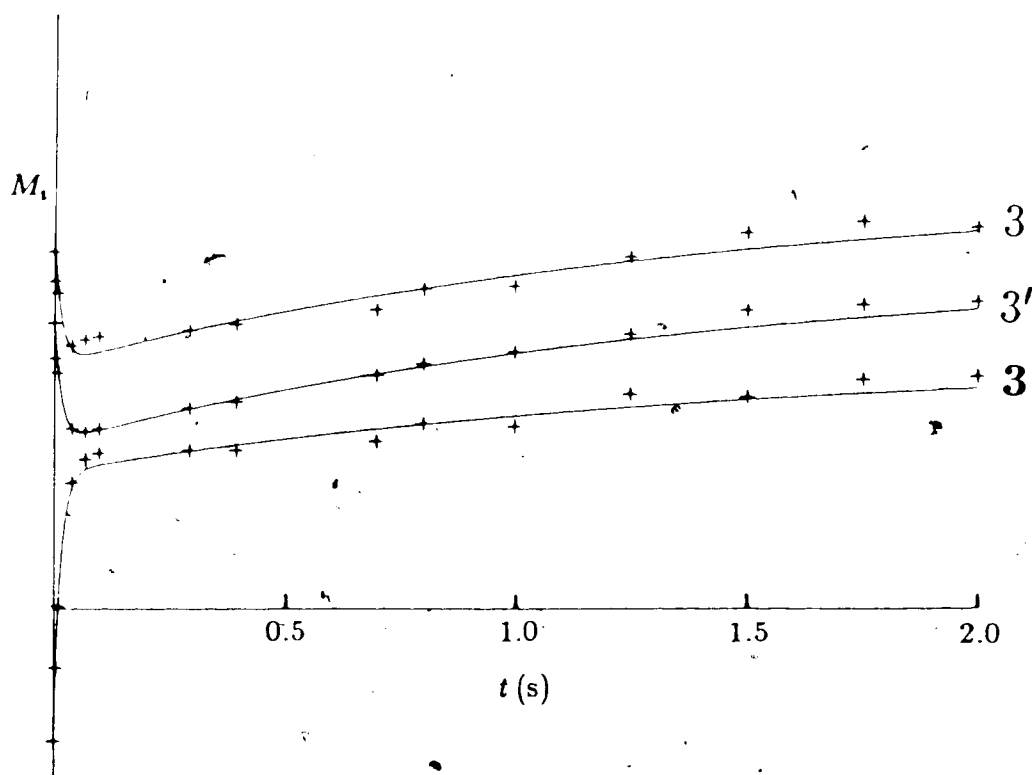


Fig. 6-14 Comparison of the observed and calculated magnetizations for isomer interconversion of $(\eta^5\text{-C}_7\text{H}_7)\text{-Ru}(\text{CO})_2\text{-SnPh}_3$. + - Magnetizations $M_i(t)$ (arbitrary units) at the three sites — 3^a and $3'$ of the asymmetric isomer and 3 of the symmetric isomer — following the selective inversion of the site 3 magnetization of the symmetric isomer at 178 K. Curves represent least squares fit for $k_{(AS)} = 15.52 \text{ s}^{-1}$, $k_{(SA)} = 49.14 \text{ s}^{-1}$, and $k_{(AA')} = 0$.

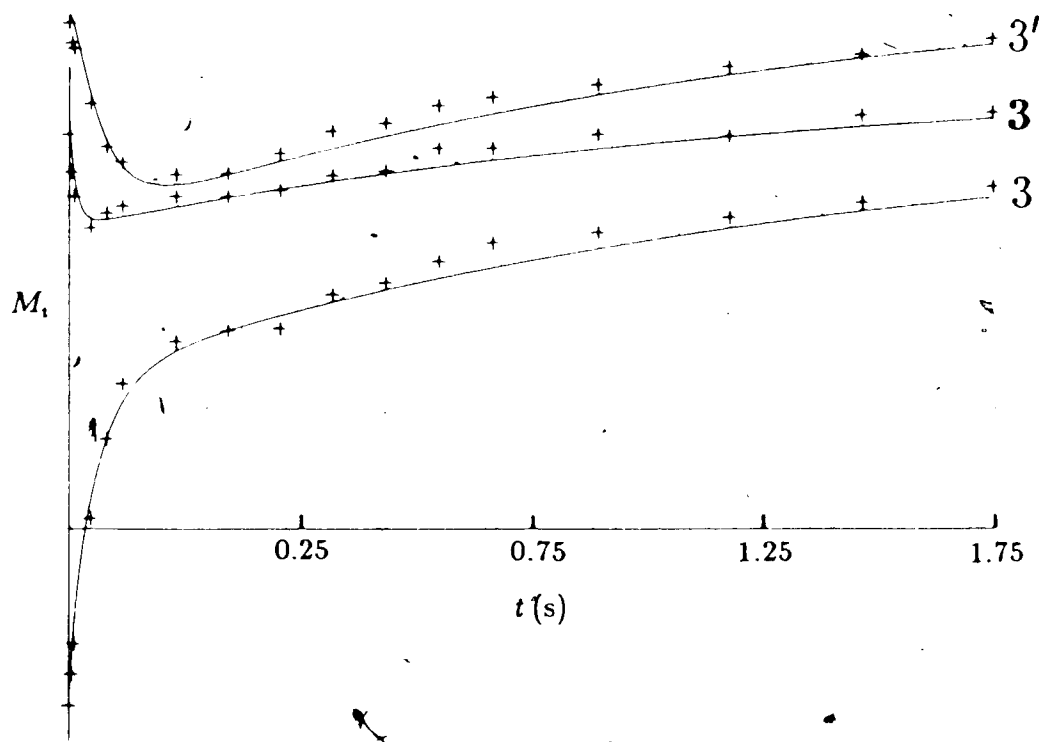


Fig. 6-15 Comparison of the observed and calculated magnetizations for isomer interconversion of $(\eta^5\text{-C}_7\text{H}_7)\text{-Ru}(\text{CO})_2\text{-SnPh}_3$. + - Magnetizations $M_1(t)$ (arbitrary units) at the three sites — 3 and 3' of the asymmetric isomer and 3 of the symmetric isomer — following the selective inversion of the site 3 magnetization of the asymmetric isomer at 178 K. Curves represent least squares fit for $k_{(AS)} = 18.06\text{ s}^{-1}$, $k_{(SA)} = 59.64\text{ s}^{-1}$, and $k_{(AA')} = 0$.

^1H NMR spectrum at this temperature, also failed to converge when both $k_{(AA')}$ and $k_{(AS)}$ were allowed to vary freely during iterations. However, when $k_{(AA')}$ was fixed at zero, it rapidly converged and yielded a value of $18.47 \pm 6.97 \text{ s}^{-1}$ for $k_{(AS)}$, and a second analysis with $k_{(AS)}$ fixed at 18.4 and allowing $k_{(AA')}$ to vary freely, yielded $k_{(AA')} = 0.24 \pm 3.66 \text{ s}^{-1}$. These results are consistent with the earlier calculations, and again show that direct enantiomeric interconversion via the symmetric intermediate $\eta^5\text{-S}'_{\text{Ru}}$ is not important. Rate constants for the isomer interconversion were obtained at two other temperatures, 183 K and 189 K, by analysing the magnetization transfer data following the inversion of the magnetization of site 3 of the asymmetric isomer $\eta^5\text{-A}_{\text{Ru}}$. Intensities of the resonances other than that of protons at sites 3, 3' and 3 did not change following the inversion of site 3 magnetization of $\eta^5\text{-A}_{\text{Ru}}$ even at 189 K, indicating the absence of Ru metal migration processes in this temperature range. It was possible to obtain the values of $k_{(AS)}$ and $k_{(SA)}$, only by fixing $k_{(AA')} = 0$, at these two temperatures and the values are given in Table 6.7.

Table 6.7

Rate constants for the isomer interconversion in $(\eta^5\text{-C}_7\text{H}_7)\text{-Ru(CO)}_2\text{-SnPh}_3$

T (K)	K_{eq}	Inverted site	$k_{(AS)}(\text{s}^{-1})$	$k_{(SA)}(\text{s}^{-1})$	$1/T_1(\text{s}^{-1})$
178.0	3.4	3	15.52 ± 9.86	49.14 ± 20.17	0.70
		3	18.06 ± 6.32	59.64 ± 32.38	
183.0	3.8	3	30.41 ± 10.26	108.50 ± 58.45	0.85
189.0	4.8	3	69.76 ± 20.37	240.42 ± 103.50	0.95

The activation parameters for the isomer interconversion were evaluated using the average values of the rate constants from the two independent determinations, and the activation parameters are tabulated in Table 6.8.

Table 6.8 Activation parameters for the isomer interconversion

	E_a (kcal/mol)	ΔH^\ddagger (kcal/mol)	ΔS^\ddagger (cal/mol K)
<i>Asym</i> \rightarrow <i>Sym</i>	8.7 ± 0.5	8.3 ± 0.5	-5.28 ± 2.96
<i>Sym</i> \rightarrow <i>Asym</i>	9.0 ± 0.1	8.7 ± 0.1	-0.88 ± 0.31

The results show that the conversion of the asymmetric isomers $\eta^5\text{-A}_{Ru}$ and $\eta^5\text{-A}'_{Ru}$ to the symmetric isomer $\eta^5\text{-S}_{Ru}$ and the reverse interconversion process occur with essentially identical activation enthalpies, but with very different activation entropies.

As the temperature is raised, the isomer interconversion rate increases rapidly, which result in the time averaging of the non-equivalent environments of sites 1 and 1; 2, 2' and 2; 3, 3' and 3; and 4, 4' and 4 at high temperatures. Thus as the temperature is raised, the 11 site spectrum at low temperature reduces to

a four site spectrum, corresponding to an effectively symmetric C_7H_7 ring, and, at higher temperatures, one should observe four sharp resonances for the C_7H_7 protons, in the absence of metal migration. At still higher temperatures, the four resonances broaden and coalesce due to the Ru metal migration process until only a single resonance is observed at room temperature. In the temperature range 223 K to 238 K, the rate of metal migration is slow, but only the three resonances, due to $\{H_1, H_1\}$, $\{H_2, H_2', H_2\}$, and $\{H_4, H_4', H_4\}$ are well resolved in CD_2Cl_2 . The resonance due to $\{H_3, H_3', H_3\}$ is very broad and significantly overlapped with the $\{H_4, H_4', H_4\}$ resonance in this solvent. In toluene- d_8 , the 1H NMR spectrum of the isomeric mixture showed a well resolved resonance due to protons 1 and 1, and the three other resonances, which are in fairly close proximity, were reasonably well resolved in the temperature range 221 K to 233 K. Thus the fluxional behaviour of this complex was studied in toluene- d_8 in this temperature range as a four site exchange problem similar to the study of fluxional behaviour of the Fe and Os complexes. It should be noted that in the Ru complex, the four sites 1, 2, 3 and 4 are time-averaged resonances due to $\{H_1, H_1\}$, $\{H_2, H_2', H_2\}$, $\{H_3, H_3', H_3\}$, and $\{H_4, H_4', H_4\}$ respectively (See Fig. 6-4), while the sites in the Fe complex were time averages of the two asymmetric isomer environments, and in the Os complex the sites are those of the symmetric isomer.

6.5.2 Delineation of the Metal migration mechanism in $(\eta^5-C_7H_7)-Ru(CO)_2-SnPh_3$

Although the 1H NMR spectrum of the $(\eta^5-C_7H_7)-Ru(CO)_2-SnPh_3$ complex in CD_2Cl_2 corresponds to that of a symmetric C_7H_7 ring, the resonance due to the site 3 magnetization, arising from protons 3,3' of the asymmetric isomer and 3 of the symmetric isomer, is so broad and significantly overlapped the site 4 resonance at most temperatures in the range of ~ 223 K to ~ 233 K (400 MHz). The

proton spectra of the complex in toluene- d_8 showed four resolved resonances in this temperature range, and hence selective inversion experiments were performed using toluene- d_8 in order to establish the migration pathways. However, even in toluene- d_8 , resonances due to site 3 and 4 overlap, but not so strongly as in CD_2Cl_2 solution since the resonance due to site 3 is not so broad. The site 2 resonance lies very close to the site 4 resonance in toluene- d_8 solution (see Fig. 6-4).

Selective inversion experiments at 221 K, following the inversion of magnetization at site 1, showed a rapid decrease in magnetization at site 3, a smaller and slower decrease in magnetizations at sites 2 and 4. These observations indicate that there are no dominant "1-2" metal shifts in this complex. The rapid decrease at site 3 indicates that "1-3" shifts are occurring, but the decrease in magnetization at site 4, which appears to be more rapid than at site 2, cannot be qualitatively accounted for. Thus a least squares analysis of the data was performed, with all the three rate constants $k_{(12)}$, $k_{(13)}$ and $k_{(14)}$ allowed to vary freely, and the values obtained were $k_{(12)} = -0.53 \pm 1.67 s^{-1}$, $k_{(13)} = 7.89 \pm 2.52 s^{-1}$ and $k_{(14)} = 3.55 \pm 2.51 s^{-1}$. This shows that "1-2" metal shifts are not important in the fluxionality of this complex, but also indicates the presence of "1-4" metal shifts, which was not observed in any other $\eta^5-C_7H_7$ complexes. Analysis of the data with $k_{(12)}$ fixed at zero during iterations, yielded $k_{(13)} = 8.01 \pm 2.53 s^{-1}$ and $k_{(14)} = 2.90 \pm 1.48 s^{-1}$. A third least squares analysis with both $k_{(12)}$ and $k_{(14)}$ fixed at zero during iterations resulted in $k_{(13)} = 13.35 \pm 3.03 s^{-1}$, but the variance for this fit was twice as large as that for the fit with both "1-3" and "1-4" processes allowed. It was not certain at this point whether the apparent presence of "1-4" shifts was a genuine "1-4" shift mechanism operating in the molecule or an artifact arising from the overlap of the resonances from sites 3 and 4. Selective inversion experiments performed at different temperatures at which different degrees of overlap of resonances 3 and 4 were observed, were analysed in two ways;

(i) $k_{(12)}$ fixed at zero, $k_{(13)}$ and $k_{(14)}$ allowed to vary freely; and (ii) only $k_{(13)}$ allowed to vary, with $k_{(12)}$ and $k_{(14)}$ fixed at zero. The rate constants obtained, and variances of these fits are shown in Table 6.9.

Table 6.9

T (K)	$k_{(13)}(s^{-1})$	$k_{(14)}(s^{-1})$	variance
221	13.35 ± 3.03	0	0.0184
	8.01 ± 2.53	2.90 ± 1.48	0.0100
227	26.21 ± 8.29	0	0.0187
	11.35 ± 6.39	7.43 ± 4.15	0.0105
231	51.59 ± 13.97	0	0.0219
	38.26 ± 17.40	8.89 ± 9.89	0.0183
234	58.56 ± 9.19	0	0.0045
	47.86 ± 6.10	6.10 ± 6.10	0.0036

The data in Table 6.9 show that the variance of the fit always improved when both "1-3" and "1-4" shifts were included. However, at temperatures 231 K and 234 K, where the overlap of resonance 3 with resonance 4 is minimal (see Fig. 6-4), $k_{(14)}$ values have large errors. Furthermore, the value obtained for $k_{(14)}$ at 234 K is smaller than the value at the lower temperature 231 K. At temperatures 221 K and 227 K for which fits with "good" "1-4" rate constants were observed, the overlap of resonances 3 and 4 is significantly larger than at 231 K and 234 K. These results indicate that the appearance of "1-4" shifts is an artifact due to the overlap of resonances rather than due to true "1-4" shifts. However "1-4" shifts cannot be ruled out firmly on the basis of these results. It was possible to investigate this further by studying the complex in CD_2Cl_2 at 232 K, where the resonances of sites 1, 2 and 4 are very well resolved, and the resonance due to site 3 is extremely broad. The resonance due to site 3 is so broad at this temperature that it resembles the flat

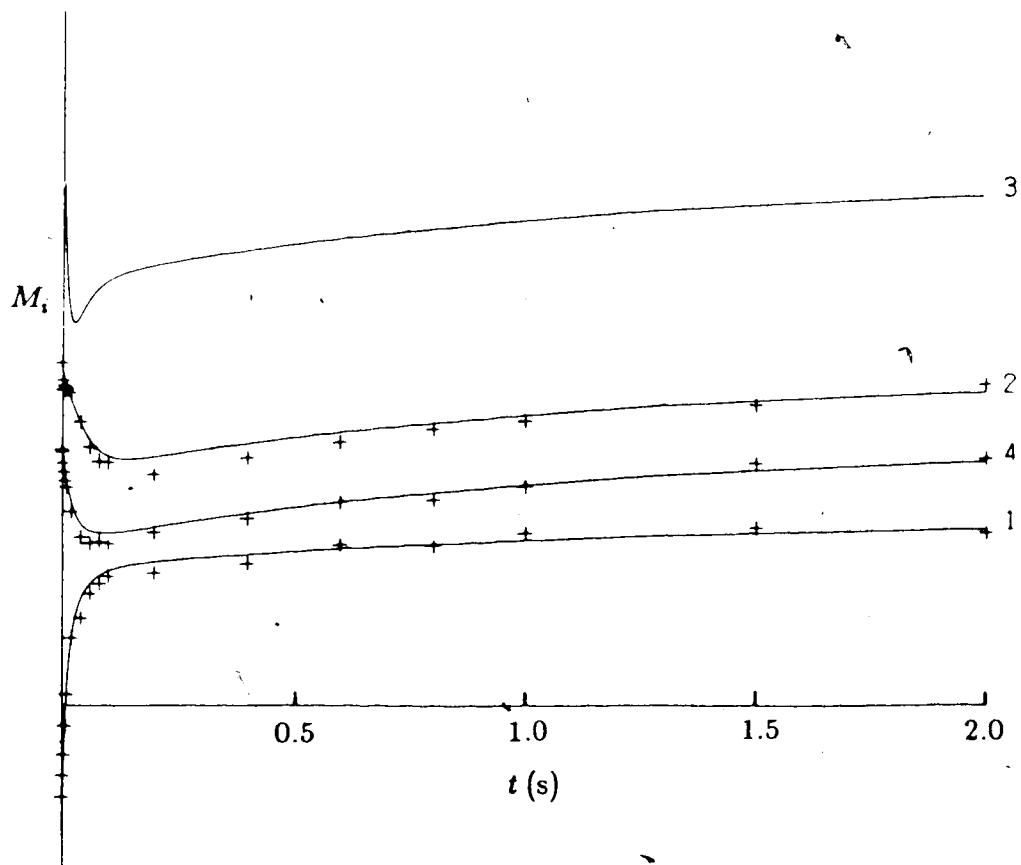


Fig. 6-16 Comparison of the observed and calculated magnetizations for "1-3" shifts for $(\eta^5\text{-C}_7\text{H}_7)\text{-Ru(CO)}_2\text{-SnPh}_3$. + - Magnetizations $M_i(t)$ (arbitrary units) at the four sites of $(\eta^5\text{-C}_7\text{H}_7)\text{-Ru(CO)}_2\text{-SnPh}_3$ in CD_2Cl_2 following the selective inversion of the site 1 magnetization at 232 K. Curves represent least squares fit for $k_{(13)} = 35.52 \text{ s}^{-1}$ and $k_{(12)} = k_{(14)} = 0$.

baseline, and hence its effect on the intensities of the other resonances, particularly resonance 4, is minimal. Selective inversion experiments were performed in which the magnetization at site 1 or at site 2 was inverted in different experiments. The results were analysed as a four site exchange system with data unavailable for one of the sites (site 3). The observed magnetization following the inversion of magnetization at site 1 are shown in Fig. 6-16 and confirm the absence of "1-2" metal shifts as in measurements in toluene- d_8 solution indicated. The results of least squares analyses in which (i) $k_{(12)}$ was fixed at zero and both $k_{(13)}$ and $k_{(14)}$ allowed to vary; and (ii) $k_{(12)}$ and $k_{(14)}$ fixed at zero and only $k_{(13)}$ allowed to vary, are given below in Table 6.10.

Table 6.10

Inverted site	$k_{(13)}(s^{-1})$	$k_{(14)}(s^{-1})$	variance
1	35.52 ± 11.38	0	0.0158
	37.51 ± 26.23	-0.88 ± 11.15	0.0161
2	33.45 ± 6.89	0	0.0141
	28.73 ± 25.48	1.80 ± 9.39	0.0142

These data show that when both $k_{(13)}$ and $k_{(14)}$ were allowed to vary, the errors in $k_{(14)}$ were much larger than the small values of the rate constants, and the variances were larger than in fits with $k_{(14)}$ fixed at zero. The errors in $k_{(13)}$ were almost comparable in magnitude to the values of the rate constants. When $k_{(14)}$ is fixed at zero, the values of the rate constants for the "1-3" shift process were much larger than the errors estimates, and the values from the two experiments were in excellent agreement. These results support the earlier conclusion that the "1-4" shift mechanism is not important in the Ru complex, and that the apparent "1-4"

shifts obtained in the analysis of data from toluene- d_8 solutions can be attributed to overlap between the resonance for sites 3 and 4.

6.5.3 Estimation of activation parameters for $(\eta^5\text{-C}_7\text{H}_7)\text{-Ru(CO)}_2\text{-SnPh}_3$

Although the resonances due to sites 1,2 and 4 are well resolved in CD_2Cl_2 and it was possible to delineate the exchange mechanism as "1-3" shifts at 232 K in CD_2Cl_2 , it is not possible to obtain precise values for the rate constants $k_{(13)}$ at other temperatures due to the significant overlap of resonance 3 and 4 in this solvent. Thus, values of $k_{(13)}$ obtained from magnetization transfer experiments in toluene- d_8 were used to obtain approximate values of the activation parameters for the "1-3" metal migration process. The values of $k_{(13)}$ given in Table 6.9 for $k_{(12)} = k_{(14)} = 0$, for the temperatures in the range 221 K to 234 K yielded activation parameters, $E_a \approx 12.3 \text{ kcal/mol}$, $\Delta H^\ddagger \approx 11.8 \text{ kcal/mol}$ and $\Delta S^\ddagger \approx 0.58 \text{ cal/mol K}$ for the "1-3" metal shifts. These crude values are consistent with the observation that isomer interconversion has a lower activation energy ($\sim 8.5 \text{ kcal/mol}$) than the metal migration process. The crudeness of the activation parameters reported here for the "1-3" metal shifts in this Ru complex, has to be taken into account when comparing the fluxionality of this system with other η^5 complexes, and in trying to draw conclusions from comparisons based on activation parameters.

6.6 Comparison of the Fluxional Behaviour of $(\eta^5\text{-C}_7\text{H}_7)\text{-M}(\text{CO})_2\text{-SnPh}_3$ systems (M=Fe,Ru,Os)

The results obtained from the studies of the fluxional behaviour of $(\eta^5\text{-C}_7\text{H}_7)$ complexes of the group 8B transition metals Fe, Ru and Os, show that when two different metal shift processes are responsible for the metal migration process, both occur with essentially identical activation parameters. The results obtained for the metal migration processes, as determined from multisite magnetization transfer experiments, are summarized in Table 6.11.

Table 6.11 Exchange processes and activation parameters for the fluxional behaviour of $(\eta^5\text{-C}_7\text{H}_7)\text{-M}(\text{CO})_2\text{-SnPh}_3$ (M = Fe, Ru, Os)

M	Observed exchange process	E_a (kcal/mol)	ΔH^\ddagger (kcal/mol)	ΔS^\ddagger (cal/mol K)	
Fe	"1-2" shifts	17.20 ± 0.19	16.66 ± 0.19	3.73 ± 0.70	$k_{(13)} \approx$
	"1-3" shifts	16.70 ± 0.42	16.16 ± 0.42	2.65 ± 1.55	$1.5k_{(12)}$
Ru	"1-3" shifts	~ 12.0	~ 11.8	~ 0.6	
Os	"1-2" shifts	16.96 ± 1.80	16.39 ± 1.81	1.06 ± 6.32	$k_{(12)} \approx$
	"1-3" shifts	18.07 ± 0.44	17.50 ± 0.45	1.90 ± 1.56	$4k_{(13)}$

Although it is not clear why, it is interesting to note that, contrary to the Ru derivative which executes "1-3" metal shifts exclusively, the Fe and Os complexes exhibit both "1-2" and "1-3" metal migrations. This is exactly the opposite to the standard complexities displayed by these molecules in solution where the Ru complex exists as a mixture of symmetric and asymmetric isomers whereas the Fe and Os complexes conform to the asymmetric and symmetric situations respectively. Furthermore it is seen that in the, Fe and Os complexes, where the metal

migration occurs via two different shift mechanisms the activation energies (E_a and ΔH^\ddagger) for the two processes are essentially identical although the rates of metal migration are significantly different. In the Fe complex the "1-3" metal migration is ~ 1.5 times faster than the "1-2" shifts, and conversely in the Os complex it is the "1-2" shift that is faster by a factor of almost four. It is unfortunate that, owing to the lack of precise activation parameters for the Ru complex, it is difficult to extend the quantitative discussion to include this molecule as well. Nevertheless, it is clear that the process here is significantly easier ($E_a \approx 12$ kcal/mol) than in either Fe or Os complexes. This is contrary to the normal behaviour of activation energy for metal migration increasing down a transition metal triad (99-101).

A comparison of the exchange processes that occur with lower activation energy than metal migration and hence occur at lower temperatures, shows that the activation energy of 9 kcal/mol obtained for the isomer interconversion in the Ru complex (see Table 6.7), is similar in magnitude to the estimated activation barrier (54) of ≤ 9.5 kcal/mol for the enantiomer interconversion of the asymmetric Fe complex (see Eq. [6-1]). The results obtained for the isomer interconversion in the Ru complex allow one to postulate the predominant pathway of this enantiomer interconversion in both Fe and Ru asymmetric complexes. In the Fe complex, it was not possible to ascertain whether the enantiomeric interconversion (Eq. [6-1]) was occurring via the symmetric intermediate η^5-S_{Fe} , or the symmetric intermediate $\eta^5-S'_{Fe}$ (54). However, in the Os complex, only the symmetric isomer with structure η^5-S_{Os} was found to exist over the large temperature range 173 K to 373 K (98), and results of the isomer interconversion in the Ru complex reported here show that the asymmetric enantiomers interconvert only via the symmetric isomer η^5-S_{Ru} . Thus it seems likely that the enantiomer interconversion in $(\eta^5-C_7H_7)-Fe(CO)_2-SnPh_3$ also occurs via the symmetric intermediate η^5-S_{Fe} and not via $\eta^5-S'_{Fe}$. This is not surprising since sterically and

electronically (107), the pseudo-octahedral structure of η^5-S_M ($M=Fe, Ru, Os$) with its staggered conformation is preferred over the trigonal prismatic structure of $\eta^5-S'_M$ with eclipsed conformation, although it may be noted (108) that in $(\eta^5\text{-cycloheptadienyl})-M(CO)-(EPTB)_2$ complexes, ($M=Fe, Ru$), isomer interconversion occurs via both types of intermediates. Further information about the enantiomer interconversion pathway could be obtained by measuring the activation parameters for the process of carbonyl exchange in the asymmetric isomer of the Ru complex, and this information would be useful in assessing the validity of the mechanism postulated above.

6.7 Comparison of the fluxionality of general $(\eta^5-C_7H_7)$ transition metal complexes

As mentioned above, only a few $(\eta^5-C_7H_7)$ complexes of transition metals have been reported in the literature (91, 102-105). The activation parameters available for metal migration in these systems are listed in Table 6.12 together with the values reported in this work.

Table 6.12 Fluxional ($\eta^5\text{-C}_7\text{H}_7$)- ML_x complexes

ML_x	E_a (kcal/mol)	ΔH^\ddagger (kcal/mol)	ΔS^\ddagger (cal/mol K)	$\Delta G^\ddagger_{(T)}$ (kcal/mol)	Ref
$\text{Mn}(\text{CO})_3$				$\sim 14_{(300)}$	102, 103
$\text{Re}(\text{CO})_3$		14.8	-1.3	15.1 ₍₃₀₀₎	91
$[\text{Fe}(\text{CO})_3]^\ddagger$				$\sim 11_{()}$	102, 103
$\text{Fe}(\eta^5\text{-C}_7\text{H}_9)$	16.9				105
$\text{Ru}(\eta^5\text{-C}_7\text{H}_9)$				16.7 _()	104
$\text{Fe}(\text{CO})_2\text{SnPh}_3$	17.0	16.4	3.2	15.5 ₍₃₀₀₎	* \ddagger
$\text{Ru}(\text{CO})_2\text{SnPh}_3$	~ 12	~ 11	~ 0.6	~ 11	*
$\text{Os}(\text{CO})_2\text{SnPh}_3$	17.5	16.9	1.5	16.5 ₍₃₀₀₎	* \ddagger

* - This work, \ddagger - Average value for "1-2" and "1-3"

In all of the ($\eta^5\text{-C}_7\text{H}_7$) systems listed in Table 6.12, other than the systems reported in this work, the "ring whizzing" process has been studied using ^1H or ^{13}C NMR lineshapes. The activation parameters in most systems were obtained by fitting the ^{13}C NMR or ^1H NMR lineshapes assuming exclusively "1-2" shifts. It is difficult to obtain precise quantitative rate constants from lineshape analysis when two metal migration processes occur simultaneously, as in the case of ($\eta^5\text{-C}_7\text{H}_7$)- $\text{Fe}(\text{CO})_2\text{-SnPh}_3$ complex described by Reuvers (54). It should also be mentioned here that in a case like ($\eta^5\text{-C}_7\text{H}_7$)- $\text{Os}(\text{CO})_2\text{-SnPh}_3$, where a predominant "1-2" shift mechanism is operative with slower "1-3" metal shifts, it is likely that a lineshape analysis would fail to detect the effects due to the slower process. One cannot therefore preclude the presence of the "1-3" metal shift mechanism in addition to the "1-2" metal shifts in the work reported in literature.

It is interesting to note that all complexes shown in Table 6.12 violate the prediction based on the Woodward-Hoffman rules to which predict that ($\eta^5\text{-C}_7\text{H}_7$) systems should be rigid or at least exhibit metal migration with high activation energies. Thus it seems reasonable to assume that fluxional behaviour of these systems is not an isolated exception to these symmetry rules, and that symmetry rules have little predictive validity in the case of ($\eta^5\text{-C}_7\text{H}_7$), transition metal complexes.

6.8 Summary

Fluxional behaviour of the group 8B transition metal complexes ($\eta^5\text{-C}_7\text{H}_7$)- $\text{M}(\text{CO})_2\text{-SnPh}_3$, $\text{M}=\text{Fe, Ru, Os}$, was studied in detail using the multisite magnetization transfer method. The selective inversion method and the method of data analysis described in earlier chapters enabled the precise quantitative determination of the rates of competing "1-2" and "1-3" metal shifts in the Fe complex whose ground state structure conforms to asymmetric disposition of the ligands with C_1 symmetry, and rates of the dominant "1-2" and slower "1-3" shifts in the Os complex which exhibits C_s symmetry. Metal shifts in both complexes were found to occur with the same activation energy. Fluxional behaviour of the Ru complex, which exists as a mixture of interconverting symmetric (C_s) and asymmetric (C_1) isomers, was found to occur only by "1-3" metal shifts, but it was not possible to obtain precise activation parameters for this process due to significant overlap of exchanging resonances. Activation parameters for the isomer interconversion process were obtained from selective inversion experiments at low temperatures, and the results indicated that enantiomeric interconversion of the asymmetric isomer occur via the symmetric species, although a determination of the carbonyl exchange rate would be helpful for further clarification. Comparison with the fluxionality of ($\eta^5\text{-C}_7\text{H}_7$) systems reported in the literature shows

that this study seems to be the first detailed quantitative study of (η^5 -C₇H₇) systems where different but simultaneous metal shifts are responsible for fluxional behaviour. The results discussed here also show that predictions based on the Woodward-Hoffmann rules are not applicable for these systems.

CHAPTER 7

Conclusions and Suggestions For Future Consideration

In NMR experiments where only the transverse or longitudinal magnetizations are involved (coherences of order 0, + 1), chemical exchange effects are easily handled by the modified Bloch equations (76). Many modern pulse experiments like DEPT involve multiple quantum coherences which cannot be described in simple terms. The description of the DEPT magnetization transfer experiment on exchanging CH ... CH and CH₃ ... CH₃ systems was developed in Chapter 2, to demonstrate the general applicability of the product operator description to investigate the effects of chemical exchange in experiments employing complicated pulse sequences. The product operator representation of the density operator (26) is a convenient way in which to describe pulse experiments (45-47). In order to determine the ¹³C DEPT intensities it is necessary to establish the identity of the product operators involved in each precession period τ of the DEPT experiment and to determine the corresponding **K** matrices in Eq. [2-6]. Since the requisite product operators and the structure of the **K** matrices depend on particular chemical system, the CH ... CH and CH₃ ... CH₃ exchange systems were considered in detail. DEPT experiments were performed on N-acetylpyrrole (CH ... CH exchange) and N,N-dimethylacetamide (CH₃...CH₃ exchange) for a series of τ values, not only the $1/2J_{CH}$ value which is normally used. It was shown both experimentally and theoretically, that the ¹³C intensities from DEPT magnetization transfer experiments are influenced by the rate of chemical exchange. The variation of ¹³C intensities with τ has a damped periodic time dependence, with

the degree of damping being strongly dependent on exchange rate at intermediate exchange rates (from the onset of significant exchange broadening, coalescence, to exchange narrowing). In the region of intermediate exchange, the comparison of observed and calculated DEPT intensities affords the determination of the exchange rate to within 5–15%. Near the coalescence temperature, the DEPT magnetization transfer experiment is expected to give a more precise determination of the exchange rate than the conventional lineshape fitting procedure because reliable peak intensities and integrals from DEPT experiments are more easily obtained than precise visual fitting of the broad signals with low signal-to-noise. In the limits of very slow and very fast exchange, the τ -dependence of the DEPT intensities, like the NMR lineshape, is found to be relatively insensitive to the exchange rate, and relaxation effects contribute significantly to the damping of the periodic τ -dependence of the intensities. In the region of intermediate exchange rates, relaxation effects are of negligible importance. Quantitative agreement of the theoretical and observed DEPT intensities for acetylpyrrole and dimethylacetamide, and the agreement between the exchange rate constants obtained from this method and those obtained from lineshape analysis, with the promise that DEPT method can yield more precise rate constants near the coalescence temperature, prompt us to believe that the use of DEPT in the study of exchange processes may prove a useful adjunct to conventional lineshape analysis.

The development of selective inversion multisite magnetization transfer experiments and the method of data analysis was described in chapter 3. Selective inversion, as opposed to selective saturation, was preferred since selective inversion creates the maximum initial perturbation, and hence gives rise to responses over a larger dynamic range and more precise results. Since only the longitudinal magnetization is important (coherence level 0), this type of homonuclear magnetization transfer experiment can be described by the modified Bloch equations.

Experimentally, selective inversion is achieved very efficiently using the DANTE sequence (61), for protons and other nuclei such as ^{13}C . Transverse magnetization is created only for the purpose of detecting the magnetization at exchanging sites, after an evolution period following the initial selective perturbation. In the magnetization transfer data analysis, k^α , $1/T_{1i}$, $M_i(\infty)$ and $(M_i(0) - M_i(\infty))$, ($i = 1, \dots, N$ sites; $\alpha = 1, \dots, P$ number of rate constants), are all variable parameters. k^α is the rate constant for a particular exchange process, such as a "1-2" metal shift in a fluxional organometallic complex, and not a rate constant for exchange from a site l to a site m . The different exchange processes are described by different matrices of exchange coefficients Π^α . The least squares method utilizes the analytic first derivatives of $M_i(t)$ with respect to each of the parameters in order to minimize the computation time. The method allows one to fix a certain number of chosen variables during the least squares iterations, and usually the values of $1/T_1$ are fixed at values which are independently determined from a nonselective inversion-recovery experiment. The errors in the rate constants k^α are also estimated in the least squares procedure using the F-variance ratio distribution.

In chapter 4, the application of the selective inversion multisite magnetization transfer method to delineate exchange mechanisms, and to determine the rate constants for these mechanisms was illustrated fully using the transition metal organometallic complex $(\eta^3\text{-C}_7\text{H}_7)\text{-Os}(\text{CO})_3\text{-SnPh}_3$ as a test case. It was demonstrated that the method can be successfully applied to delineate exchange mechanisms and to determine reliable rate constants, even under non-ideal conditions such as imperfect selectivity of inversion, baseline distortions and absence of data from one of the sites. The power of the technique was clearly demonstrated in this particular example of a mixture of fluxional but noninterconverting symmetric and asymmetric isomers. It was possible to quantitatively investigate

the fluxional behaviour of the symmetric isomer in the presence of interfering exchange broadened signals due to the fluxional asymmetric isomer: Classical lineshape analysis would be practically impossible to use in such a case. The data analysis also showed that the accuracy of the relaxation rates is not very critical in the determination of reliable rate constants.

The results of a detailed investigation of the fluxional behaviour of the $(\eta^3\text{-C}_7\text{H}_7)\text{-Os}(\text{CO})_3\text{-SnPh}_3$ complex, using the multisite magnetization transfer method, were presented in chapter 5. The activation parameters were determined for the "1-2" metal migration process which was shown to be the dominant exchange process in both symmetric and asymmetric isomers. The symmetric isomer was shown to have a higher activation barrier (9.5 kcal/mol) for "1-2" metal shifts than that in the asymmetric isomer (6.4 kcal/mol). The activation energy for axial-equatorial carbonyl exchange in the asymmetric isomer (98) is significantly higher than that for the metal migration in either isomer. This difference in activation energies, together with the absence of carbonyl scrambling in the symmetric isomer, suggests that the two processes occur independently. It is interesting to note that, although the activation energy reported here for the metal migration in the symmetric isomer of the Os complex is similar to that reported for symmetric $(\eta^3\text{-C}_7\text{H}_7)\text{-Fe}(\text{CO})_3\text{-SnPh}_3$ (97), carbonyl exchange was observed in the Fe complex but not in the Os analogue. It was not possible to make any generalizations from a comparison of the fluxional behaviour of other similar $(\eta^3\text{-C}_7\text{H}_7)$, symmetric and asymmetric systems, due to the lack of reliable quantitative information from other studies. Hence it would be interesting to undertake selective inversion magnetization transfer experiments on the complexes $(\eta^3\text{-C}_7\text{H}_7)\text{-Re}(\text{CO})_3\text{-PMe}_3$ (91), which exists as a noninterconverting mixture of symmetric and asymmetric isomers below room temperature, and $(\eta^3\text{-C}_7\text{H}_7)\text{-Mn}(\text{CO})_3\text{-PMe}_3$ (91) which exists as an interconverting mixture of isomers.

In chapter 6, the results of the investigation of the fluxional behaviour of group 8B transition metal complexes ($\eta^5\text{-C}_7\text{H}_7\text{)-M(CO)}_2\text{-SnPh}_3$, (M=Fe,Ru,Os), using the multisite magnetization transfer method, were presented. It has been established that the Fe complex exists as the asymmetric isomer (54), the Os complex only as the symmetric isomer and the Ru complex as a mixture of interconverting symmetric and asymmetric isomers (98). All complexes were fluxional due to the metal migration around the C_7H_7 ring, enantiomer interconversion in the Fe complex (54), and isomer interconversion in the Ru complex (98). At higher temperatures, ^1H NMR spectra of both Fe and Ru complexes correspond to those of an effective symmetric isomer and hence it was possible to investigate the metal migration in all three complexes as four site exchange problems. Unlike the ($\eta^3\text{-C}_7\text{H}_7$) Fe and ($\eta^3\text{-C}_7\text{H}_7$) Os complexes discussed in chapter 5, where only "1-2" metal shifts were observed, two metal migration processes were found to occur simultaneously in ($\eta^5\text{-C}_7\text{H}_7$) Fe and Os complexes. In the $\eta^5\text{-Fe}$ complex, competing "1-2" and "1-3" metal shifts occur, with the rate of "1-3" shifts being about 1.5 times faster than the rate of "1-2" shifts, while dominant "1-2" shifts and slower "1-3" shifts occur in the Os complex, with the rate of "1-2" shifts being about four times faster than "1-3" shifts. In both cases, precise rate constants and hence activation parameters were obtained, from the results of selective inversion, multisite magnetization transfer experiments. Metal shifts in both Fe and Os complexes were found to occur with similar activation energies. In the Ru complex, only "1-3" metal shifts occur, but it was not possible to obtain precise values for the rate constants and activation parameters for this complex due to the significant overlap of some of the exchanging resonances. For the Ru complex, activation parameters for the isomer interconversion were obtained from selective inversion experiments at low temperature. The results show that enantiomeric

interconversion of the asymmetric isomer occurs via the symmetric isomer not by direct exchange between the enantiomers. To further clarify this result, it would be helpful to undertake selective inversion magnetization transfer experiments to investigate the mechanism and rate of carbonyl exchange in the isomer interconversion process in this complex.

Comparison of the fluxional ($\eta^5\text{-C}_7\text{H}_7$) systems reported in the literature (91,102-105) shows that the "ring whizzing" process has been studied using ^1H or ^{13}C lineshape and only "1-2" shifts were reported to be responsible for the fluxional behaviour. It is difficult to delineate mechanisms and to obtain precise quantitative rate constants from lineshape analysis when two metal migration mechanisms occur simultaneously. It is also likely that in a case like ($\eta^5\text{-C}_7\text{H}_7$)- $\text{Os}(\text{CO})_2\text{-SnPh}_3$ where a predominant "1-2" mechanism is operative with slower "1-3" metal shifts, that a lineshape analysis would fail to detect the effects due to the slower process and one should not preclude the presence of "1-3" metal shifts, in addition to "1-2" metal shifts, in the work reported in the literature. Therefore it would be useful to reinvestigate the fluxionality of the complexes reported in the literature, using the selective inversion, multisite magnetization transfer method. The complexes discussed in chapter 6, and other ($\eta^5\text{-C}_7\text{H}_7$) complexes reported in literature (see Table 6.12) are all fluxional and violate the prediction based on Woodward-Hoffmann rules that ($\eta^5\text{-C}_7\text{H}_7$) systems are rigid. This indicates that the Woodward-Hoffmann symmetry rules have little predictive validity in the case of ($\eta^5\text{-C}_7\text{H}_7$) complexes of transition metals.

REFERENCES

1. L. M. Jackman and F. A. Cotton, (Ed.) "Dynamic NMR spectroscopy", Academic Press, New York, 1975.
2. J. Sandström, "Dynamic NMR spectroscopy", Academic Press, London, 1982.
3. C. S. Johnson, Jr., *Adv. Magn. Reson.* **1**, 33 (1965).
4. G. Binsch, *Top Stereochem.* **3**, 97, (1968).
5. N. S. Ham and T. Mole, *F. NMR Spectrosc.* **4**, 91, (1969).
6. I. O. Sutherland, *Ann. Rep. on NMR Spectrosc.* **4**, 71, (1971).
7. S. Aime and L. Milone, *Prog. NMR Spectrosc.* **11**, 183, (1977).
8. B. E. Mann, *Prog. NMR Spectrosc.* **11**, 95, (1977).
9. A. Steigel in *NMR Basic Principles and Progress*, vol 15 (Ed. P. Diehl, E. Fluck, R. Kosfeld), p. 1ff, Springer-Verlag, Berlin, (1978).
10. G. Binsch and H. Kessler, *Angew. Chem. Int. Ed. Engl.* **19**, 411, (1980).
11. M. L. Martin, X. Y. Sun, and G. J. Martin, *Ann. Rep. on NMR Spectrosc.* **16**, 187 (1985).
12. H. S. Gutowsky, D. W. McCall and C. P. Slichter, *J. Chem. Phys.* **21**, 279 (1953).
13. H. S. Gutowsky and A. Saika, *J. Chem. Phys.* **21**, 1688 (1953).
14. H. S. Gutowsky and C. H. Holm, *J. Chem. Phys.* **25**, 1228 (1956).
15. H. M. McConnell, *J. Chem. Phys.* **28**, 430 (1958).
16. R. A. Sack, *Mol. Phys.* **1**, 163 (1958).
17. P. W. Anderson, *J. Phys. Soc. Japan* **9**, 316 (1954).
18. R. Kubo, *J. Phys. Soc. Japan* **9**, 935 (1954).
19. J. I. Kaplan, *J. Chem. Phys.* **28**, 278 (1958).

20. J. I. Kaplan, *J. Chem. Phys.* **28**, 462 (1958).
21. S. Alexander, *J. Chem. Phys.* **37**, 967 (1962).
22. S. Alexander, *J. Chem. Phys.* **37**, 974 (1962).
23. S. Alexander, *J. Chem. Phys.* **38**, 1787 (1963).
24. S. Alexander, *J. Chem. Phys.* **40**, 2741 (1964).
25. F. Bloch, *Phys. Rev.* **70**, 460 (1946).
26. U. Fano, *Rev. Mod. Phys.* **29**, 74 (1957).
27. R. M. Lynden-Bell, *Prog. NMR. Spectrosc.* **2**, 163 (1967).
28. G. Binsch, *J. Amer. Chem. Soc.* **91**, 1304 (1969).
29. D. A. Kleier and G. Binsch, *J. Magn. Reson.* **3**, 146 (1970).
30. R. A. Hoffmann, *Adv. Magn. Reson.* **4**, 87 (1970).
31. J. I. Kaplan and G. Fraenkel, *J. Amer. Chem. Soc.* **94**, 2907 (1972).
32. P. D. Buckley, K. W. Jolly and D. N. Pinder, *Prog. NMR Spectrosc.* **10**, 1 (1975).
33. S. Szymanski, M. Witanowsky and A. Gryff-Keller, *Ann. Rep. on NMR Spectrosc.* **8**, 228 (1978).
34. J. I. Kaplan and G. Fraenkel, "NMR of Chemically Exchanging Systems", Academic Press, New York 1980.
35. R. Benn and H. Gunther, *Angew. Chem. Int. Ed. Engl.* **22**, 350 (1983).
36. A. Bax in *Topics in Carbon-13 NMR Spectroscopy*, Vol. **4** (G. C. Levy, Ed.), p. 197ff, Wiley, New York, 1984.
37. H. Y. Carr and E. M. Purcell, *Phys. Rev.* **94**, 630 (1954).
38. A. Allerhand and H. S. Gutowsky, *J. Chem. Phys.* **41**, 2115 (1964).
39. A. Allerhand and H. S. Gutowsky, *J. Chem. Phys.* **42**, 1587 (1965).
40. A. Allerhand and H. S. Gutowsky, *J. Chem. Phys.* **42**, 4203 (1965).
41. H. S. Gutowsky, R. L. Vold and E. J. Wells, *J. Chem. Phys.* **43**, 4107 (1965).

42. N. Boden, in *Determination of Organic Structures by Physical Methods* (Ed. F. C. Nachod and J. J. Zuckerman), Vol 4, p.85 ff, Academic Press, New York, 1971.
43. J. Frahm, *J. Magn. Reson.* **47**, 209 (1982).
44. J. Jeener, B. H. Meier, P. Bachmann, and R. R. Ernst, *J. Chem. Phys.* **71**, 4546 (1979).
45. O. W. Sorensen, G. W. Eich, M. H. Levitt, G. Bodenhausen, and R. R. Ernst, *Prog. NMR Spectrosc.* **16**, 163 (1983).
46. K. J. Packer and K. M. Wright, *Mol. Phys.* **50**, 797 (1983).
47. T. T. Nakashima and R. E. D. McClung, *J. Magn. Reson.* **70**, 187 (1986).
48. D. T. Pegg, D. M. Doddrell, and M. R. Bendall, *J. Chem. Phys.* **77**, 2745 (1982).
49. R. C. Neuman, Jr and V. Jones, *J. Amer. Chem. Soc.* **90**, 1970 (1968).
50. R. C. Neumann Jr., W. R. Woolfenden, and V. Jonas, *J. Phys. Chem.* **73**, 3177 (1969).
51. T. Matsuo and H. Shosenji, *Chem. Commun.* 501 (1969).
52. K. I. Dahlquist and S. Forsen, *J. Phys. Chem.* **73**, 4142 (1969).
53. T. Matsuo, H. Shosenji, and R. Miyamoto, *Bull. Chem. Soc. Japan* **46**, 1437 (1973).
54. J. G. A. Reuvers, Ph. D. Thesis, University of Alberta 1979.
55. S. Forsen and R. Hoffmann, *Acta. Chem. Scand.* **17**, 1787 (1963).
56. S. Forsen and R. Hoffmann, *J. Chem. Phys.* **39**, 2892 (1963).
57. S. Forsen and R. Hoffmann, *J. Chem. Phys.* **40**, 1189 (1964).
58. F. Dahlquist, K. Longmuir and R. Duvernet, *J. Magn. Reson.* **17**, 406 (1975).
59. J. R. Alger and J. H. Prestegard, *J. Magn. Reson.* **27**, 137 (1977).

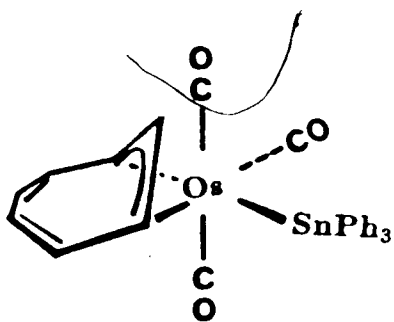
60. I. D. Campbell, C. M. Dobson, R. G. Ratcliffe and R. J. P. Williams, *J. Magn. Reson.* **29**, 397-1978.
61. G. A. Morris and R. Freeman, *J. Magn. Reson.* **29**, 433 1978.
62. J. J. Led and H. Gesmar, *J. Magn. Reson.* **49**, 444 1982.
63. J. W. Faller, in *Determination of Organic Structures by Physical Methods* vol.5 (Ed. F. C. Nachod and J. J. Zuckerman) p. 75ff Academic Press, New York, 1973.
64. J. R. Alger and R. G. Shulman, *Quart. Rev. Bio Phys.* **17**, 83 (1984).
65. G. Y. Kiel and J. Takats, *Organometallics* (in press 1987).
66. F. A. Cotton, *Acct. Chem. Res.* **1**, 257 (1968).
67. F. A. Cotton, *J. Organometallic Chem.* **100**, 29 (1975).
68. J. W. Faller, *Adv. Organometallic Chem.* **16**, 211 (1977).
69. B. E. Mann, in *Comprehensive Organometallic Chemistry* vol.3 (Ed. E. W. Abel, F. G. A. Stone, and G. Wilkinson) Pergamon Press, Oxford, 89 (1982).
70. B. E. Mann, *Chem. Soc. Rev.* **15**, 167 (1986).
71. D. M. P. Mingos, *J. Chem. Soc. Dalton Trans.* 31, 1977
72. R. B. Woodward and R. Hoffmann, "The Conservation of Orbital Symmetry", Academic Press, New York, 1970.
73. G. S. Reddy, *Chem and Ind.* 1426 (1965).
74. D. W. Marquardt, R. G. Bennett, and E.J. Burell *J. Mol. Spectrosc.* **7**, 269 (1961).
75. H. M. McConnell and D. D. Thompson, *J. Chem. Phys.* **31**, 85 (1959).
76. H. M. McConnell, *J. Chem. Phys.* **28**, 430 (1958).
77. A. Abragam, "Principles of Nuclear Magnetism", p. 45 ff, Clarendon Press, Oxford 1961.
78. B. T. Smith, J. M. Boyle, B. S. Garbow, Y. Ikebe, V. C. Kleme and C. B. Moler, "Matrix Eigenvalue Systems", Springer-Verlag, Berlin, 1974

79. G. Forsythe and C. B. Moler, "Computer solution of Linear algebraic systems", Englewood Cliffs, N. J. Prentice-Hall Inc. 1967, Chap. 9, 13, 24.
80. J. H. Wilkinson, "The Algebraic Eigenvalue Problem", chapter 2, Clarendon Press, Oxford, 1965.
81. P. D. Lark, B. R. Craven and R. C. L. Bosworth, "The Handling of Chemical Data", p. 149 ff, Pergamon Press, Oxford, 1968.
82. A. Abramowitz and I. A. Stegun "Handbook of Mathematical functions", p. 946 Dover Publications, New York 1970
83. H. Gesmar and J. Led, J. Magn. Reson. **68**, 95 (1986).
84. M. Grassi, B. E. Mann, B. T. Pickup and C. M. Spencer, J. Magn. Reson. **69**, 92 (1986).
85. T. C. Farrar and E. D. Becker, "Pulse and Fourier Transform NMR", p. 20 ff, Academic Press, New York, 1971.
86. J. B. Lambert and J. W. Keepers, J. Magn. Reson. **38**, 233 1980.
87. A. Abragam, "Principles of Nuclear Magnetism", p295, Clarendon Press, Oxford, 1961.
88. R. B. Larabee, J. Amer. Chem. Soc. **93**, 1510 (1971).
89. B. E. Mann, B. F. Taylor, N. A. Taylor and R. Wood, J. Organomet. Chem. **162**, 137 (1978).
90. D. M. Heinekey and W. A. G. Graham, J. Amer. Chem. Soc. **101**, 6115 (1979).
91. D. M. Heinekey, Ph. D. Thesis, University of Alberta 1982.
92. M. H. Hails, B. E. Mann and C. M. Spencer, J. Chem. Soc., Dalton Trans. 693 (1985).
93. M. A. Bennett, R. Bramley and R. Watt, J. Amer. Chem. Soc. **91**, 3089 (1969).

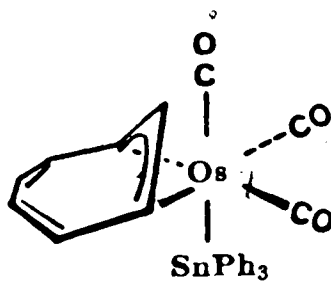
94. J. W. Faller, *Inorg. Chem.* **8**, 767 (1969).
95. D. Ciapennelli and R. Rosenblum, *J. Amer. Chem. Soc.* **91**, 6876 (1969).
96. J. L. Calderon, F. A. Cotton and A. Shaver, *J. Organomet. Chem.* **42**, 419 (1972).
97. J. G. A. Reuvers and J. Takats, Manuscript in preparation.
98. G. Y. Kiel and J. Takats, Personal communication.
99. M. Cooke, R. J. Goodfellow, M. Green, J. P. Maher and J. R. Yandle, *Chem. Commun.* 565 (1970).
100. F. A. Cotton and D. L. Hunter, *J. Amer. Chem. Soc.* **98**, 1413 (1976).
101. M. A. Bennett, T. W. Matheson, G. B. Robertson, A. K. Smith and P. A. Tucker, *Inorg. Chem.* **19**, 1014 (1980).
102. T. H. Whitesides and R. A. Budnik, *Chem. Commun.* 1514 (1971).
103. T. H. Whitesides and R. A. Budnik, *Inorg. Chem.* **15**, 874 (1976).
104. J. Muller, C. G. Kreiter, B. Mertschenk and S. Schmitt, *Chem. Ber.* **108**, 273 (1975).
105. R. J. Blackborrow, R. H. Grubbs, K. Hildenbrand, E. A. Koerner von Gustorf, A. Miyashita and A. Scrivanti, *J. Chem. Soc., Dalton Trans.* 2205 (1977).
106. J. G. A. Reuvers and G. Bigam, Unpublished results.
107. T. Albright, P. Hofmann and R. Hoffmann, *J. Amer. Chem. Soc.* **99**, 7546 (1977).
108. T. H. Whitesides and R. A. Budnik, *Inorg. Chem.* **14**, 664 (1975).

APPENDIX A

Perspective views of the asymmetric/meridional ($\eta^3\text{-AO}_8$) and symmetric/faceal ($\eta^3\text{-SO}_8$) isomers of $(\eta^3\text{-C}_7\text{H}_7)\text{-Os}(\text{CO})_3\text{-SnPh}_3$.



$\eta^3\text{-AO}_8$



$\eta^3\text{-SO}_8$